LICENTIATE THESIS

Orientational dynamics of small non-spherical particles in fluid flows

JONAS EINARSSON

Department of Physics
University of Gothenburg
Göteborg, Sweden 2013

Orientational dynamics of small non-spherical particles in fluid flows
Jonas Einarsson
ISBN 978-91-637-4473-0

This thesis is electronically published, available at
http://hdl.handle.net/2077/34320

Department of Physics
University of Gothenburg
SE-412 96 Göteborg
Sweden
Telephone: +46 (0)31-786 00 00

Front cover: Illustration of spheroidal particle tumbling in a shear flow. Flipbooks: Ellipsoidal particles rotating in a simple shear flow. *Odd pages:* Symmetric particle with major aspect ratio $\lambda = 7$ and minor aspect ratio $\kappa = 1$. *Even pages:* Slightly asymmetric particle with $\lambda = 7$ and $\kappa = 1.2$. Both particles started with identical initial conditions. See Sections 2.3 and 3 for further explanation.

Printed by Kompendiet
Göteborg, Sweden 2013

ABSTRACT

Particles suspended in fluid flows are common in nature. Important examples are drops of water or particulate matter in the atmosphere, and planktonic microorganisms in the ocean. Due to fluid velocity gradients, non-spherical particles are subject to a hydrodynamic torque. The torque leads to rotational motion of the particle. This thesis describes our work on the orientational dynamics of non-spherical particles suspended in fluid flows. We consider the viscous Stokes regime, where the particle Reynolds number $\mathrm{Re}_\mathrm{p} \ll 1$ ($\mathrm{Re}_\mathrm{p} = u_0 a/\nu$, where u_0 is a typical flow speed, a is the particle size and ν is the kinematic viscosity of the fluid). In this *advective limit*, the hydrodynamic torques are given by Jeffery's theory [JEFFERY, G. B. *Proc. R. Soc. Lond. A* **102**, 161–179 (1922)].

First, we describe a microfluidic experiment where we observe periodic and aperiodic tumbling of rod-shaped particles. We argue that the aperiodic tumbling is commensurate with the quasi-periodic and chaotic tumbling predicted by the inertia-free limit of Jeffery's theory.

Second, we calculate a modification to Jeffery's theory for axisymmetric particles, that takes into account the first effects of particle inertia. In a simple shear flow the particle inertia induces a drift towards a limiting orbit. We describe how the stationary orientational distribution of an ensemble of particles is determined by the competition between particle inertia and Brownian noise.

Third, by averaging Jeffery's equation along particle trajectories, we make a connection between rotation rates and the third-order Lagrangian correlation functions of the flow. Our result explains recent numerical and experimental observations of different tumbling rates for disks and rods in turbulence.

Finally, this thesis contains a non-technical introduction to the study of particle dynamics in fluid flows, aimed at a wider audience.

List of papers

This thesis consists of an extended summary and the following three appended papers:

Paper A
Einarsson, J., Johansson, A., Mahato, S. K., Mishra, Y. N., Angilella, J. R., Hanstorp, D. & Mehlig, B. 2013 Periodic and aperiodic tumbling of microrods advected in a microchannel flow. *Acta Mechanica* **224** (10), 2281–2289.

Paper B
Einarsson, J., Angilella, J. R. & Mehlig, B. 2013 Orientational dynamics of weakly inertial axisymmetric particles in steady viscous flows. *In review*, available as arXiv e-print **1307.2821.**

Paper C
Gustavsson, K., Einarsson, J. & Mehlig, B. 2013 Tumbling of small axisymmetric particles in random and turbulent flows. *In review*, available as arXiv e-print **1305.1822**.

ACKNOWLEDGEMENTS

Most importantly, I want to thank my supervisor Bernhard Mehlig for taking me on as a student. I cannot imagine a better scientific climate to work in: everything is up for discussion, no stone unturned.

I also want to thank the many collaborators we have: Dag Hanstorp and his students, for the microfluidic experiments; Jean-Régis Angilella for the many discussions and calculations, some of which resulted in paper B; Kristian Gustavsson for teaching me all I know about random flows and Kubo-numbers.

Finally, a big thank you to my friends and collegues who improved this thesis by their scrutinous reading and helpful comments: Kajsa, Tora, Rasmus, Bernhard, Kristian, Erik and Marina.

CONTENTS

PART I
INTRODUCTION

The motion of small particles suspended in fluid flows is a fundamental research topic attracting interest in many branches of science, as well as in technical applications. In some cases it is the actual motion of the particles that is of interest. For example, in the atmospheric sciences the collisions and aggregation of small drops are important to the formation of rain [1]. Similarly, in astronomy it is believed that the collisions of small dust grains lead eventually to the formation of planets in the accretion disk around a star [2]. Another example is in marine biology, where the dynamics of small planktonic organisms swirled around by the ocean is fundamental in understanding their feeding and mating patterns [3].

In other contexts the motion of the individual particle is of lesser interest. Instead its effects on the suspending fluid is the topic of study. The properties of so-called complex fluids, meaning fluids with suspended particles, are studied in the field of rheology. For instance, the "ketchup effect" (where ketchup is stuck in the bottle, and nothing happens, and then suddenly all the ketchup pours out at once, only to become innocently solid again on the plate) exists because of how all the microscopic particles suspended in the liquid orient themselves [4]. On a more serious note, the similarly sudden onset of landslides in clay soils is related to the complex fluid of water and clay particles [5]. A fundamental question in rheology is how to relate the microscopic motion of the suspended particles to the macroscopic behaviour of the complex fluid.

In many circumstances it is important to consider the non-spherical shape of particles, and how they are oriented. For instance, the ash clouds from volcanic eruptions play an important role in the radiation budget of our planet, and therefore its climate [6]. The ash particles are non-spherical [7], and their shapes

and orientations influence how light and energy is absorbed in the volcanic cloud [8]. Similarly, the orientation of non-spherical plankton influences the light propagation through the upper layers of the oceans, determining to which depth life-supporting photosynthesis is possible [9].

Despite their diversity, all the above examples share a basis in a fundamental question. How do particles respond to a given flow, and how does the flow in return respond to the presence of particles? The underlying goal of our research is to find an answer to this fundamental question. But with such grand aims there must be plenty of room for humility regarding which particular questions we seek answers to. The mathematics of fluid dynamics have challenged physicists and mathematicians alike for several hundred years. Before moving on to the description of my work, I allow myself to digress into the story of a seemingly innocent question: what is the drag force on a perfect sphere moving with constant velocity through a still fluid?

Until the early 19th century the prevailing theory was the following: a moving sphere drags along some of the surrounding fluid in its motion, and the force upon the sphere is equal to the force required to drag along the extra weight. The force must then be dependent on the weight, or more precisely the density, of the fluid. But in 1829, Captain Sabine of the Royal Artillery performed detailed experiments with a pendulum in different gases [10]. By observing the attenuation of the pendulum motion in both hydrogen gas and in air, he concluded beyond doubt that the damping force on the pendulum is not simply proportional to the density of the surrounding gas - there has to be another force.

It was Sir George Gabriel Stokes who first computed the force on a *slowly moving* sphere due to the internal friction of the fluid [11]. and found that it depends on the "index of friction", which we today know as the kinematic viscosity of a fluid. From his calculation, Stokes immediately concluded that "the apparent suspension of the clouds is mainly due to the internal friction of air." The *Stokes drag force* was a great success, and it correctly predicts the forces for slowly moving particles.

But for swiftly moving particles the solution turned out to be

very elusive. The question of how to correctly amend Stokes drag force to account for slightly faster motion took around a century of hard work, and the invention of a new branch of mathematics [12]. If we dare ask how to properly calculate the drag force on a particle moving quickly, in a curved path, and in a fluid which itself moves, the answer is still debated.

Meanwhile, the Stokes solution for slow motion has been extended to encompass both forces and torques on particles of any conceivable shape [13, 14, 15]. Much of modern research on particles in fluid flows still relies directly on these well-known results. Indeed, all results presented in this thesis are based on the Stokes drag on non-spherical particles. Despite its apparent simplicity, we shall see in this thesis that it can lead to very non-trivial physical behaviour. However, we shall keep in mind that there is a largely unexplored world beyond the slow-motion approximation.

Today we enjoy access to tools undreamed of in Stokes' time. We have computers that can solve otherwise unsolvable equations numerically. Albeit still expensive, it is even possible to create artificial computer "experiments" with turbulent flows. With the advent of electronics and microtechnology also our experimental techniques have improved tremendously. There are groups recording the detailed real-time motion of particles in turbulent fluid flows [16, 17], raising the bar for theorists as well.

In my research I work in an environment where we have experiments on one hand, and the methods of mathematical physics to attack the theory on the other. We work simultaneously on two main tracks. The first aims to understand which equations are appropriate to describe the rotation of non-spherical particles in simple flows, such as the ones Stokes himself considered. To this end we have an experimental setup where we observe the motion of single particles (see Section 3 & Paper A). Based on the experimental observations, we try to deduce which physical mechanisms are responsible for the particle motion. The second track concerns the motion of non-spherical particles in turbulent and other random flows. It is theoretical work on our part, but the corresponding experiments are being performed in other parts of the world [16, 17]. We aim to explain the complicated relation

between the statistics of the turbulent flow, and the statistics of the particle motion (see Section 5 & Paper C).

Disposition of this thesis

The thesis contains three papers A–C, and this extended introduction & summary. The extended summary serves three distinct purposes, and thus addresses several different readers. I intend this text to

1. introduce our field of research to a non-expert,
2. give a brief technical introduction of the field, intended for a fellow student or researcher, and
3. introduce the papers, and elaborate on some results related to the papers.

The material is divided into the following four parts:

- Part I: Introduction & background,
- Part II: Present work,
- Part III: Appendices with calculations, and
- Part IV: Research papers.

The parts are divided in Sections, and the Section numbering is sequential throughout the entire thesis.

The non-technical reader is directed to the Background chapter, directly following this Section, for an introduction to our field of study.

The second half of Part I introduces some technical key concepts, prerequisite to understanding the appended research papers. This introduction is aimed at a peer, who has some technical background, but perhaps is not familiar with this particular field of research. It is necessarily brief, and selective in subject, but my intention is that it should enable for instance a fellow student to read and understand the appended research papers.

The reader familiar with the subject matter likely wants to jump directly to the papers in Part IV, and return to Part II at his or her own convenience for elaborations, particularly regarding Papers A and C.

I expect the calculations in Part III to serve as a technical reference, and they are only required for a full technical understanding of the papers.

1 Background

Every now and then I get the question "what is it you do, anyway?" Often enough the question is posed out of sheer politeness, and I can simply say "Physics! Tiny particles, like plankton, they tumble in the oceans, and stuff." But sometimes the question is sincere, and I find that it is quite a challenge to explain to a non-expert. I may say that we calculate how non-spherical particles rotate in flows. But that is comparable to if I was designing a gearbox, and said that I work with cars. It is true, but not very helpful. The following is an attempt at a description which is readable and not too complicated, but still complicated enough to get a glimpse of the physics.

1.1 Our field of study: particles in flows

Where do particles go when I put them into a flow? Which way do they face? how fast do they spin? These are all valid questions, but they are unspecific. Of course the answers depend on if the particle is an aircraft or a grain of particulate carbon soot, and if the liquid is air or water.

I will start with an elaboration on fluid physics, move through why we consider rigid particles specifically, then say something about the forces acting on the particles. This will naturally lead us to why we must consider "small" particles, which is not obvious from the outset. But let's start from the beginning.

Fluids

Many physical systems around us are fluids. The air we breathe, the water we drink, the blood in our veins are all fluids. As a working definition we can think of a fluid as a system where the constituent molecules move around more or less freely. Sometimes they interact with each other and exchange some energy. These collisions give rise to what you perceive as friction. You know that syrup has more friction than water: if you pull a spoon through syrup, more of your energy is expended colliding molecules than

if you were to pull the spoon through water. A measure of how often and how violently the molecules collide is the *viscosity* of a fluid, and we say that syrup has higher viscosity than water. Now, it gets interesting when something else, for example a drop of oil or a particle, is added to the fluid. Consider dripping a drop of oil into water. Then what happens depends on how the water molecules interact with the oil molecules. As you probably have experienced, the oil molecules prefer to stick together. Therefore the oil concentrates into a drop where as many oil molecules as possible may be neighbours with other oil molecules.

But so far, the above is a very qualitative, and you may rightly say naive, description of what happens. One could say that a fundamental problem of fluid physics is to figure out where all the different molecules go. From the detailed knowledge of every molecule we may proceed to deduce where the oil drop goes, and how fast, or if it perhaps breaks up, or maybe merges with another drop. However, making something useful out of this molecular picture is very difficult[1]. Just consider that in one litre of water there are about 10^{25} molecules (that is a very large number; about the weight of the Earth in kg). In fact, we are not even particularly interested in the specific details of every molecule – we are interested in the macroscopic, observable world that is built up from all these molecules. Now, this thesis is not at all concerned with the detailed motion of molecules, but I still wanted to start with this picture because sometimes it becomes important to remember the origin of the macroscopic motion.

Fluid dynamics

The discipline studying the macroscopic properties and motion of fluids is called fluid dynamics. Some typical quantities studied there are the fluid velocity and pressure. We can think of the velocity at a certain position in the fluid as the average velocity of all the molecules at that point. The pressure is the force per area an object in contact with the fluid experiences, due to the

[1] Modern computers now allow simulation of surprisingly large numbers of molecules. Here is a video showing the interface between two molten metals using exactly this approach: http://www.youtube.com/watch?v=Wr7WbKODM2Q

constant bombardment of molecules. Think for example of the forces in a bottle of soda. There are well-known equations called the Navier-Stokes equations (you can see them in Eq. (2.1) on p. 16) which describe the velocity and pressure, if we can solve them. We will soon return to how this helps us, but first we must restrict ourselves to avoid a difficult hurdle.

Recall our example of a drop of oil in water. The switch from a molecular view to a fluid dynamical view presents a new problem: if we do not keep track of every molecule, we instead have to keep track of which points in space contain oil and which contain water. Separating the two materials, there is a boundary surface which can deform over time as the oil drop changes shape. This sounds very complicated. Indeed, drop dynamics is a topic of its own, which this thesis does not intend to cover. Instead, this thesis concerns *rigid particles*.

Rigid bodies

A rigid body in physics is an object whose configuration can be described by the position of one point (usually the center-of-mass) and the rotation of the body around that point. Simply put: it cannot deform. The dynamics of a rigid body is described by Newton's laws. In particular, the center-of-mass motion is described by Newton's second law: the force $\boldsymbol{F}$ on a body equals its mass m times its acceleration $\boldsymbol{a}$,

$$\boldsymbol{F} = m\boldsymbol{a}.$$

While the above equation describes the movement of the position, there is a corresponding law for the rotation. Since this thesis concerns *orientational dynamics* of particles, we need equations also for the rotation of a rigid body. Newton's second law governing rotations says that the torque $\boldsymbol{T}$ on a rigid body equals its moment of inertia $\mathbb{I}$ times its angular acceleration $\boldsymbol{\alpha}$,

$$\boldsymbol{T} = \mathbb{I}\boldsymbol{\alpha}.$$

The two equations above are deceivingly simple-looking, but their solutions contain full knowledge of the motion of a rigid body. I

state the equations here only to draw a conclusion: in order to extract all the information about the motion of a particle, we need to know both the force and the torque acting on the particle at all times.

There are many kinds of forces which can potentially act on a particle. For example there is gravity if the particle is heavy, or magnetic forces if the particle is magnetic. But for now we consider the forces on a particle due to the surrounding fluid, so called hydrodynamic forces. In everyday terms the hydrodynamic force is the drag, as experienced by the spoon you pull through syrup. Uneven drag over a body may also result in a hydrodynamic torque. For instance, turbulent air striking the wings of an aircraft will induce a torque which you feel as a rotational acceleration while the pilot compensates.

Hydrodynamic forces

In order to find out what the force on a particle is, we need to know how the fluid around the particle behaves. And for that, we need to solve the Navier-Stokes equations of fluid dynamics around the particle. What does it mean to "solve" the equations? We imagine the fluid in some environment (we call this "boundary conditions"), for example the air in a cloud. A solution of the equations tells us for example the velocity of the fluid at any given point at any given instant. If we have a solution, we know how to extract the resulting forces and torques on a particle in the fluid.

The problem is that we cannot solve the equations. Not only can we not find solutions as mathematical formulas – in many cases we can not even find numerical solutions using a supercomputer. For example, computing the motion of the air in a cloud is utterly out of reach with the computer resources of today.

I think it is worthwhile to emphasise that some problems are inherently very hard, and cannot be solved by brute force. From time to time I get the question why we struggle with difficult mathematical work, why not just "run it through the computer?" A numerical computer solution is like an experiment: it will give you the numbers for a particular case, but not necessarily any understanding of why. We aim to extract all possible physical un-

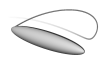

derstanding available from the equations, even if it not possible to solve them in general. It is the understanding of the underlying physics that enables us to simplify the equations until it is practical to solve them. This requires knowledge of which particular details may be neglected, and which details are crucial to keep track of.

And indeed, the meteorologists now have methods of simulating the flows of air in the atmosphere. The trick is to ignore parts of the equation dealing with very small motions, and spend the resources on describing the large eddies of the flow, it is called "Large Eddy Simulations". The game of simplifying without oversimplifying is at the heart of fundamental research.

At any rate, we wish to figure out what the forces on a rigid body in a fluid flow are. By now it is clear that some type of simplification has to be made. The great simplification is embodied in the word *small* in the title of this thesis. The particles we consider are small. But how small is a small particle? The answer I have to give right away is a rather unsatisfactory "it depends". The smallness of the particle has to be relative to something else. This simple principle is formalised by scientists, who discuss smallness in terms of *dimensionless numbers*. Because dimensionless numbers are very common in our work I will spend a few paragraphs to explain the basic idea.

Dimensionless numbers

In principle all physical quantities have some units. For example, the size of a particle has units of "length", and the speed of the particle has units of "length per time", which we write as length/time. Whenever we multiply or divide quantities with dimensions, we also multiply or divide their units. For example dividing the length 20 m with the time 5 s gives the speed 4 m/s. Now suppose we divide the speed 4 m/s with the speed 2 m/s. The result is 2, without any units – they cancelled in the division. The idea is that in order to determine if a quantity x_1 is "small" we have to divide it with another quantity x_2 of the same units. Then if the resulting dimensionless number is smaller than 1, we say that x_1 is small, and implicitly mean *relative to* x_2. This concept seems simple

enough. Let's consider a slightly more complicated example.

Imagine a rubber boat on the sea. There are waves on the sea, rising and falling periodically. The boat speeds along, also rising and falling as it crosses the waves. Now I propose to find a dimensionless number to tell us if the boat is "fast". It has to be fast relative to something else, and the only thing we know of are the waves.

There are two distinct mechanisms at play for the rising and falling of the boat. First, if the boat stays in a fixed position the sea will rise and fall beneath it periodically. Call this period time τ. Second, the boat may cross different waves by travelling over them. Let's call the speed of the boat v, and the distance between different waves on the sea is a length η. In the paragraph above we concluded that we have to divide v with another speed, and check if the dimensionless number is smaller or larger than 1. With the quantities we know of, that is the wave period time τ and the wave distance η, we can form the speed η/τ. We divide the boat speed v with the speed η/τ. The ratio is a number which I will call the *Kubo number*, for reasons I will explain shortly. The Kubo number is defined by

$$\mathrm{Ku} = v\tau/\eta.$$

I will now give a brief interpretation of what it means when Ku is smaller or larger than 1. If $\mathrm{Ku} > 1$, it means that $v\tau > \eta$. The quantity $v\tau$ is a length, more precisely the length that the boat travels during the period time of a wave. Thus, $\mathrm{Ku} > 1$ means that the boat travels more than one wave distance during the period time of a single wave. So when the Kubo number is very large, then the boat travels over many different waves before the wave landscape changes. In this case we may rightly say that the boat is *fast*. On the other hand, if $\mathrm{Ku} < 1$, the boat does not cover the distance between waves in a single wave period time. Before the boat reaches the next wave, the entire wave landscape has changed underneath it.

I made this example of the Kubo number because it is one of the fundamental quantities in Paper C, which is about rotation rates of particles in turbulence. In Paper C a particle plays the

role of the boat, and a turbulent flow plays the role of the waves. As I did here, we describe the limits of very small Ku, and very large Ku. In a real turbulent flow Ku is around 1. That is to say neither of the extremes are true, but in the paper we argue that together they bring some insight into the tumbling of the particles. The use of dimensionless numbers simplifies our work. Instead of considering the effects of all three separate parameters, we can understand the physics by analysing a single dimensionless number.

The dimensionless numbers tell us which physical quantities are important in relation to each other. In the example above, the actual speed of the boat is not important – the speed only matters in relation to the waves. We know that all situations with the same Kubo number are, in some sense, equivalent. This very fact is also what enables engineers to use scale models in wind tunnels. They know that to test a model of a suspension bridge in a wind tunnel, they can not use full-scale wind speeds, but instead a scaled down version of the wind. The dimensionless numbers reveal what scaling is appropriate to match the model bridge to real conditions.

Small particles

We are now equipped to understand what it means for a particle to be *small* in the context of fluid flows. It turns out, for our purposes, that there are two dimensionless numbers that determine whether a particle is small. One has to do with how quickly the particle adjusts to the fluid, the other with how quickly the fluid adjusts to the particle.

The first dimensionless number is the Stokes number, St for short. We can understand it as a comparison of two different time scales. The first is the time it takes for the particle to stop if thrown in an otherwise still fluid. If you throw a stone in air, it takes quite some time for the drag force to stop the stone. But if you try to throw a piece of paper, the drag force overcomes the inertia almost immediately. On the other hand, if you try to throw the stone under water, the time to stop is shorter than in air. We call this time the relaxation time of the particle in the fluid.

The other time is simply how long time it takes for the the fluid velocity to change appreciably. The Stokes number is then defined as

$$\mathrm{St} = \frac{\text{Particle relaxation time}}{\text{Time for fluid velocity change}}.$$

A small Stokes number means that the particle adjusts to the fluid faster than the fluid changes. Such particles stick closely to the flow velocity. Conversely, a large Stokes number means that the fluid changes before the particle has time to adjust, and the particle is relatively unaffected by the fluid velocity. Thus the first meaning of a *small* particle is in the sense that the Stokes number is small, and the particle relaxes to the surrounding drag forces before they change.

The other dimensionless number measuring particle smallness is the particle Reynolds number. It is a measure of how quickly disturbances in the flow settle down. If you stir with a spoon in your cup of tea there is a wake behind the spoon, perhaps even a vortex is created. When you stop stirring, the tea will splash about for a moment and then settle down. The time it takes for a small vortex to settle down is called the viscous time, because it is related to the viscosity of the fluid. Imagine stirring with a spoon in syrup instead of tea, the wake behind the spoon relaxes more quickly in the viscous fluid. But of course it also matters how vigorously you stir, or equivalently, how fast the fluid moves relative to the spoon. To find the particle Reynolds number we compare the viscous time to how fast the spoon, or particle, moves the distance of one particle length:

$$\mathrm{Re}_\mathrm{p} = \frac{\text{Viscous time}}{\text{Time for fluid to flow one particle length}}.$$

A small particle Reynolds number implies that the viscous time is short, and the fluid disturbances we create settle down before the fluid has time to move past the particle. A large particle Reynolds number means that the vortices and disturbances produced by the particle are transported away from the particle, such as the wake and vortices you observe in your cup of tea. A *small* particle

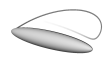

corresponds to small particle Reynolds number, so that there is no wake, and no vortices created by the particle.

Recall the story about the Stokes drag in the very beginning of this thesis. When Stokes in 1851 called a particle "slowly moving", he meant exactly the condition that the particle is small, in the sense just described here.

There is one more dimensionless number we encounter in this thesis. It is the Péclet number. I started this story with a molecular picture of the fluid, and said that the drag force on a particle is the combined result of many molecular collisions. But molecules move in a random fashion, and the number of collisions is not exactly the same all the time. Some times there will be more collisions, and other times there will be fewer collisions. The drag force we have considered thus far is the result of the *average* number of collisions. But if the *variation* around the average number of collisions is large, the randomness of the molecular collisions will induce a degree of randomness also in the force on the particle. The Péclet number measures whether the random fluctations are "large" in this sense:

$$\mathrm{Pe} = \frac{\text{Strength of average (hydrodynamic) force}}{\text{Strength of random force}}.$$

If Pe is large, we may disregard the randomness and consider the hydrodynamic force we discussed above. But if Pe is small, we must expect a degree of randomness in the particle dynamics.

Conclusion

Hopefully we have established enough common language to put the appended research papers in context.

Paper A describes an experiment where we observe the rotation of rod-shaped particles. We try to keep $\mathrm{Re_p} = 0$ and $\mathrm{St} = 0$ ("small" particle), and Pe very large ("low randomness"). The aim is to understand the hydrodynamic force on non-spherical particles.

Paper B is a theoretical study of how the particle rotation changes when we allow for a small value of St (weak particle inertia), but still enforce $\mathrm{Re_p} = 0$ (no fluid inertia). It turns out that there is a

big difference between rod-shaped particles and disk-shaped particles, which is not present when $\mathrm{St} = 0$. As a second part, we also introduce random variations, as measured by the Péclet number. When there is enough noise (small Pe), the difference between rods and disks disappear.

Paper C concerns the speed of rotation of particles in turbulence. Also here we consider small particles: $\mathrm{Re}_\mathrm{p} = 0$ (no fluid inertia) and $\mathrm{St} = 0$ (no particle inertia). It turns out that disk-shaped particles rotate, on average, faster than rod-shaped particles. In the manuscript we make a connection between the particle rotation statistics and the statistics of the turbulent flow.

The presentation in Part II may, or may not, be too technical for the casual reader. But even if, I hope I may encourage an ever so brief look.

At the very least, we have an interpretation of the technical title "Orientational dynamics of small non-spherical particles suspended in fluid flows." The interpretation is that we aim to understand the rotational motion of a non-spherical rigid body immersed in a fluid bath of molecules. We know the forces and torques driving the rotation through the macroscopic description of fluid dynamics. But in order to have a fair chance at progress, we consider the case of very small particles, as characterised by the Stokes and particle Reynolds dimensionless numbers.

2 Prerequisite concepts

In this section I introduce some basic concepts needed to understand the appended research papers.

2.1 Forces on particles in fluids

We are studying the dynamics of small particles suspended in flows. Specifically, we consider particles small enough to not create disturbances in the fluid flow. In such cases, one can consider the fluid flow as a prescribed input, and calculate the response of the particles. What I mean is that the particle does not induce long-lived disturbances in the fluid, which survive to affect the particle at a later time. In order to understand this requirement, and how the particle forces are calculated, we start at the Navier-Stokes equation.

The governing equation for an incompressible, Newtonian fluid is the Navier-Stokes equation

$$\rho_f \left(\frac{\partial}{\partial t} \boldsymbol{u} + \boldsymbol{u} \cdot \nabla \boldsymbol{u} \right) = -\nabla p + \mu \nabla^2 \boldsymbol{u}, \tag{2.1}$$

with the incompressibility condition

$$\nabla \cdot \boldsymbol{u} = 0.$$

Here ρ_f is the density of the fluid, which by the incompressibility condition is assumed to be the same everywhere. The vector field $\boldsymbol{u}(\boldsymbol{x}, t)$ is the fluid velocity, defined at all points in space, and $p(\boldsymbol{x}, t)$ is the scalar pressure field, also defined at all points in space. The parameter μ is the dynamic viscosity of the fluid, which by definition is the relation between stress and strain in a Newtonian fluid. Sometimes we instead use the kinematic viscosity $\nu = \mu/\rho_f$. The definition of a Newtonian fluid is that the viscosity is constant. One commonly used boundary condition to Eq. (2.1) is the no-slip condition, meaning zero relative velocity between the boundary and the fluid.

We will often, especially when discussing the orientational dynamics of particles, encounter the fluid flow gradient $\mathbb{A} = \nabla \boldsymbol{u}^{\mathrm{T}}$, or on component form

$$A_{ij} = \frac{\partial u_i}{\partial x_j}.$$

The incompressibility condition $\nabla \cdot \boldsymbol{u} = 0$ transfers directly to the condition $\mathrm{Tr}\mathbb{A} = 0$.

Throughout this thesis I employ the implicity summation convention for repeated indices. The implied summation is over the number of spatial degrees of freedom, for example

$$A_{ii} = \sum_{i=1}^{d} A_{ii} = \mathrm{Tr}\mathbb{A}.$$

The gradient $\mathbb{A}$ is often split into its symmetric and anti-symmetric parts such that

$$\mathbb{O} = \frac{1}{2}(\mathbb{A} - \mathbb{A}^{\mathrm{T}}), \quad \mathbb{S} = \frac{1}{2}(\mathbb{A} + \mathbb{A}^{\mathrm{T}}), \quad \mathbb{A} = \mathbb{O} + \mathbb{S}.$$

The symmetric part $\mathbb{S}$ is called the rate-of-strain tensor, and it contains the local rate of deformation of the flow. The anti-symmetric part $\mathbb{O}$ is related to the vorticity vector. The vorticity vector $\boldsymbol{\omega}_f$ of a flow $\boldsymbol{u}$ is defined by $\boldsymbol{\omega}_f = \nabla \times \boldsymbol{u}$. The matrix $\mathbb{O}$ is related to the vorticity vector $\boldsymbol{\omega}_f$, because for any given vector $\boldsymbol{x}$

$$\mathbb{O}\boldsymbol{x} = \frac{1}{2}\boldsymbol{\omega}_f \times \boldsymbol{x} \equiv \boldsymbol{\Omega} \times \boldsymbol{x}. \tag{2.2}$$

The vector $\boldsymbol{\Omega}$, defined as half the vorticity, is a common quantitiy in our calculations, and therefore is given its own symbol. Expressed in index notation the elements of $\mathbb{O}$ are related to $\boldsymbol{\Omega}$ by $O_{ij} = -\varepsilon_{ijp}\Omega_p$. Here and in this thesis ε denotes the anti-symmetric third-order tensor

$$\varepsilon_{ijk} = \begin{cases} +1 & \text{if } (i,j,k) \text{ is a cyclic permutation of } (1,2,3), \\ -1 & \text{if } (i,j,k) \text{ is a cyclic permutation of } (3,2,1), \\ 0 & \text{if two indices are equal.} \end{cases}$$

The stress tensor $\mathbb{T}$ of a fluid is a symmetric second order tensor defined at each point in space. Its elements T_{ij} are defined as the i:th component of the force on a surface with (outward pointing) normal in the j:th direction. That is, if a surface has outward normal $\boldsymbol{n}$, the force $\boldsymbol{f}$ per unit area is

$$\boldsymbol{f} = \mathbb{T}\boldsymbol{n}.$$

Due to this interpretation, the diagonal elements of $\mathbb{T}$ are called normal stresses, and the off-diagonal elements shear stresses. For an incompressible and Newtonian fluid the stress tensor is

$$\mathbb{T} = -p\mathbb{I} + 2\mu\mathbb{S},$$

where $\mathbb{I}$ denotes the identity tensor. This relation is not a result, as much as part of the definition of Newtonian fluids. The relation is in fact used in the derivation of the Navier-Stokes equation (2.1) [18].

There are two steps to compute the force on a particle suspended in the fluid. First one has to solve the Navier-Stokes equation, with the particle as a boundary. Then one must integrate the resulting stress tensor over the entire particle surface. The Navier-Stokes equation (2.1) contains non-linear terms, and does not, in general, admit an analytical solution. We may understand that the problem is very hard just by imagining a particle in a fluid: as the particle moves and rotates, it stirs up a wake and vortices in its trail. These disturbances may linger and affect the particle at a later time. It seems that we are, in general, obliged to take into account the whole joint history of the particle and the fluid to predict the final state of the two.

But if the particle is sufficiently small, the disturbances will be smeared out by the viscous forces before they make any secondary impact. The condition is precisely that the particle Reynolds number is small. As stated in Sec. 1.1,

$$\mathrm{Re_p} = \frac{\text{Viscous time}}{\text{Time for fluid to flow one particle length}}.$$

More specifically,

$$\mathrm{Re_p} = \frac{u_0 a}{\nu},$$

where u_0 is a typical flow speed relative to the particle surface, a is the size of the particle and ν is the kinematic viscosity of the fluid. In the extreme case when $\mathrm{Re}_\mathrm{p} = 0$, the Navier-Stokes equation (2.1) reduces to the linear steady Stokes equation [15, 18]

$$\mu \nabla^2 \boldsymbol{u} = \nabla p.$$

This type of flow condition is called viscous flow, or creeping flow. Because the governing equation is linear, many more problems admit analytical solutions. In particular, the force and torque on a particle in viscous flow has been worked out in quite some detail. The formalism of resistance tensors was introduced by Brenner [14, 19], but here I follow the notation used in the book *Microhydrodynamics* by Kim & Karrila [15].

The fundamental result is that the force and torque on a particle suspended in a flow is linearly related to the undisturbed flow. Given the particle velocity $\boldsymbol{v}$ and angular velocity $\boldsymbol{\omega}$, we write the force $\boldsymbol{F}$ and torque $\boldsymbol{T}$ as

$$\begin{aligned} \boldsymbol{F} &= \mathscr{A}(\boldsymbol{u} - \boldsymbol{v}) + \mathscr{B}(\boldsymbol{\Omega} - \boldsymbol{\omega}), \\ \boldsymbol{T} &= \mathscr{B}^{\mathrm{T}}(\boldsymbol{u} - \boldsymbol{v}) + \mathscr{C}(\boldsymbol{\Omega} - \boldsymbol{\omega}) + \mathscr{H} : \mathbb{S}. \end{aligned} \tag{2.3}$$

The resistance tensors $\mathscr{A}$, $\mathscr{B}$, $\mathscr{C}$ and $\mathscr{H}$ depend only upon particle shape, and can be computed once and for all. The tensor $\mathscr{H}$ of is third order, and the double dot product $\mathscr{H} : \mathbb{S}$ is a contraction over two indices. In index notation it reads $(\mathscr{H} : \mathbb{S})_i = H_{ijk} S_{jk}$.

The resistance tensors in the case of a sphere of radius a are $\mathscr{A} = 6\pi\mu a \mathbb{I}$, $\mathscr{B} = \mathscr{H} = 0$ and $\mathscr{C} = 8\pi\mu a^3 \mathbb{I}$. In fact, for any particle which is mirror-symmetric in all three cartesian planes it holds that $\mathscr{B} = 0$. In such cases there is neither coupling between rotation and force, nor between translation and torque. An example of the contrary is a cork-screw-shaped particle. For such particles one can exploit the coupling between rotation and translation to sort left-handed screws from right-handed screws [20, 21]. Sorting particles by handedness, or *chirality*, is important in for example pharmacological chemistry. However, this thesis concerns particles with shapes such that the orientational dynamics decouple from the translational motion.

For non-spherical particles there is a hidden complication in Eq. (2.3): the flow is usually known in a fixed frame of reference, but the resistance tensors are known in the frame of reference of the particle. Expressing the resistance tensors in the fixed frame of reference entails a rotation dependent on the particle orientation. Thus, the torque is in general a non-linear function of particle orientation.

The hydrodynamic resistance of an ellipsoid was computed in a now famous paper by Jeffery in 1922 [13]. The result therein is of course not expressed in the subsequently invented tensor notation, but all the necessary calculations are there. The adaptation to current notation is found in *Microhydrodynamics* (Ref. 15 p. 56). All calculations in this thesis, and the appended papers, proceed from forces and torques obtained in this manner. Therefore the assumption of $\mathrm{Re}_\mathrm{p} = 0$ is implicit everywhere, even if not explicitly stated.

When the force and torque on a particle are known, its trajectory is determined by Newton's equations of motion for a rigid body. Since the torque may depend non-linearly upon particle orientation, solving the rigid-body equations is in general not possible. The first approximation, introduced already by Jeffery in 1922, is the over-damped limit where particle inertia is neglected. The resulting equation of motion is discussed in Sec. 2.3, but first we will discuss the anatomy of the simple shear flow in Sec. 2.2.

2.2 Simple shear flow

The simple shear flow is a uni-directional linear flow which varies magnitude in only one transversal direction. It is shown in Fig. 2.2. The equation describing the shear flow is simply,

$$\boldsymbol{u}(y) = s\, y\, \hat{\boldsymbol{x}}.$$

Here s is a scalar called the shear strength, and y is the coordinate along the $\hat{\boldsymbol{y}}$-axis. Fig. 2.1 shows the coordinate system we use for shear flows in this thesis and in the appended papers. The three principal directions are the flow direction $\hat{\boldsymbol{x}}$, the shear direction $\hat{\boldsymbol{y}}$

and the vorticity direction $\hat{\boldsymbol{z}}$. The vorticity direction $\hat{\boldsymbol{z}}$ is also the direction of $\boldsymbol{\Omega}$ introduced in Sec. 2.1.

The flow gradient of the simple shear flow is constant and given by

$$\mathbb{A} = \begin{bmatrix} 0 & s & 0 \\ 0 & 0 & 0 \\ 0 & 0 & 0 \end{bmatrix}.$$

The shear flow is important for two reasons. First, it is one of the fundamental flows in rheology, the study of fluids. It is the flow inside a Couette device, used for example to measure viscosity. Second, as far as particle dynamics go, the simple shear flow is relevant for *any* flow with parallel streamlines. Consider for example the flow of a suspension through a pipe. The pipe is assumed to be large compared to the suspended particles, and the flow profile is most likely a complicated function of position y in the pipe cross section[1]:

$$\boldsymbol{u}(y) = f(y)\hat{\boldsymbol{x}},$$

and the flow gradient is

$$\mathbb{A} = \begin{bmatrix} 0 & f'(y) & 0 \\ 0 & 0 & 0 \\ 0 & 0 & 0 \end{bmatrix}.$$

Thus, if the flow profile f varies slowly over the particle size, the particle experiences a simple shear flow of strength $f'(y)$. This is exactly the case in the experiment described in Paper A (see Section 3).

Curiously, the dynamics of non-spherical particles in simple shear flow offers a rich variety of behaviours. There is no stationary state, but a particle tumbles end-to-end indefinitely. If the particle is axisymmetric, the tumbling is periodic. The technical details and explanations of this are discussed in Sec. 2.3, but we

[1] In principle the function should also depend on the position in the z-direction. In that case the result is also a simple shear flow, although rotated.

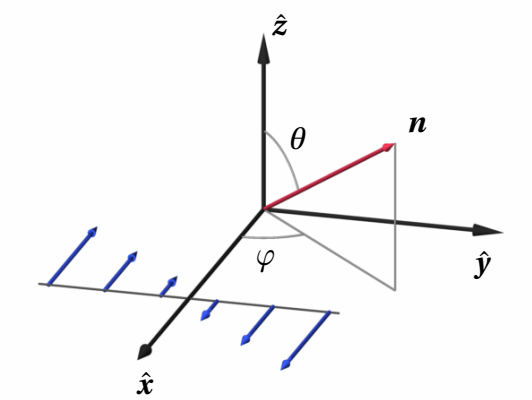

Figure 2.1: Coordinate system of simple shear flow in this thesis. The same system is used in Papers A & B. The directions are the flow direction $\hat{\boldsymbol{x}}$, the shear direction $\hat{\boldsymbol{y}}$, and the vorticity direction $\hat{\boldsymbol{z}}$. The angles (θ, φ) are the spherical coordinates of the particle direction vector $\boldsymbol{n}$.

can understand the underlying reason from the composition of the shear flow. Fig. 2.2 illustrates schematically how the shear is a superposition of two flows. One is a pure rotation, corresponding to the antisymmetric part $\mathbb{O}$ of the flow gradient. The other is a pure strain, the symmetric part $\mathbb{S}$ of the flow gradient. Now imagine a rod-shaped particle in these flows. The pure rotation, the vorticity, will rotate the rod with a constant angular velocity, regardless of the rod's orientation. The strain, on the other hand, has a preferred direction to which it will attract the long axis of the rod. Sometimes the vorticity and strain will cooperate to turn the rod onto the strain eigendirection, and sometimes the vorticity will struggle to rotate the rod out of the attracting direction. The result is that the rod will always rotate, but sometimes faster and sometimes slower. When the difference between the fast and the slow rotations is large, we perceive this as intermittent tumbling.

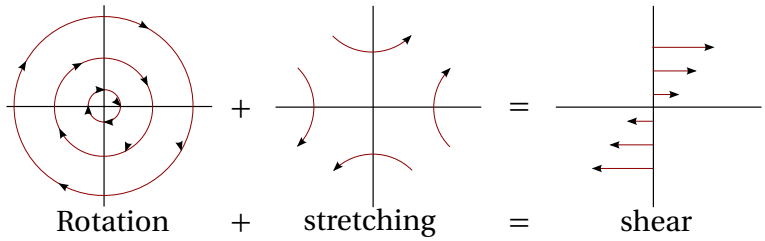

Figure 2.2: Decomposition of the simple shear flow into rotation and strain.

2.3 The Jeffery equation and its solutions

In this section we consider axisymmetric particles: particles which are rotationally symmetric around an axis of symmetry. For such particles the orientational configuration may be represented by a unit vector $\boldsymbol{n}$, attached to the axis of symmetry. As alluded to in Sec. 2.1, Jeffery presents two major results in his seminal paper from 1922 [13]. First, he calculates the hydrodynamic torque on a ellipsoid, not necessarily axisymmetric, in any linear flow. Second, he derives the equation of motion of an inertia-free, axisymmetric ellipsoid (a spheroid). This equation of motion is often referred to as the Jeffery equation. In our notation the Jeffery equation is

$$\dot{\boldsymbol{n}} = \mathbb{O}\boldsymbol{n} + \Lambda\left(\mathbb{S}\boldsymbol{n} - \boldsymbol{n}\boldsymbol{n}^{\mathrm{T}}\mathbb{S}\boldsymbol{n}\right). \tag{2.4}$$

Here $\mathbb{O}$ and $\mathbb{S}$ are the anti-symmetric and symmetric parts of the fluid gradient, as introduced in Sec. 2.1. The parameter Λ is a particle shape factor. For a spheroid of aspect ratio λ the shape factor is

$$\Lambda = \frac{\lambda^2 - 1}{\lambda^2 + 1}.$$

For most conceivable particle shapes, $-1 < \Lambda < 1$. Negative Λ correspond to flat, disk-shaped particles, while positive Λ correspond to elongated, rod-like particles. It was shown by Bretherton [22] that, given the correct shape factor Λ, Jeffery's equation is valid not only for spheroids, but for any axisymmetric particle. He also

showed that there are extreme cases where $|\Lambda| > 1$. In this thesis we consider particles with $|\Lambda| < 1$, like the spheroid.

The equation of motion for an inertia-free particle is given by force and torque balance on the particle. Then the center-of-mass velocity equals the fluid velocity at the center-of-mass position, a condition called *advection*. Jeffery's equation is the rotational analogue of center-of-mass advection. In Paper B, we demonstrate how to derive Jeffery's equation. We start from the hydrodynamic torque and Newton's equation of motion, and take the limit $\mathrm{St} \to 0$. See also Appendix A and the discussion in Section 3 for the generalisation to non-axisymmetric particles. In the following, we will instead consider the possible solutions of the Jeffery equation (2.4).

Jeffery's equation is a non-linear vector equation, and as such it is seemingly hard to solve. However, the non-linearity is only apparent: it is due to the geometric constraint that $\boldsymbol{n}$ is a unit vector. The underlying dynamics is in fact linear. I will now explain two ways to understand this fact.

The vorticity $\mathbb{O}$ rotates $\boldsymbol{n}$, and the strain $\mathbb{S}$ aligns and stretches $\boldsymbol{n}$ towards its strongest eigendirection. The non-linear term $\boldsymbol{n}\boldsymbol{n}^{\mathrm{T}}\mathbb{S}\boldsymbol{n}$ is simply the stretching component of the strain, which is subtracted in order to prevent elongation of $\boldsymbol{n}$. Bretherton (Sec. 6 in Ref. [22]) realised that we may instead model the orientation of the particle with any vector $\boldsymbol{q}$ which obeys the same linear terms, but without compensating for any elongation:

$$\dot{\boldsymbol{q}} = \big(\mathbb{O} + \Lambda\mathbb{S}\big)\boldsymbol{q}. \tag{2.5}$$

Owing to the common linear terms in Eq. (2.4) and Eq. (2.5), the vector $\boldsymbol{q}$ will have the same angular dynamics as $\boldsymbol{n}$. In addition, $\boldsymbol{q}$ may be stretched and compressed by the strain $\mathbb{S}$. But since we are only interested in the angular degrees of freedom, we can at any instant recover $\boldsymbol{n}$ by normalising $\boldsymbol{q}$ to unit length. Thus, the general solution of the Jeffery equation is given by solving Eq. (2.5) for $\boldsymbol{q}(t)$, then the solution to Eq. (2.4) is given by normalising $\boldsymbol{q}(t)$ to unit length:

$$\boldsymbol{n}(t) = \frac{\boldsymbol{q}(t)}{|\boldsymbol{q}(t)|}. \tag{2.6}$$

Another, more mathematical, way of understanding how the linear companion equation (2.5) arises is the following. Like above, we choose to represent the particle orientation by a vector $\boldsymbol{q}$ which is parallel to $\boldsymbol{n}$. Define $\boldsymbol{q} = \alpha(t)\boldsymbol{n}$, with $\alpha(t)$ an arbitrary function of time. We know from this definition that we may always recover $\boldsymbol{n}$ by normalising $\boldsymbol{q}$ to unit length. Now, we can calculate the equation of motion for $\boldsymbol{q}$:

$$\begin{aligned}\frac{\mathrm{d}\boldsymbol{q}}{\mathrm{d}t} &= \frac{\mathrm{d}}{\mathrm{d}t}(\alpha\boldsymbol{n}) \\ &= \dot{\alpha}\boldsymbol{n} + \alpha\dot{\boldsymbol{n}} \\ &= \dot{\alpha}\boldsymbol{n} + \alpha\left(\mathbb{O}\boldsymbol{n} + \Lambda\left(\mathbb{S}\boldsymbol{n} - \boldsymbol{n}\boldsymbol{n}^{\mathrm{T}}\mathbb{S}\boldsymbol{n}\right)\right). \end{aligned} \tag{2.7}$$

But $\alpha(t)$ is an arbitrary function which we may choose. In particular we can choose $\alpha(t)$ to be a function satisfying

$$\dot{\alpha} = \alpha\Lambda\boldsymbol{n}^{\mathrm{T}}\mathbb{S}\boldsymbol{n}.$$

By inserting this choice of $\alpha(t)$ into Eq. (2.7), we again arrive at Eq. (2.5).

We will now consider the solutions of Jeffery's equation in time-independent flows. This case includes for example the simple shear flow, and indeed any linear flow. It is also a useful model when the flow changes only slowly in time, compared to the time it takes for the gradients to affect the particle orientation. First, I will describe the possible solutions of Eq. (2.4) in linear flows. This picture is vital in understanding our argument in Paper C (see also Section 5 in this thesis). Second, I will discuss the solutions of Jeffery's equation in a simple shear flow. The solutions are called the Jeffery orbits, and they play an important role in both Paper A and B.

When $\mathbb{O}$ and $\mathbb{S}$ are time-independent the linear companion equation (2.5) is solved by the matrix exponential:

$$\boldsymbol{q}(t) = e^{(\mathbb{O}+\Lambda\mathbb{S})t}\boldsymbol{q}(0).$$

This solution implies that the long-time dynamics of $\boldsymbol{q}$, and therefore $\boldsymbol{n}$, is determined by the eigenvalues and eigenvectors of the matrix $\mathbb{B} = \mathbb{O} + \Lambda\mathbb{S}$. For an incompressible flow $\mathrm{Tr}\mathbb{B} = 0$, because

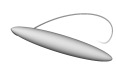

$\mathrm{Tr}\mathbb{A} = 0$. In three spatial dimensions, the three eigenvalues of $\mathbb{B}$ must sum to zero. Thus, as noted by Bretherton [22], there are three distinct possibilities for the eigensystem of $\mathbb{B}$:

1. Three real eigenvalues, then

   $\boldsymbol{q}$ will align with the eigenvector corresponding to the largest eigenvalue.

2. One real eigenvalue $a > 0$, and a complex pair $-a/2 \pm i\omega$, then

   $\boldsymbol{q}$ will spiral into alignment with the eigenvector corresponding to the real eigenvalue.

3. One real eigenvalue $a \leq 0$, and a complex pair $-a/2 \pm i\omega$, then

   $\boldsymbol{q}$ will spiral out and finally rotate in the plane spanned by the real and imaginary parts of the complex eigenvector.

The characteristic equation for the eigenvalues b of a 3×3-matrix $\mathbb{B}$ is

$$-b^3 + b^2\mathrm{Tr}\mathbb{B} + \frac{b}{2}\left(\mathrm{Tr}\mathbb{B}^2 - (\mathrm{Tr}\mathbb{B})^2\right) + \det\mathbb{B} = 0.$$

But for a traceless matrix $\mathrm{Tr}\mathbb{B} = 0$ and $\det\mathbb{B} = \mathrm{Tr}\mathbb{B}^3/3$, because

$$\mathrm{Tr}\mathbb{B} = b_1 + b_2 + b_3 = 0 \implies b_3 = -(b_1 + b_2),$$

therefore

$$\begin{aligned}\mathrm{Tr}\mathbb{B}^3 &= b_1^3 + b_2^3 + b_3^3 = -3(b_1^2 b_2 + b_1 b_2^2),\\ \det\mathbb{B} &= b_1 b_2 b_3 = -(b_1^2 b_2 + b_1 b_2^2).\end{aligned}$$

Thus the characteristic equation simplifies to

$$-b^3 + \frac{b}{2}\mathrm{Tr}\mathbb{B}^2 + \frac{1}{3}\mathrm{Tr}\mathbb{B}^3 = 0. \tag{2.8}$$

It is possible to solve Eq. (2.8) exactly for the eigenvalues, but the important observation is that they are determined by only two

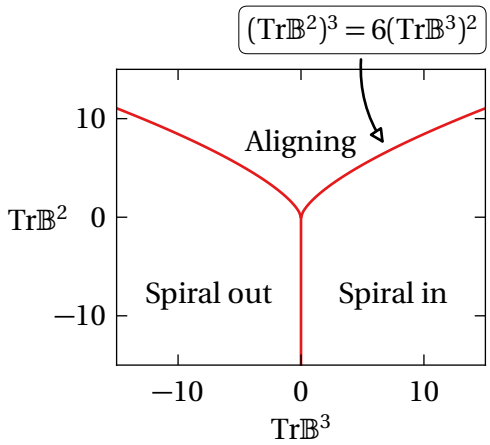

Figure 2.3: Map of the three possible types of particle motion, as determined by the eigensystem of $\mathbb{B} = \mathbb{O} + \Lambda\mathbb{S}$.

parameters: $\mathrm{Tr}\mathbb{B}^2$ and $\mathrm{Tr}\mathbb{B}^3$. In Fig. 2.3 I illustrate how the three cases outlined above correspond to different values of $\mathrm{Tr}\mathbb{B}^2$ and $\mathrm{Tr}\mathbb{B}^3$. The boundary curve of the region of three real eigenvalues is where the discriminant Δ of the characteristic equation is zero:

$$\Delta = \left(\mathrm{Tr}\mathbb{B}^2\right)^3 - 6\left(\mathrm{Tr}\mathbb{B}^3\right)^2 = 0.$$

In the region where there is a pair of complex eigenvalues, the two cases of spiral in or out are separated by $\mathrm{Tr}\mathbb{B}^3 = 0$. Now, what follows is one of the key observations in our argument in Paper C. For any given flow gradient, changing the particle from rod-like to disk-shaped (or vice versa) transforms $\mathrm{Tr}\mathbb{B}^3 \rightarrow -\mathrm{Tr}\mathbb{B}^3$ and therefore change the qualitative dynamics from aligning to rotating (or vice versa). This transformation may be understood because

$$\mathrm{Tr}\mathbb{B}^3 = 3\Lambda\mathrm{Tr}\mathbb{O}\mathbb{O}\mathbb{S} + \Lambda^3\mathrm{Tr}\mathbb{S}\mathbb{S}\mathbb{S}.$$

The other combinations of $\mathbb{S}$ and $\mathbb{O}$ which could be expected to contribute, such as $\mathrm{Tr}\mathbb{O}\mathbb{O}\mathbb{O}$, vanish identically because of symmetries of $\mathbb{O}$ and $\mathbb{S}$. As explained above, changing a particle from

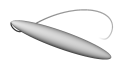

rod-like to disk-shaped implies a change of sign of the shape factor Λ. The implications of this observation for the tumbling of particles in turbulent and random flows are further discussed in Sec. 5 in Part II, and in Paper C.

The remainder of this section concerns the case of simple shear flow. This case is characterised by $\mathrm{Tr}\mathbb{B}^3 = 0$ and $\mathrm{Tr}\mathbb{B}^2 < 0$. The simple shear has a special position among flows, and we understand the significance of the condition $\mathrm{Tr}\mathbb{B}^3 = 0$ from the above discussion. First, a change of particle shape does not change the qualitative dynamics. Both disk-shaped particles and rod-like particles rotate in a shear flow. Second, $\mathbb{B}$ has a zero eigenvalue, as seen from the characteristic equation (2.8). The zero eigenvalue is important, because it implies that the particle dynamics never forgets its initial condition. The eigenvector of the zero eigenvalue is the vorticity direction[2], thus the component of $\boldsymbol{q}$ in the vorticity direction is constant in a shear flow. The other two eigenvalues are an imaginary pair, resulting in a periodic rotation of $\boldsymbol{q}$.

In summary, the dynamics of $\boldsymbol{q}$ in a simple shear flow is a periodic rotation in a plane. The plane is normal to the vorticity direction, and determined by the initial condition of $\boldsymbol{q}$.

When the trajectories $\boldsymbol{q}(t)$ are projected onto the unit sphere, the result $\boldsymbol{n}(t)$ are the Jeffery orbits. I visualise this in Fig. 2.4 where the trajectories $\boldsymbol{q}(t)$ and $\boldsymbol{n}(t)$ are shown for three different initial conditions.

The solutions to Jeffery's equation in a simple shear flow are degenerate: the orientational trajectory depends on the initial condition indefinitely. In many realistic situations this long-time memory hardly seems plausible. The degeneracy is a result of the assumptions made in the course deriving the Jeffery orbits. Each assumption corresponds to a physical mechanism, and in order to understand how the degenaracy may be broken these mechanisms must be investigated. The three assumptions we believe most important to investigate are the following.

First, the particle may not be axisymmetric. In this case the dynamics is more complicated, but still depends on the initial

[2] See Fig. 2.1 and Sec. 2.2 for the definition of the coordinate system and the terminology of its directions in a simple shear flow.

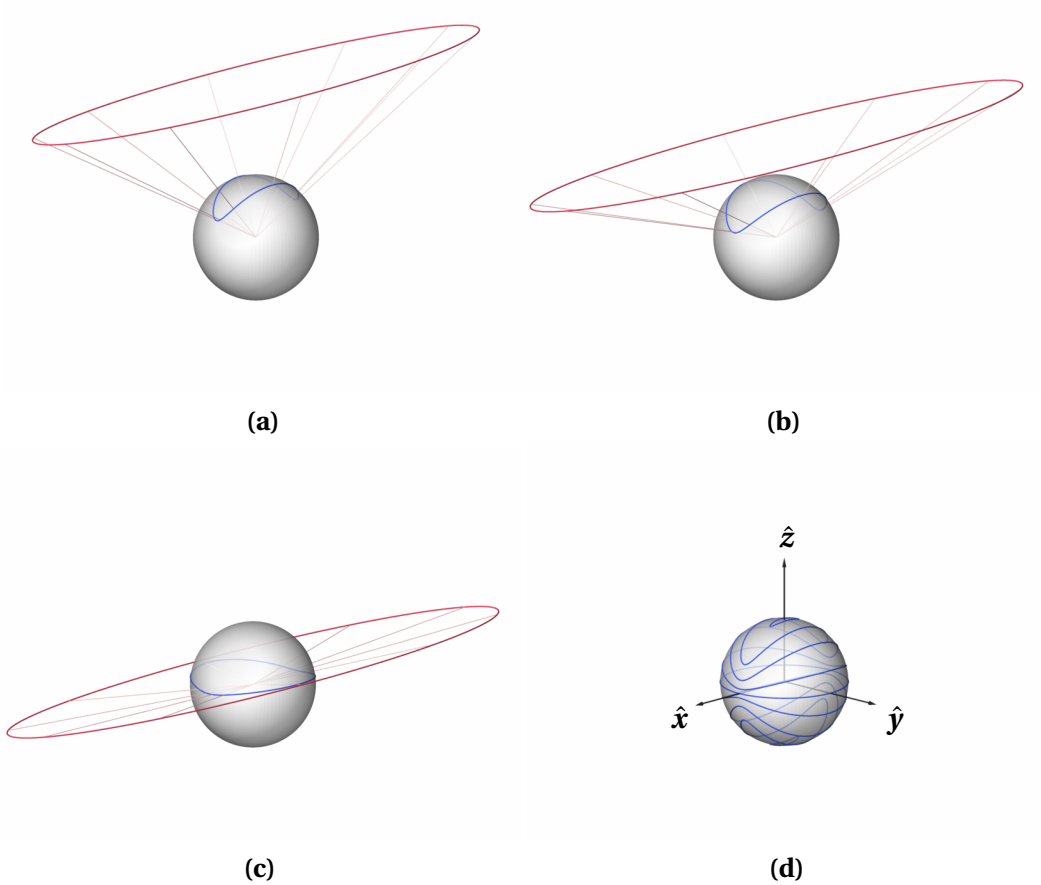

Figure 2.4: (a-c) Illustrations of how the trajectories $\boldsymbol{q}(t)$ (red) produces the Jeffery orbits $\boldsymbol{n}(t)$ (blue) upon projection onto the unit sphere. **(d)** Sample of resulting Jeffery orbits with coordinate system. All trajectories correspond to a particle of aspect ratio $\lambda = 5$ in a simple shear flow.

conditions indefinitely. Triaxial particles are discussed further in relation to Paper A in Sec. 3.

Second, there may be inertial effects. Fluid inertia was neglected when we used the resistance tensor formulation (2.3) for the torque on a particle. Particle inertia was neglected when Newton's equation reduced to Jeffery's equation in the advective limit $\mathrm{St} \to 0$. In Paper B we describe how the effects of a small amount of particle inertia break the degeneracy of the solutions $\boldsymbol{n}(t)$. See the discussion in Section 4 for an outlook on the case of fluid inertia.

Finally, the third mechanism is Brownian noise. The idea is that thermal fluctuations kick the particle out of one Jeffery orbit and into another. After some time, the initial condition is forgotten and the state of the particle is described by an orientational probability distribution. The problem of computing the orientational distribution has a long history, and in the next Section I briefly review some of the methods and results.

2.4 Orientational distributions

In this Section we consider the orientational dynamics of an axisymmetric particle, represented by the vector $\boldsymbol{n}$. In this case the orientational distribution is a function $P(\boldsymbol{n}, t)$ which describes the probability of observing the particle with orientation[3] $\boldsymbol{n}$ at time t. Instead of asking for the orientational trajectory $\boldsymbol{n}(t)$ of a particle given the initial condition $\boldsymbol{n}(0)$, we now ask what the orientational distribution $P(\boldsymbol{n}, t)$ is, given the initial condition $P(\boldsymbol{n}, 0)$.

The by far most common approach is to consider a diffusion equation for the unit vector $\boldsymbol{n}$. My view of the diffusion approximation is the following. The orientation of the particle is driven by very many, very small and very fast kicks. In the case of particles in fluids, the small kicks originate in the bombardment of fluid molecules onto the particle surface. These *microscopic* kicks are so small and fast that we never see them directly. But after a short time, enough kicks have accumulated into an observable

[3] Strictly, $P(\boldsymbol{n}, t)\mathrm{d}S$ is the probability to find $\boldsymbol{n}$ on the surface element $\mathrm{d}S$ at time t.

change. If we reset the particle orientation and start over, the microscopic kicks will again accumulate into an observable change. But because the molecular bombardment is not exactly the same every time, the accumulated change is different every time. The "diffusion approximation" is to not consider all the details of the random kicks, but to only consider the *mean value* and *variance* of the accumulated changes. The idea is to replace the complicated accumulation of microscopic kicks with randomly chosen changes. The randomly chosen steps will have the correct mean value and variance, but all other details are neglected. The idea is based mathematically in the "Central Limit Theorem" of statistics, stating that if you add many random numbers the sum will converge to be normally distributed (under certain conditions). For a complete and very readable account of the method I point to the book *Stochastic Processes in Physics and Chemistry*, by van Kampen [23].

The governing equation for the orientational distribution of an axisymmetric particle in the diffusion approximation is the Fokker-Planck equation

$$\frac{\partial}{\partial t}P(\boldsymbol{n},t) = -\frac{\partial}{\partial \boldsymbol{n}}\left[\boldsymbol{J}(\boldsymbol{n},t)P(\boldsymbol{n},t)\right] + \mathscr{D}\frac{\partial^2}{\partial \boldsymbol{n}^2}P(\boldsymbol{n},t). \tag{2.9}$$

The first term on the right hand side is referred to as the drift, and the second as the diffusion. The drift is due to the deterministic fluid flow, and $\boldsymbol{J}(\boldsymbol{n},t)$ represents the right hand side of the Jeffery equation (2.4). The diffusion term is due to the random kicks, and $\mathscr{D}$ is the rotational diffusion constant. Since $\boldsymbol{n}$ is a unit vector, the Fokker-Planck equation is defined on the unit sphere. Therefore the derivative with respect to $\boldsymbol{n}$ is defined as $\partial/\partial_{\boldsymbol{n}} = (\mathbb{I} - \boldsymbol{n}\boldsymbol{n}^{\mathrm{T}})\nabla$, with ∇ the usual gradient in $\mathbb{R}^3$. In Appendix B I explain this in more detail, and present a full derivation of Eq. (2.9).

For the purposes of this thesis, and more specifically Paper B, we consider the case when a particle is suspended in a simple shear flow, and at the same time is subject to Brownian noise. As mentioned in the Section 2.3, the solutions to Jeffery's equation in a simple shear flow are degenerate. The orientational distribution of $\boldsymbol{n}$ under the influence of, for example, thermal noise has been extensively studied, as a means of explaining how particles in

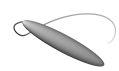

shear "forget" their initial conditions. A thorough review is given in [14], and what follows is a brief summary.

The dynamics is governed by a single dimensionless parameter, the Péclet number $\mathrm{Pe} = s/\mathscr{D}$. Here $\mathscr{D}$ is the diffusion constant in Eq. (2.9), and s is the shear strength, or the strength of the drift term in Eq. (2.9). A small value of Pe means that the noise is strong, and vice versa.

For small Pe, when the noise dominates, the orientational distribution is uniform – all orientations are equally likely. When the noise is decreased, the orientational distribution begins to reflect the Jeffery orbits. As Pe becomes larger and the shear grows increasingly important, the probability of seeing a particle aligned with the flow direction increases. But surprisingly, when Pe becomes large enough, the stationary orientational distribution converges and becomes *independent of* Pe. In other words, when the noise is small enough, the particles follow the Jeffery orbits, but every now and then jump to a different orbit.

The stationary orientational distribution in general depends on the value of Pe and the particle aspect ratio λ. In order to quantify the above discussion, I show numerical solutions[4] for the stationary average $\langle \sin^2\theta \rangle$ in Fig. 2.5. The angle θ is the polar angle of $\boldsymbol{n}$, such that $n_z = \cos\theta$. It is also the angle to the vorticity direction, see Fig. 2.1.

For small Pe we see that $\langle \sin^2\theta \rangle = 2/3$, the expected value for a uniformly random distribution. But for large Pe, the average reaches a plateau, depending on particle aspect ratio λ. The asymptotic solutions of Eq. (2.9) described in [14] are shown as dotted lines. In particular, Hinch & Leal [24] solved the case of weak noise, that is large Pe. They obtained an expression for the height of the plateau valid for thin particles, $\lambda \gg 1$. The numerical solution confirms their prediction.

In Paper B we compute the same orientational average, $\langle \sin^2\theta \rangle$, when the particle has a small but finite mass, as characterised by the Stokes number.

[4] The details of how I solve Eq. (2.9) numerically can be found in Appendix C.

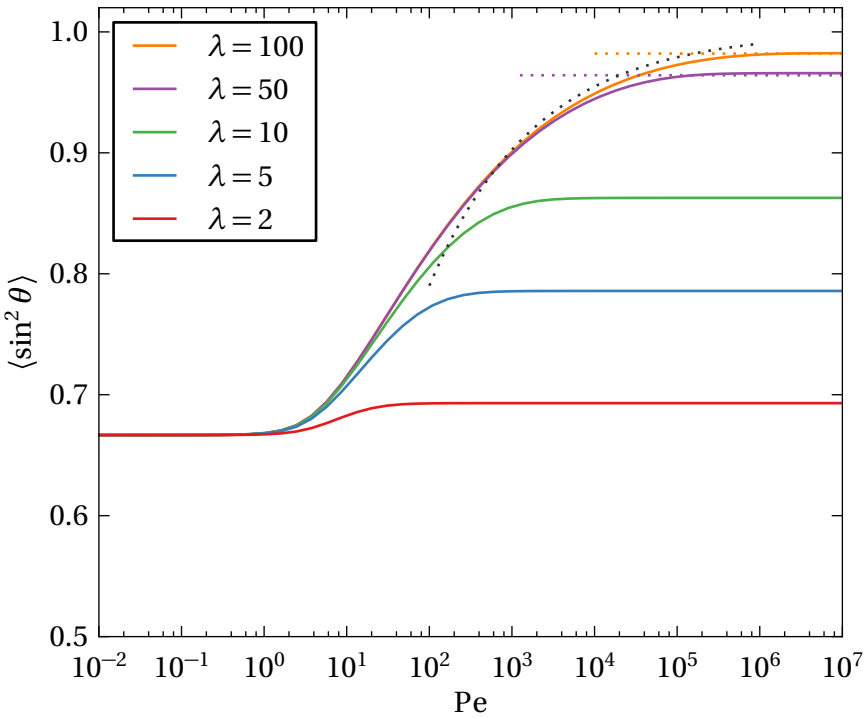

Figure 2.5: Stationary average $\langle \sin^2 \theta \rangle$ for an axisymmetric particle in a shear flow subject to random noise, shown as function of the Péclet number $\mathrm{Pe} = s/\mathscr{D}$ for different values of the particle aspect ratio λ. Larger Pe corresponds to less noise. Solid lines are numerical solutions. Dotted lines show asymptotes in regimes of weak and intermediate noise, given by Eqs. (9.5) and (9.13a) with (9.15) in [14].

PART II
PRESENT WORK

The following Sections describe the research that I have performed with my collegues and collaborators over the last two and a half years. The material is organised according to different "projects", or questions. Sections 3-5 roughly correspond to the Papers A–C.

3 Experimental observation of single particle orientational dynamics

In a collaborative project with the group of Dag Hanstorp (Gothenburg university) we developed an experimental setup for observing the orientational dynamics of single particles. The aim is to understand which mechanisms that are crucial to include in a description of the particle dynamics. By quantitatively measuring the trajectories of individual particles, we aim to narrow down the possible choices of mechanisms driving the particle dynamics. The project has thus far resulted in Paper A of this thesis[1], which describes observations of both periodic and aperiodic tumbling of rod-shaped particles. At the time of this writing a round of refined experiments are ongoing, and a publication describing the corresponding results is planned.

3.1 Overview & setup

Since we want to study the orientational dynamics of single particles, our ideal physical system is a fluid flow, with one small,

[1] A description of the experimental setup and some preliminary results were published in a conference proceeding not included in this thesis, see Ref. [25].

Figure 3.1: Photograph of a microchannel of the type used in our experiment. The channel is molded in a block of PDMS plastic. In the picture the channel is filled with dye. To the left and right are inlet/outlet tubes. The channel is ca 5 cm long.

suspended particle. In particular, we would like the following features:

- A known fluid flow, which does not change in time as the particle moves.
- A known particle geometry, so that the hydrodynamic force can be calculated.
- Small particles, in the sense that $\mathrm{St} \ll 1$ and $\mathrm{Re_p} \ll 1$.
- But not too small particles, in the sense that $\mathrm{Pe} \gg 1$.

We realise this system in a tiny rectangular pipe, a microfluidic channel. Its cross-section is $0.2\,\mathrm{mm} \times 2.5\,\mathrm{mm}$ and it is manufactured by molding plastic in a precision machined metal mold. The channel is made several centimeters long, and in each end a thin teflon tube is connected as inlet or outlet. A photograph of a channel is shown in Fig. 3.1. The fluid consists of a mix of glycerol and water, and it is pumped through the channel with a syringe. The channel is mounted in a microscope equipped with a video camera, which in turn is connected to a computer that stores the image sequences.

The particles are plastic rods produced by stretching epoxy glue as it hardens. The rods measure around 20-40 μm in length and

1-2 μm in thickness. When we calculate the Stokes and particle Reynolds numbers for a rod in our experiment, we find that $\mathrm{St} \approx 10^{-6}$ and $\mathrm{Re_p} \approx 10^{-5}$, which qualifies the rod as a small particle. We also compute the rotational Peclét number and find that $\mathrm{Pe} \approx 10^4$. Thus we realise the condition of small, but not too small particles.

The more complicated features on our wish list are the fluid flow, and the particle geometry. By designing the channel to be wide and shallow we can consider the fluid flow as known. How is discussed in detail in Paper A. In contrast, the exact shape of the particles remains unknown. As mentioned above, the particles are roughly rod-shaped, with a length ten times longer than its diameter. In a microscope we can easily see features of about 10 μm, but it cannot resolve anything much smaller than 1 μm. Resolving such small scales may seem unnecessary, but can in fact make all the difference. The observation of the effects of these small asymmetries is the main point of Paper A. In the next section I will extend the discussion of this point a bit further than what is published in the paper.

3.2 Results & discussion

In Paper A we suggest, without much elaboration, that the data shown in Fig. 8 of the paper correspond to chaotic tumbling of triaxial particles. In this section I want to explain our reasons for this suggestion.

The main results presented in Paper A are the trajectories of $\boldsymbol{n}$ shown in Figs. 6 through 8 in the paper. Recall that $\boldsymbol{n}$ is a unit vector pointing along the axis of symmetry of the rod. From the recorded image sequences we extract $\boldsymbol{n}$ as function of time[2]. For an axisymmetric rod, the two degrees of freedom contained in $\boldsymbol{n}$ fully determines the orientation of the rod. A third degree of freedom not contained in $\boldsymbol{n}$ is the rotation around the symmetry axis of the rod. Clearly, also an axisymmetric rod may rotate around its

[2]Actually, we extract $\boldsymbol{n}(d)$, where d is the distance advected along the streamline. As shown in the paper this corresponds to time t when writing down for instance Jeffery's equation. This technical detail is of no importance to the present discussion.

symmetry axis, but this *rolling rotation* makes no physical difference. But in the case of an asymmetric rod the rolling is physically relevant, and a description of the orientational dynamics must contain all three rotational degrees of freedom. In our experiment we can not resolve the rolling rotation, so in order to analyse the effects of asymmetry we have to figure out what its signature is in the observable $\boldsymbol{n}$. In the following paragraphs I explain how the signature shows up in the trajectories of n_z, shown in panels (c) in all figures in Paper A.

For the purpose of this discussion we treat the rod as an ellipsoid. An ellipsoid has three perpendicular axes, and the vector $\boldsymbol{n}$ is attached to one of them. We introduce the third degree of freedom by an additional unit vector $\boldsymbol{p}$, attached to another of the ellipsoid axes, perpendicular to $\boldsymbol{n}$. The geometry of the ellipsoid is characterised by two aspect ratios. The aspect ratio λ is associated with the axis in the direction of $\boldsymbol{n}$, like in the paper. We denote the second aspect ratio κ, it is associated with the axis in the direction of $\boldsymbol{p}$.

In the case of axisymmetric particles, the Jeffery equation of motion for $\boldsymbol{n}$ is derived from a torque balance. In the same way we derive an equation of motion for $\boldsymbol{n}$ and $\boldsymbol{p}$ in the case of a triaxial ellipsoid. The details of this calculation are found in Appendix A. The equations of motion are

$$\begin{aligned}
\frac{\mathrm{d}\boldsymbol{n}}{\mathrm{d}t} &= \mathbb{O}\boldsymbol{n} + \frac{\lambda^2-1}{\lambda^2+1}\big(\mathbb{S}\boldsymbol{n} - \boldsymbol{n}^{\mathrm{T}}\mathbb{S}\boldsymbol{n})\boldsymbol{n}\big) + \frac{2\lambda^2(1-\kappa^2)}{(\lambda^2+\kappa^2)(\lambda^2+1)}(\boldsymbol{n}^{\mathrm{T}}\mathbb{S}\boldsymbol{p})\boldsymbol{p}, \\
\frac{\mathrm{d}\boldsymbol{p}}{\mathrm{d}t} &= \mathbb{O}\boldsymbol{p} + \frac{\kappa^2-1}{\kappa^2+1}\big(\mathbb{S}\boldsymbol{p} - \boldsymbol{p}^{\mathrm{T}}\mathbb{S}\boldsymbol{p})\boldsymbol{p}\big) + \frac{2\kappa^2(1-\lambda^2)}{(\kappa^2+\lambda^2)(\kappa^2+1)}(\boldsymbol{n}^{\mathrm{T}}\mathbb{S}\boldsymbol{p})\boldsymbol{n}.
\end{aligned} \tag{3.1}$$

Here, as in the introduction, $\mathbb{S}$ and $\mathbb{O}$ are the symmetric and antisymmetric parts of the flow gradient,

$$\mathbb{O} = \frac{1}{2}(\mathbb{A} - \mathbb{A}^{\mathrm{T}}), \quad \mathbb{S} = \frac{1}{2}(\mathbb{A} + \mathbb{A}^{\mathrm{T}}), \quad \mathbb{A} = \nabla\boldsymbol{u} = \mathbb{O} + \mathbb{S}.$$

We note the similarity between the equations for $\boldsymbol{n}$ and $\boldsymbol{p}$ in Eq. (3.1). Exchanging the aspect ratios $\lambda \longleftrightarrow \kappa$ and the meaning of $\boldsymbol{n} \longleftrightarrow \boldsymbol{p}$, must result in the same equations – it is the same

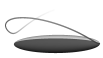

particle. Secondly, we see that the complicated coupling between $\boldsymbol{n}$ and $\boldsymbol{p}$ occurs through the strain $\mathbb{S}$. The vorticity $\mathbb{O}$ generates a simple solid-body rotation.

In absence of any constraint, the action of the strain matrix $\mathbb{S}$ is to collapse both $\boldsymbol{n}$ and $\boldsymbol{p}$ onto its primary eigendirection. But the rigidity of the particle prevents this, and instead a rotation is induced. Exactly which rotation is determined by the particle shape: the strain has more influence on an elongated axis. This is especially clear in the special case where the axis in the direction of $\boldsymbol{p}$ is not elongated at all, that is the axisymmetric case $\kappa = 1$. Then

$$\begin{aligned}\frac{\mathrm{d}\boldsymbol{n}}{\mathrm{d}t} &= \mathbb{O}\boldsymbol{n} + \frac{\lambda^2-1}{\lambda^2+1}\left(\mathbb{S}\boldsymbol{n} - \boldsymbol{n}^{\mathrm{T}}\mathbb{S}\boldsymbol{n})\boldsymbol{n}\right)\\ \frac{\mathrm{d}\boldsymbol{p}}{\mathrm{d}t} &= \mathbb{O}\boldsymbol{p} - \frac{\lambda^2-1}{\lambda^2+1}(\boldsymbol{n}^{\mathrm{T}}\mathbb{S}\boldsymbol{p})\boldsymbol{n}.\end{aligned} \tag{3.2}$$

In this case we recognise the Jeffery equation for $\boldsymbol{n}$, without any coupling to $\boldsymbol{p}$. But the equation for $\boldsymbol{p}$ is coupled to $\boldsymbol{n}$. In addition to the simple rotation of the vorticity, the action of the strain on $\boldsymbol{n}$ dictates the motion of $\boldsymbol{p}$ through the rigidity condition. As soon as an asymmetry, that is $\kappa \neq 1$, is introduced, our observable quantity $\boldsymbol{n}$ will be influenced by $\boldsymbol{p}$.

We now move on to discuss the solutions of Eq. (3.1) in simple shear flows. For the axisymmetric case, Eq. (3.2) admits analytical solutions for $\boldsymbol{n}$. The solutions, described in Section 2.3, are the periodic Jeffery orbits. Two important characteristics of the Jeffery orbits are

1. they describe monotonous tumbling, the vector $\boldsymbol{n}$ always rotates around the vorticity vector with positive angular velocity,

2. the orbits are periodic, the particle always returns to its initial condition after one period time.

The general triaxial case does not allow any closed form solution, and generally the solutions are not periodic. Depending on initial condition the solution may be periodic, quasi-periodic or chaotic

[26, 27]. However, as discovered by Hinch and Leal [26], the property of monotonous tumbling still holds. That is, the vector $\boldsymbol{n}$ will rotate around the vorticity vector with a positive angular velocity. This allows us to reduce the dimensionality of the problem with a Poincaré surface-of-section. In practise this means that we only look at the trajectories as they pass through a plane of our choice. If we choose a plane containing the vorticity vector $\boldsymbol{\Omega}$, the monotonous tumbling guarantees that the trajectory always returns to the surface-of-section.

We choose as surface-of-section the plane $n_x = 0$, which is when the rod is perpendicular to the flow direction. In the surface-of-section we choose the coordinates (ψ, n_z).

The coordinate n_z is the cosine of the angle between $\boldsymbol{n}$ and $\boldsymbol{\Omega}$. It is the same n_z shown in the results of the experiment. For an axisymmetric rod n_z is interpreted as the Jeffery orbit. In the time series $n_z(t)$, the moments where $n_x = 0$ correspond exactly to the peak height of the oscillation. The n_z-coordinate in the surface-of-section is therefore a quantity easily read from the experimentally observed time series.

The coordinate ψ is the angle of rolling rotation. As explained above the rolling rotation is not an observable in our experiment.

By numerical solution of Eq. (3.1) we construct a plot of the Poincaré map by choosing an initial condition and computing a long time series. At each crossing of the surface-of-section, we plot a point at (ψ, n_z).

The Poincaré map for an axisymmetric rod with aspect ratio $\lambda = 10$ and $\kappa = 1$ is shown in Fig. 3.2. It consists of only horizontal lines, each corresponding to a constant value of n_z. In other words each line corresponds to a different Jeffery orbit. Each line is actually a torus (or a circle) since the angle ψ is periodic. The dynamics is confined to stay on the torus on which it begins. Also shown in Fig. 3.2 are examples of trajectories. The successive markers on the surface-of-section correspond in the lower panel to what the experimentally observed time series $n_z(t)$ would look like.

In general the particle does *not* return to exactly its initial position in (ψ, n_z)-space. The dynamics proceeds in jumps of $\Delta\psi$,

and the trajectory is periodic if and only if $\pi/\Delta\psi$ is rational. Nevertheless, if we disregard the rolling rotation, the dynamics does appear periodic in n_z.

In Fig. 3.3 we show the corresponding Poincaré map for a slightly asymmetric rod. Here $\lambda = 10$ as before, but $\kappa = 1.1$, that is a 10 % asymmetry. In the experiment this small amount of asymmetry corresponds to about 200 nm asymmetry in the particle cross-section. The effect of the asymmetry is to bend or destroy the tori. Most tori survive, but in a deformed state. Others are are broken up into a chaotic region, seen as a continuum of unordered dots in the surface-of-section. When the dynamics begins on a torus, it confined to that torus, like before. But if started in the chaotic region, it may, and will eventually, visit all parts of the chaotic region.

The picture is further distorted when we turn the asymmetry up to 20 %, as shown in Fig. 3.4. Here the chaotic region has grown, and more tori have broken up. But it is still true that trajectories which started on a torus, are confined to that torus. In the examples of $n_z(t)$ given in Figs. 3.2-3.4 the dynamics on the torus shows up as a quasi-periodic variation. The trajectory started in the chaotic region results in a chaotic variation in $n_z(t)$.

In Paper A it is rather briefly suggested (p. 12) that the data corresponds to chaotic tumbling of a triaxial particle. I have here explained the reasons for making this suggestion. The data presented in Paper A is consistent with the trajectories in the surface-of-section, given an asymmetry of 10-30 %. We see regular motion, corresponding to the tori, but also chaotic motion. The tori close to $n_z = 0$ are the first to break up, and are very rarely observed, while tori close to $n_z = 1$ are more common.

3.3 Outlook

A complicating factor in our analysis is that each experimentally recorded trajectory corresponds to a different particle, and therefore to a different surface-of-section. Removing this problem was a main aim in the design the current iteration of the experiment.

The idea is to use a laser, an optical tweezer, to control the initial

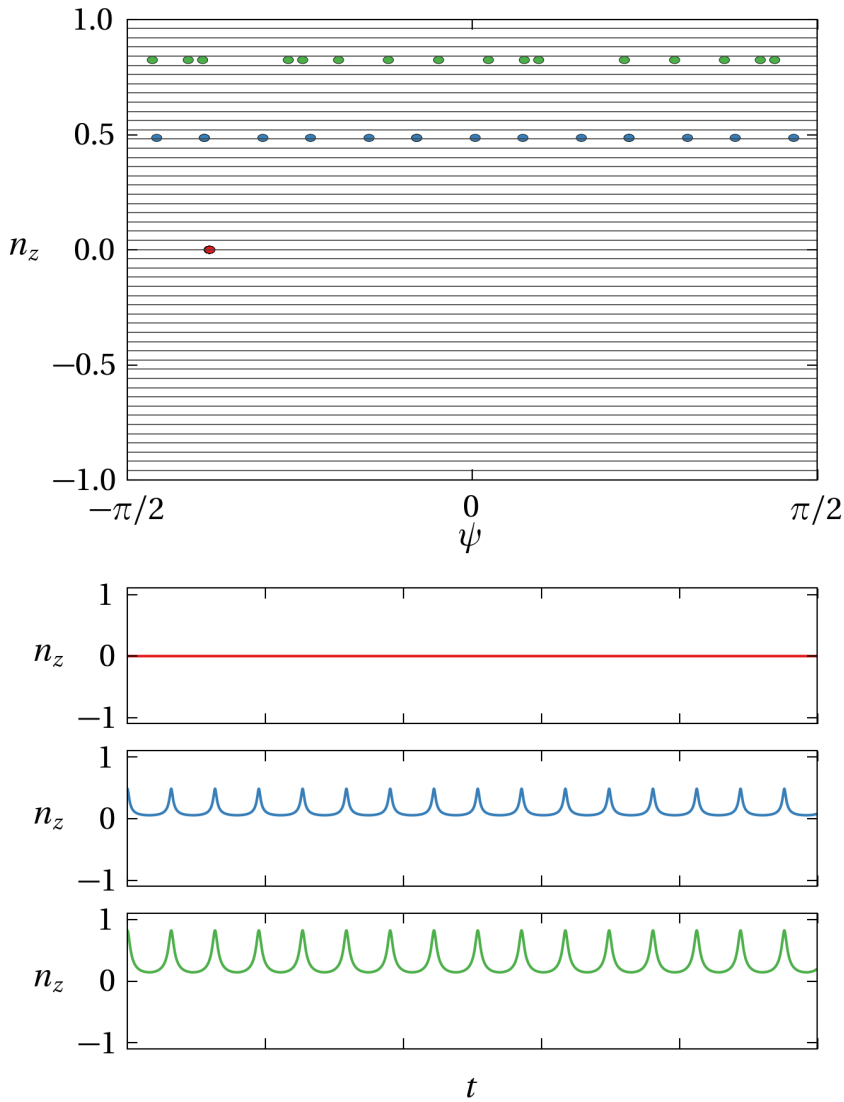

Figure 3.2: Top: Poincaré surface-of-section of an axisymmetric particle with aspect ratios $\lambda = 10$, $\kappa = 1$. Bottom: Examples of what $n_z(t)$ looks like, given the trajectory indicated by the color coded markers on the surface-of-section. Surface-of-section image made by Anton Johansson, reproduced under a CC-BY license.

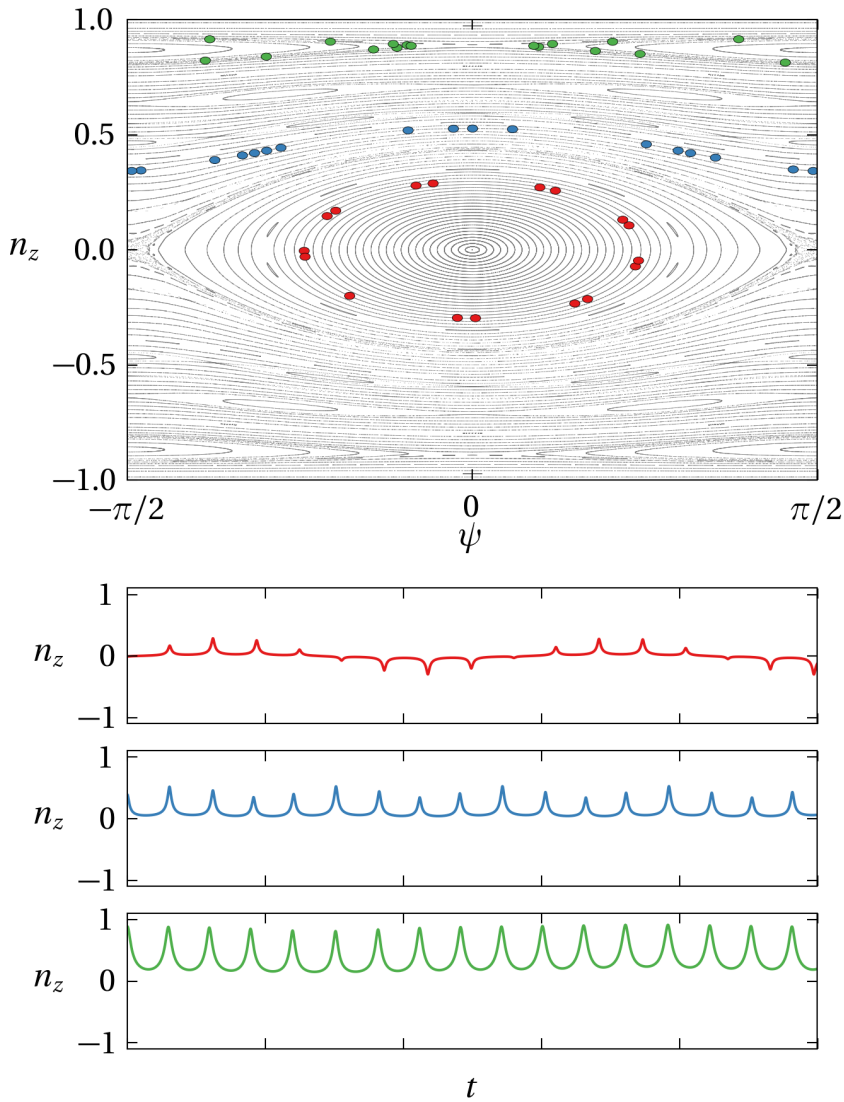

Figure 3.3: Top: Poincaré surface-of-section of an asymmetric particle with aspect ratios $\lambda = 10$, $\kappa = 1.1$. Bottom: Examples of what $n_z(t)$ looks like, given the trajectory indicated by the color coded markers on the surface-of-section. Surface-of-section image made by Anton Johansson, reproduced under a CC-BY license.

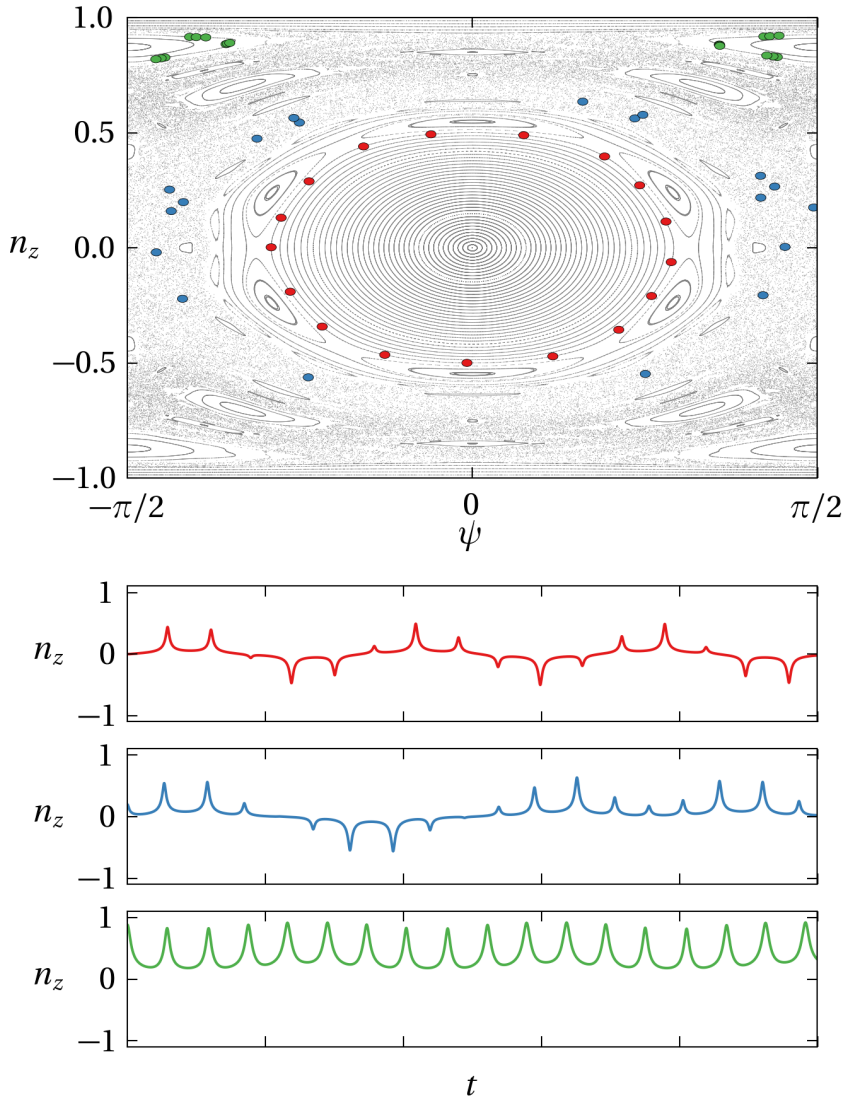

Figure 3.4: Top: Poincaré surface-of-section of an axisymmetric particle with aspect ratios $\lambda = 10$, $\kappa = 1.3$. Bottom: Examples of what $n_z(t)$ looks like, given the trajectory indicated by the color coded markers on the surface-of-section. Surface-of-section image made by Anton Johansson, reproduced under a CC-BY license.

condition n_z of a rod. After observing the trajectory of a tumbling particle, the laser is used to capture the very same particle again. The particle is brought back to its starting position and reset with a new initial condition. By repeating this procedure we want to map out which tori are bent, and which are unaffected. This work is underway by M.Sc. students Staffan Ankardal & Alexander Laas.

Another important question is to consider the alternative mechanisms that could affect the particle dynamics. The effect of thermal noise has been studied by many authors for the case of axisymmetric particles. A little bit of noise invalidates the rule that a trajectory is confined to its tori, in the case of axisymmetric particle this means a Jeffery orbit. Instead there is an orientational distribution over different tori.

But the corresponding question arises also for non-axisymmetric particles. A little bit of noise allows for transport between tori, and we expect an orientational distribution to exist.

Finally, for larger triaxial particles both fluid and particle inertia contribute to the dynamics. In Paper B (see Section 4) we compute the first effects of particle inertia ($\mathrm{St} > 0$) on the dynamics of an axisymmetric particle. The corresponding calculation for a triaxial particle remains as an open question. Fluid inertia ($\mathrm{Re_p} > 0$) is more difficult, even in the case of axisymmetric particles (see Section 4.2).

4 Effects of particle and fluid inertia

This project is a collaboration with Jean-Régis Angilella at the University of Caen, in France. Our aim is to understand the effects of inertia on the particle dynamics.

4.1 Overview

The simplest approach to modeling small particles, as measured by the Stokes and particle Reynolds numbers, is to simply let $\mathrm{St} = 0$ and $\mathrm{Re_p} = 0$. Clearly there is no real physical system which fulfills this condition strictly. However, it may be very close, as for example in the experiment we describe in Paper A. It is therefore natural to ask the question what happens when St and $\mathrm{Re_p}$ are small, but not strictly equal to zero.

In Paper B we treat the case of $\mathrm{St} > 0$, but $\mathrm{Re_p} = 0$. As explained in the paper this case corresponds to particles of larger density than the surrounding fluid. Paper B is self-contained and rather detailed, so I will not repeat any technical detail here. The main results are, first, a modification of the Jeffery equation, that takes into account small values of the Stokes number. Second, we employ the new equation of motion to compute the stationary orientational distribution of weakly inertial particles under the influence of noise.

The effect of inertia, however small, is particularly interesting for particles in a simple shear flow. When $\mathrm{St} = 0$, Jeffery's equation predicts that the orientational trajectory is periodic and always return to the initial orientation. But when $\mathrm{St} > 0$, there is instead a drift so that all trajectories, regardless of initial condition, will converge onto the same final orbit. This has previously been shown by Lundell in numerical simulation [28]. For the case of almost spherical particles, the orbit drift was computed by Subramanian and Koch [29]. Our equation of motion confirms and extends these results to arbitrary axisymmetric particle shapes.

We then show how the new equation of motion enables us to compute the orientational distribution of weakly inertial particles under the additional influence of noise. This calculation would be

rather difficult without the new equation of motion. The point is that the noise and particle inertia are two different physical effects which independently break the degeneracy of the Jeffery orbits.

Noise tends to scatter particle orientations, creating a stationary orientational distribution. As explained in Section 2.4, for weak noise the orientational distribution converges and becomes independent of the noise strength. On the other hand, in absence of noise the particle inertia drives particles into a final orbit. Moreover, the final orbit is different for rod-shaped particles and disk-shaped particles. Therefore we expect a qualitative difference when inertial effects compete with noise. We quantify this competition between inertia and noise in Figs. 4 and 5 in the paper. The results may also be compared to Fig. 2.5 in this thesis (p. 33).

Finally, as a technical note, in order to compute the orientational distribution we numerically solve a Fokker-Planck equation on the unit sphere. The equation is Eq. (2.9) in Section 2.4, but with $\boldsymbol{J}(\boldsymbol{n}, t)$ corresponding to the new equation of motion. The numerical approximation is calculated by rewriting the equation with quantum mechanical angular momentum operators, and expanding the solution in spherical harmonics. I include the details of this calculation as Appendix C to this thesis, and it is also an Appendix of Paper B.

4.2 Outlook

The case of $\mathrm{St} > 0$ but $\mathrm{Re_p} = 0$ is only valid for small particles, with much larger density than the surrounding fluid. One example are aerosols. A natural next step is to consider also $\mathrm{Re_p} > 0$, which is a relevant case for our experiment. I think it is fair to say that treating a non-zero Stokes number is the simpler task, compared to non-zero particle Reynolds number. A finite St means that we do perturbation theory on Newton's equations of motion, while a finite $\mathrm{Re_p}$ entails perturbation theory of the Navier-Stokes equation.

But there exists methods to perform this calculation. Subramanian and Koch [29, 30] calculated the orbit drift due to finite

particle and fluid inertia for two special cases: nearly spherical particles and very elongated rods. The curious outcome is that the drift is opposite in the two cases, suggesting that there is a transition somewhere inbetween. An interesting proposition is to compute the existence and stability of periodic orbits, for a general axisymmetric particle.

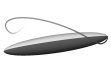

5 Tumbling in turbulent flows

Together with Kristian Gustavsson we investigate the orientational dynamics of small particles in random and turbulent flows. Kristian is an expert on particle dynamics in random flows. In the previous Sections, describing Papers A & B, we considered only steady and uniform fluid flows. In this project we combine our knowledge of random and turbulent flows with that of the dynamics of non-spherical particles. The collaboration has thus far resulted in Paper C (in review).

5.1 Overview

The dynamics of turbulent flow is fundamentally complicated. It is non-linear and chaotic, and reliable numerical solutions are computationally very expensive. One of the motivations for studying random flows is that, with properly chosen statistics, they may be a model system for understanding the dynamics of particles in turbulence.

This idea works well for quantities which are not crucially dependent on the specifics of turbulence. For example, one of Kristian's results concerns the relative collision velocities of particles [31]. Through a random flow model he worked out properties universal to colliding particles in any flow. In other cases, however, it turns out that the particle dynamics depends on details of the turbulent flow which are not present in the random flow.

A random flow with a single length scale is characterised by the Kubo number $\mathrm{Ku} = u_0\tau/\eta$, where u_0 is a typical flow speed, τ a typical correlation time, and η a typical correlation length. For a basic explanation of the Kubo number, see Section 1.1 (p. 6). A small Kubo number corresponds to a rapidly fluctuating flow, with the limit $\mathrm{Ku} \to 0$ representing the white-noise limit. Large Kubo numbers correspond to steady flows.

When Parsa et. al. published numerical (DNS) and experimental results on the rotation rates of non-spherical particles in turbulence [17], they highlighted a case where the random flow predicts a qualitatively different result from the observation in

turbulence. They showed that disk-shaped particles rotate, on average, about twice as fast as rod-shaped particles in turbulence. The naive prediction from a random-flow model is that disks and rods rotate alike. The questions we try to answer in Paper C are, which mechanisms are responsible for the differences in particle rotation rates? How do the statistics of the flow relate to the statistics of the particles?

It is a well-known fact that the distribution of velocity gradients in turbulent flow is strongly skewed [32, 33]. We argue in Paper C that there is a relation between the skewed distribution of velocity gradients and the differing tumbling rates of disks and rods. The broken symmetry means that some flow configurations are more likely than others. We use Jeffery's equation of motion for axisymmetric particles to argue how this asymmetry propagates to the particle rotation.

As I explained in Section 2.3 about *steady flows*, the orientational dynamics of a particle switches from rotation to alignment when one replaces a rod with a disk, or vice versa. Therefore, if rods and disks are to tumble alike on average, we must require that particles experience equal amounts of "rotating" gradients and "aligning" gradients – otherwise the result will be different if we switch the particle type. In other words, the distribution of flow gradients $\mathbb{A}$ must be symmetric in $\mathrm{Tr}\mathbb{A} \to -\mathrm{Tr}\mathbb{A}^{\mathrm{T}}$, in particular over the line $\mathrm{Tr}\mathbb{A}^3 = 0$ (see[1] Fig. 2.3 in Section 2.3.) This symmetry does not exist in turbulence.

However, this argument does not close the case, because it is only true for *steady* flow ($\mathrm{Ku} \to \infty$), and turbulence is absolutely not steady. The more technical part of the paper is a calculation valid at the other extreme: $\mathrm{Ku} \ll 1$, or very unsteady flows, more so than turbulence. As shown in the paper, the calculation reinforces the picture outlined above.

It turns out that the first contribution to the rotation rate which is different for rods and disks comes from the third-order correlation functions of the flow velocity gradients. Specifically, the correlation function $\langle \mathbb{O}(0)\mathbb{O}(0)\mathbb{S}(-t)\rangle$ makes a strong contribution. Here, as throughout this thesis, $\mathbb{O}$ and $\mathbb{S}$ are the antisymmetric

[1] Recall, $\mathbb{B} = \mathbb{O} + \Lambda\mathbb{S}$, but $\mathbb{B} \to \mathbb{A}$ $(-\mathbb{A}^{\mathrm{T}})$ as the particle shape $\Lambda \to 1$ (-1).

and symmetric parts of the Lagrangian[2] flow gradient matrix. The interpretation is that flow regions where there is first stretching flow ($\mathbb{S}$) and then high vorticity ($\mathbb{O}^2$) makes disks rotate, but rods align.

The manuscript is necessarily brief on some technical details, and in the following I elaborate on two of them. First, I show how to arrive at Eq. (4) starting from Eq. (3) in the manuscript. Second, I give some detail on how we collected and verified Lagrangian statistics in a turbulent flow, along with some more data we did not find space for in the paper.

5.2 Derivation of the result Eq. (4)

In order to derive the final result, we need to establish some facts about Lagrangian correlation functions in isotropic and incompressible flow. We denote the matrix of flow gradients by

$$\mathbb{A}(\boldsymbol{r}(t),t)=\nabla \boldsymbol{u}(\boldsymbol{r}(t),t),$$

or in component notation

$$A_{ij}(\boldsymbol{r}(t),t)=\frac{\partial}{\partial r_j}u_i(\boldsymbol{r}(t),t).$$

The correlation functions between elements of a matrix $\mathbb{A}$ are denoted

$$C^{AA}_{ijkl}(t_1)\equiv\left\langle A_{ij}(\boldsymbol{r}(0),0)A_{kl}(\boldsymbol{r}(t_1),t_1)\right\rangle,$$
$$C^{AAA}_{ijklmn}(t_1,t_2)\equiv\left\langle A_{ij}(\boldsymbol{r}(0),0)A_{kl}(\boldsymbol{r}(t_1),t_1)A_{mn}(\boldsymbol{r}(t_2),t_2)\right\rangle,$$

and so on. From now on we use the shorthand $\mathbb{A}_t\equiv\mathbb{A}(\boldsymbol{r}(t),t)$. Note that we assume that the flow is statistically stationary, in the sense that the correlation between two matrix elements only depends on the time difference t_1, not on the particular value of t (here chosen to be 0). We separate the gradient into its symmetric and antisymmetric parts,

$$\mathbb{O}=\frac{1}{2}(\mathbb{A}-\mathbb{A}^{\mathrm{T}}),\quad \mathbb{S}=\frac{1}{2}(\mathbb{A}+\mathbb{A}^{\mathrm{T}}),\quad \mathbb{A}=\mathbb{O}+\mathbb{S}.$$

[2] Along a particle trajectory; as experienced by the particle.

It turns out that all the second-order and third-order correlation functions between $\mathbb{S}$ and $\mathbb{O}$ factorise in a very convenient manner. Appendix D contains the details of this factorisation and the final expressions. All the correlation functions become products of one time-dependent function, and one part which depends only on the spatial indices, but not time. For example, in three spatial dimensions

$$\begin{aligned} C^{OO}_{ijkl}(t) &= \frac{\left\langle \mathrm{Tr}\mathbb{O}_0\mathbb{O}_t \right\rangle}{6}(\delta_{il}\delta_{jk}-\delta_{ik}\delta_{jl}), \\ C^{SS}_{ijkl}(t) &= \frac{\left\langle \mathrm{Tr}\mathbb{S}_0\mathbb{S}_t \right\rangle}{30}(3\delta_{il}\delta_{jk}+3\delta_{ik}\delta_{jl}-2\delta_{ij}\delta_{kl}), \\ C^{SO}_{ijkl}(t) &= 0. \end{aligned} \tag{5.1}$$

Here $\left\langle \mathrm{Tr}\mathbb{O}_0\mathbb{O}_t \right\rangle$ and $\left\langle \mathrm{Tr}\mathbb{S}_0\mathbb{S}_t \right\rangle$ are flow-specific functions of time. They can be determined through a flow model, measurement, or, as in our case, numerical DNS data. See the Section 5.3 for details.

Similar, but lengthier, results exist for the eight three-point correlations $C^{SSS}_{ijklmn}(t)$, $C^{SSO}_{ijklmn}(t)$, ..., $C^{OOO}_{ijklmn}(t)$ (see Appendix D.)

Now we are equipped for the derivation. The dimensionless equation of motion for the particle position $\boldsymbol{r}$ and orientation $\boldsymbol{n}$ reads

$$\dot{\boldsymbol{r}} = \mathrm{Ku}\,\boldsymbol{u}\,, \quad \dot{\boldsymbol{n}} = \mathrm{Ku}\big[\mathbb{O}\boldsymbol{n} + \Lambda\big(\mathbb{S}\boldsymbol{n} - (\boldsymbol{n}^{\mathrm{T}}\mathbb{S}\boldsymbol{n})\boldsymbol{n}\big)\big]\,. \tag{5.2}$$

Here, Λ is the particle shape function, $\Lambda = -1$ for disks, and $\Lambda = 1$ for rods. The equation for $\boldsymbol{r}$ comes only implicitly into the equation for $\boldsymbol{n}$, through the dependence of $\mathbb{O}$ and $\mathbb{S}$ upon particle position.

We consider an ensemble of particles, found in the flow at a distant past time $t = 0$ with initial condition $\boldsymbol{n}_0$. Then we compute the ensemble average of the squared rotation rate $\langle \dot{n}^2 \rangle$ at a much later time t. In the calculation we will eventually take $t \to \infty$. The

average rotation rate squared is

$$\begin{aligned}\langle \dot{n}^2 \rangle &= \mathrm{Ku}^2 \left\langle \left(\mathbb{O}_t \boldsymbol{n}_t + \Lambda \left(\mathbb{S}_t \boldsymbol{n}_t - (\boldsymbol{n}_t^{\mathrm{T}} \mathbb{S}_t \boldsymbol{n}_t) \boldsymbol{n}_t \right) \right)^2 \right\rangle \\ &= \mathrm{Ku}^2 \big[- \left\langle \boldsymbol{n}_t^{\mathrm{T}} \mathbb{O}_t \mathbb{O}_t \boldsymbol{n}_t \right\rangle \\ &\qquad + \Lambda \left\langle \boldsymbol{n}_t^{\mathrm{T}} (\mathbb{S}_t \mathbb{O}_t - \mathbb{O}_t \mathbb{S}_t) \boldsymbol{n}_t \right\rangle \\ &\qquad + \Lambda^2 \left\langle \boldsymbol{n}_t^{\mathrm{T}} \mathbb{S}_t \mathbb{S}_t \boldsymbol{n}_t \right\rangle \\ &\qquad - \Lambda^2 \left\langle (\boldsymbol{n}_t^{\mathrm{T}} \mathbb{S}_t \boldsymbol{n}_t)^2 \right\rangle \big]. \end{aligned} \tag{5.3}$$

We cannot perform the average at this point, because in general the orientation $\boldsymbol{n}_t$ and the gradient matrices $\mathbb{O}_t$ and $\mathbb{S}_t$ have complicated joint statistics - the particles align preferentially to the gradients. The first approximation to the equation of motion (5.2) is $\boldsymbol{n}(t) \approx \boldsymbol{n}_0 + \mathcal{O}(\mathrm{Ku})$. We proceed to average using the Lagrangian correlation functions (5.1). For example,

$$\begin{aligned}\left\langle \boldsymbol{n}_0^{\mathrm{T}} \mathbb{O}_t \mathbb{O}_t \boldsymbol{n}_0 \right\rangle &= \boldsymbol{n}_0^{\mathrm{T}} \left\langle \mathbb{O}_t \mathbb{O}_t \right\rangle \boldsymbol{n}_0 \\ &= C^{OO}_{ijjk}(0) n_i n_k \\ &= \frac{\left\langle \mathrm{Tr} \mathbb{O}_t \mathbb{O}_t \right\rangle}{6} (\delta_{ik}\delta_{jj} - \delta_{ij}\delta_{jk}) n_i n_k \\ &= \frac{\left\langle \mathrm{Tr} \mathbb{O}_t \mathbb{O}_t \right\rangle}{3} = -\frac{\left\langle \mathrm{Tr} \mathbb{A}_t^{\mathrm{T}} \mathbb{A}_t \right\rangle}{6}. \end{aligned}$$

Here I denote the components of $\boldsymbol{n}_0$ by n_i, and employ the implicit summation convention on repeated indices. We also use $n_i n_i = 1$, and in the last step that $\langle \mathrm{Tr} \mathbb{A}^{\mathrm{T}} \mathbb{A} \rangle / 2 = \langle \mathrm{Tr} \mathbb{S} \mathbb{S} \rangle = -\langle \mathrm{Tr} \mathbb{O} \mathbb{O} \rangle$ in a homogenous flow (see App. D).

In the same fashion we evaluate all averages in Eq. (5.3) and find to second order in Ku

$$\begin{aligned}\langle \dot{n}^2 \rangle &= \mathrm{Ku}^2 \left(-\frac{1}{3} \langle \mathrm{Tr}\mathbb{O}_t \mathbb{O}_t \rangle + \frac{\Lambda^2}{3} \langle \mathrm{Tr}\mathbb{S}_t \mathbb{S}_t \rangle - \frac{2\Lambda^2}{15} \langle \mathrm{Tr}\mathbb{S}_t \mathbb{S}_t \rangle \right) + \mathscr{O}(\mathrm{Ku}^3) \\ &= \frac{\mathrm{Ku}^2}{3} \left(-\langle \mathrm{Tr}\mathbb{O}_t \mathbb{O}_t \rangle + \frac{3\Lambda^2}{5} \langle \mathrm{Tr}\mathbb{S}_t \mathbb{S}_t \rangle \right) + \mathscr{O}(\mathrm{Ku}^3) \\ &= \mathrm{Ku}^2 \frac{\langle \mathrm{Tr}\mathbb{A}_t^{\mathrm{T}} \mathbb{A}_t \rangle}{30} \left(5 + 3\Lambda^2 \right) + \mathscr{O}(\mathrm{Ku}^3). \end{aligned} \tag{5.4}$$

An equivalent expression was derived in [34]. The limit of $\mathrm{Ku} \to 0$ is called the white noise limit. Physically it means that the flow is changing so rapidly that the instantaneous gradient is always uncorrelated with the particle orientation. There is no "memory", or correlation with the near past, in the system. Hence the name white noise.

Now we proceed to compute the first effects of finite correlation time in the flow. In order to reach $\mathscr{O}(\mathrm{Ku}^3)$, we need an expression for $\boldsymbol{n}(t)$. The equation for $\boldsymbol{n}$ has the implicit solution

$$\boldsymbol{n}_t = \boldsymbol{n}_0 + \mathrm{Ku} \int_0^t \mathrm{d}t' \left[\mathbb{O}_{t'} \boldsymbol{n}_{t'} + \Lambda (\mathbb{S}_{t'} \boldsymbol{n}_{t'} - (\boldsymbol{n}_{t'}^{\mathrm{T}} \mathbb{S}_{t'} \boldsymbol{n}_{t'}) \boldsymbol{n}_{t'}) \right], \tag{5.5}$$

The perturbation expansion is computed to any order in Ku by recursively inserting the entire right hand side of Eq. (5.5) into each occurence of $\boldsymbol{n}_{t'}$. Iterating once we find

$$\boldsymbol{n}_t = \boldsymbol{n}_0 + \mathrm{Ku} \int_0^t \mathrm{d}t' \left[\mathbb{O}_{t'} \boldsymbol{n}_0 + \Lambda (\mathbb{S}_{t'} \boldsymbol{n}_0 - (\boldsymbol{n}_0^{\mathrm{T}} \mathbb{S}_{t'} \boldsymbol{n}_0) \boldsymbol{n}_0) \right] + \mathscr{O}(\mathrm{Ku}^2) \tag{5.6}$$

In principle, we could continue, however, for the present purpose, this first order expansion is enough. We insert the expansion (5.6)

into Eq. (5.3) and find to third order in Ku

$$\begin{aligned}\langle \dot{n}^2\rangle &= \mathrm{Ku}^2\frac{\langle \mathrm{Tr}\mathbb{A}_t^{\mathrm{T}}\mathbb{A}_t\rangle}{30}\left(5+3\Lambda^2\right)\\
&+\mathrm{Ku}^3\int_0^t \mathrm{d}t'\Big[-\left\langle \boldsymbol{n}_0^{\mathrm{T}}\mathbb{O}_t\mathbb{O}_t[\mathbb{O}_{t'}\boldsymbol{n}_0+\Lambda(\mathbb{S}_{t'}\boldsymbol{n}_0-(\boldsymbol{n}_0^{\mathrm{T}}\mathbb{S}_{t'}\boldsymbol{n}_0)\boldsymbol{n}_0)]\right\rangle\\
&\quad-\left\langle[-\boldsymbol{n}_0^{\mathrm{T}}\mathbb{O}_{t'}+\Lambda(\boldsymbol{n}_0^{\mathrm{T}}\mathbb{S}_{t'}-(\boldsymbol{n}_0^{\mathrm{T}}\mathbb{S}_{t'}\boldsymbol{n}_0)\boldsymbol{n}_0^{\mathrm{T}})]\mathbb{O}_t\mathbb{O}_t\boldsymbol{n}_0\right\rangle\\
&\quad+\Lambda\left\langle[-\boldsymbol{n}_0^{\mathrm{T}}\mathbb{O}_{t'}+\Lambda(\boldsymbol{n}_0^{\mathrm{T}}\mathbb{S}_{t'}-(\boldsymbol{n}_0^{\mathrm{T}}\mathbb{S}_{t'}\boldsymbol{n}_0)\boldsymbol{n}_0^{\mathrm{T}})](\mathbb{S}_t\mathbb{O}_t-\mathbb{O}_t\mathbb{S}_t)\boldsymbol{n}_0\right\rangle\\
&\quad+\Lambda\left\langle\boldsymbol{n}_0^{\mathrm{T}}(\mathbb{S}_t\mathbb{O}_t-\mathbb{O}_t\mathbb{S}_t)[\mathbb{O}_{t'}\boldsymbol{n}_0+\Lambda(\mathbb{S}_{t'}\boldsymbol{n}_0-(\boldsymbol{n}_0^{\mathrm{T}}\mathbb{S}_{t'}\boldsymbol{n}_0)\boldsymbol{n}_0)]\right\rangle\\
&\quad+\Lambda^2\left\langle\boldsymbol{n}_0^{\mathrm{T}}\mathbb{S}_t\mathbb{S}_t[\mathbb{O}_{t'}\boldsymbol{n}_0+\Lambda(\mathbb{S}_{t'}\boldsymbol{n}_0-(\boldsymbol{n}_0^{\mathrm{T}}\mathbb{S}_{t'}\boldsymbol{n}_0)\boldsymbol{n}_0)]\right\rangle\\
&\quad+\Lambda^2\left\langle[-\boldsymbol{n}_0^{\mathrm{T}}\mathbb{O}_{t'}+\Lambda(\boldsymbol{n}_0^{\mathrm{T}}\mathbb{S}_{t'}-(\boldsymbol{n}_0^{\mathrm{T}}\mathbb{S}_{t'}\boldsymbol{n}_0)\boldsymbol{n}_0^{\mathrm{T}})]\mathbb{S}_t\mathbb{S}_t\boldsymbol{n}_0\right\rangle\\
&\quad-2\Lambda^2\left\langle\boldsymbol{n}_0^{\mathrm{T}}\mathbb{S}_t\boldsymbol{n}_0\boldsymbol{n}_0^{\mathrm{T}}\mathbb{S}_t[\mathbb{O}_{t'}\boldsymbol{n}_0+\Lambda(\mathbb{S}_{t'}\boldsymbol{n}_0-(\boldsymbol{n}_0^{\mathrm{T}}\mathbb{S}_{t'}\boldsymbol{n}_0)\boldsymbol{n}_0)]\right\rangle\\
&\quad-2\Lambda^2\left\langle[-\boldsymbol{n}_0^{\mathrm{T}}\mathbb{O}_{t'}+\Lambda(\boldsymbol{n}_0^{\mathrm{T}}\mathbb{S}_{t'}-(\boldsymbol{n}_0^{\mathrm{T}}\mathbb{S}_{t'}\boldsymbol{n}_0)\boldsymbol{n}_0^{\mathrm{T}})]\mathbb{S}_t\boldsymbol{n}_0\boldsymbol{n}_0^{\mathrm{T}}\mathbb{S}_t\boldsymbol{n}_0\right\rangle\Big]\\
&\quad+\mathscr{O}(\mathrm{Ku}^4)\end{aligned}$$

There are quite a number of terms, but again, we can use the known three point correlation functions to evaluate the averages. For example,

$$\begin{aligned}&\left\langle\boldsymbol{n}_0^{\mathrm{T}}\mathbb{S}_t\mathbb{S}_t\boldsymbol{n}_0\boldsymbol{n}_0^{\mathrm{T}}\mathbb{S}_{t'}\boldsymbol{n}_0\right\rangle = C^{SSS}_{ijjklm}(0,t'-t)n_in_kn_ln_m\\
&=\frac{\left\langle\mathrm{Tr}\mathbb{S}_t\mathbb{S}_t\mathbb{S}_{t'}\right\rangle}{30}(3\delta_{im}\delta_{kl}+3\delta_{il}\delta_{km}-2\delta_{ik}\delta_{lm})\\
&=\frac{2\left\langle\mathrm{Tr}\mathbb{S}_t\mathbb{S}_t\mathbb{S}_{t'}\right\rangle}{15}.\end{aligned}$$

Moreover, the correlation functions where two of the three matrices are evaluated at the same time have an exchange symmetry. More precisely it means, for instance, $C^{OSS}_{ijklmn}(0,\tau)=C^{SOS}_{klijmn}(0,\tau)$. This symmetry reduces the number of terms considerably, for example $\langle\mathbb{S}_t\mathbb{O}_t\mathbb{O}_{t'}\rangle=\langle\mathbb{O}_t\mathbb{S}_t\mathbb{O}_{t'}\rangle$. After averaging, the result is

$$\begin{aligned}\langle\dot{n}^2\rangle &= \mathrm{Ku}^2\frac{\langle\mathrm{Tr}\mathbb{A}_t^{\mathrm{T}}\mathbb{A}_t\rangle}{30}\left(5+3\Lambda^2\right)\\
&+\frac{2\Lambda\mathrm{Ku}^3}{5}\int_0^t\mathrm{d}t'\Big[\frac{3\Lambda^2}{7}\left\langle\mathrm{Tr}\mathbb{S}_t\mathbb{S}_t\mathbb{S}_{t'}\right\rangle-\left\langle\mathrm{Tr}\mathbb{O}_t\mathbb{O}_t\mathbb{S}_{t'}\right\rangle+2\Lambda\left\langle\mathrm{Tr}\mathbb{S}_t\mathbb{O}_t\mathbb{S}_{t'}\right\rangle\Big]\end{aligned}$$

Due to the statistical stationarity of the flow, we may translate the integrals to the form given in the manuscript,

$$\begin{aligned}\int_0^t \mathrm{d}t' \left\langle \mathrm{Tr}\mathbb{S}_t \mathbb{S}_t \mathbb{S}_{t'} \right\rangle &= \int_0^t \mathrm{d}t' \left\langle \mathrm{Tr}\mathbb{S}_0 \mathbb{S}_0 \mathbb{S}_{t'-t} \right\rangle \\ &= -\int_t^0 \mathrm{d}\tau \left\langle \mathrm{Tr}\mathbb{S}_0 \mathbb{S}_0 \mathbb{S}_{-\tau} \right\rangle \\ &= \int_0^t \mathrm{d}\tau \left\langle \mathrm{Tr}\mathbb{S}_0 \mathbb{S}_0 \mathbb{S}_{-\tau} \right\rangle\end{aligned}$$

The last step is to take the time $t \to \infty$, as advertised earlier. This concludes the derivation of Eq. (4) in the manuscript:

$$\begin{aligned}\langle \dot{n}^2 \rangle = \mathrm{Ku}^2 \frac{\langle \mathrm{Tr}\mathbb{A}_t^{\mathrm{T}} \mathbb{A}_t \rangle}{30} \left(5 + 3\Lambda^2\right) \\ + \frac{2\Lambda \mathrm{Ku}^3}{5} \int_0^\infty \mathrm{d}\tau \left[\frac{3\Lambda^2}{7} \left\langle \mathrm{Tr}\mathbb{S}_0 \mathbb{S}_0 \mathbb{S}_{-\tau} \right\rangle - \left\langle \mathrm{Tr}\mathbb{O}_0 \mathbb{O}_0 \mathbb{S}_{-\tau} \right\rangle + 2\Lambda \left\langle \mathrm{Tr}\mathbb{S}_0 \mathbb{O}_0 \mathbb{S}_{-\tau} \right\rangle \right]\end{aligned} \tag{5.7}$$

5.3 Turbulent flow data

We do not ourselves have the resources to produce a numerical solution of the Navier-Stokes equations. But researchers at Johns Hopkins University (JHU) have published the data from a large direct numerical simulation[3] [35]. The JHU database contains the velocity and pressure fields of homogenous, isotropic and incompressible turbulence. The spatial domain is a periodic box, and the data covers circa 45 Kolmogorov times. The dataset corresponds to one turn-around of the largest eddy in the periodic box.

The JHU database stores the data (27 TB) in a computing cluster, which we can access with a remote programming interface. We may query for the velocity and pressure fields, as well as their derivatives, at any time and position in the dataset. The JHU

[3] http://turbulence.pha.jhu.edu/

database provides both spatial and temporal interpolation, so to us the dataset is for practical purposes continuous.

We initialise a particle at a random position $\boldsymbol{r}$, with a random orientation $\boldsymbol{n}$, and query for the velocity field $\boldsymbol{u}(\boldsymbol{r}(t),t)$ and gradient field $\mathbb{A}(\boldsymbol{r}(t),t)$. Then we update the position and orientation by

$$\begin{aligned}\dot{\boldsymbol{r}} &= \boldsymbol{u}(\boldsymbol{r}(t),t),\\ \dot{\boldsymbol{n}} &= \mathbb{O}\boldsymbol{n} + \Lambda\left(\mathbb{S}\boldsymbol{n} - \boldsymbol{n}\boldsymbol{n}^{\mathrm{T}}\mathbb{S}\boldsymbol{n}\right).\end{aligned}$$

The procedure is repeated for the entire duration of the data set. From the time series $\mathbb{A}(\boldsymbol{r}(t),t)$ we compute the required correlation functions, and other observables such as particle alignment with vorticity $\langle|\boldsymbol{\Omega}\cdot\boldsymbol{n}|\rangle$.

In Fig. 5.1 I show the probability distributions of particle alignment with the eigenvectors of the strain matrix $\mathbb{S}$, and the vorticity vector $\boldsymbol{\Omega}$. The straining direction $\boldsymbol{e}_1$ corresponds to the largest eigenvalue. We see that rods ($\lambda = 100$ in this case) align preferentially to the vorticity, as previously observed [36]. But we also see that disks ($\lambda = 1/100$) have an even stronger preference to anti-align with the vorticity. The same pattern of opposite preference holds for the eigenvectors of $\mathbb{S}$. Disks prefer the compressing direction $\boldsymbol{e}_3$, while rods prefer the weakly stretching $\boldsymbol{e}_2$. None of the particle shapes correlate strongly to the strongest straining direction $\boldsymbol{e}_1$.

In Fig. 5.2 I show the distribution of measured rotation rates for disks, rods and spheres. The sphere always rotates with the vorticity rate. We see that the disk experiences many more events of high rotation rates, which must be due to the effects of strain. The rod, on the other hand, not only rotates less than the disk, but it rotates much less than the sphere. It means that the rod's rotation is actually inhibited by the strain.

From the data set we also compute the three integrals in Eq. (5.7) in order to quantify the relative strengths of the contributions. First, we have to confirm that the correlation functions factorise according to Eq. (5.1). We compute every element of, for example, C^{SSS}_{ijklmn} and compare it to the theoretical formula, in this case Eq. (D.3) in Appendix D. The result is shown in Fig. 5.3, and

the other combinations show similar agreement with theory. We conclude that the JHU dataset indeed contains incompressible and isotropic turbulence. Second, knowing that the correlation functions factorise, we may compute the time dependence of the trace and perform the integral. In Figs. 5.4-5.6 I show the result for the integrals relevant to the expansion Eq. (5.7).

Finally, we may use the numerical turbulence correlation functions in the expansion (5.7), and compare to the numerical results of tumbling in turbulent flows. Two comments are in order. First, in turbulent flows $\mathrm{Ku} = \mathcal{O}(1)$, while Eq. (5.7) is valid for small Ku. Therefore we do not expect quantitative predictions. However, we expect the functional form of the result to be correct. That is, in this case, the dependence upon the particle shape λ. Second, in deriving Eq. (5.7) we used dimensionless variables where $\mathbb{A} = u_0/\eta\mathbb{A}'$. But here we have instead expressed the correlation functions de-dimensionalised by the Kolmogorov time τ_K, or $\mathbb{A} = 1/\tau_K\mathbb{A}''$. In order to proceed, we identify the time τ in the Kubo number with the Kolmogorov time τ_K, so that $\mathrm{Ku}\mathbb{A}' = \mathbb{A}''$. There are therefore no free parameters in Eq. (5.7) when using the numerical turbulence data. The result is shown in Fig. 5.7.

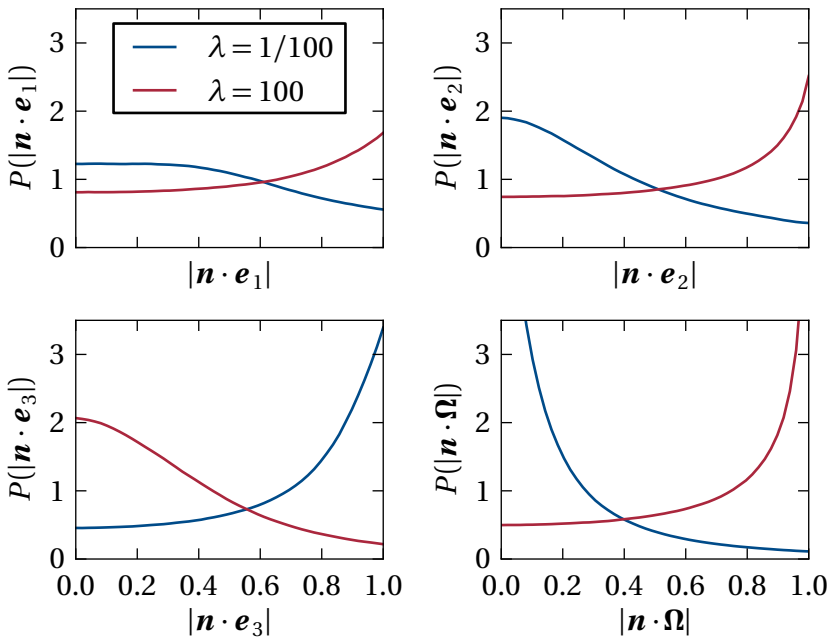

Figure 5.1: Probability distributions of particle direction alignment in turbulent flow. The lower right panel shows alignment with the vorticity direction $\hat{\boldsymbol{\Omega}}$. The three other show alignment with the eigenvectors $\boldsymbol{e}_i$ of the strain matrix $\mathbb{S}$, where $\boldsymbol{e}_1$ corresponds to the largest eigenvalue. Red line shows distribution for a rod-shaped particle, blue line shows distribution for a disk.

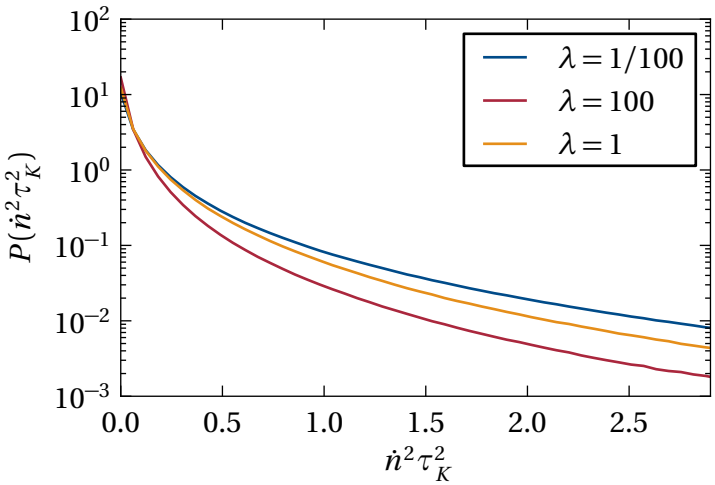

Figure 5.2: Probability of observed rotation rates of a rod (red line), disk (blue line) and sphere (orange line) in turbulent flow.

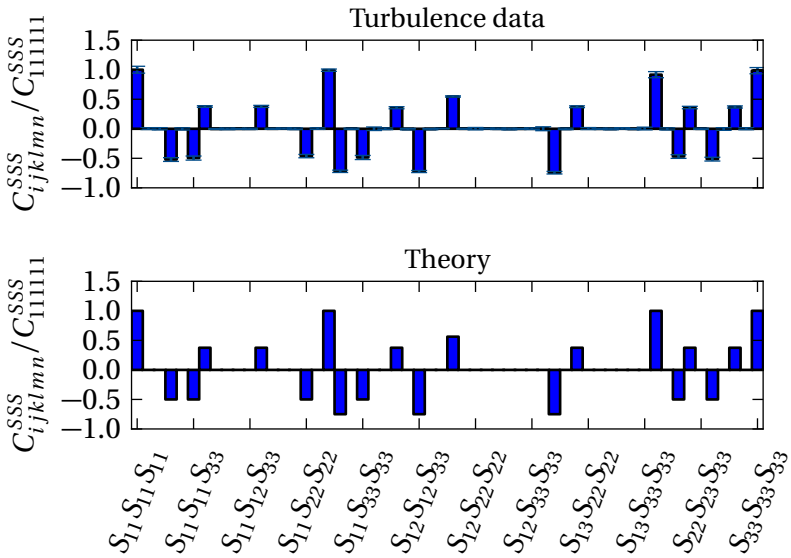

Figure 5.3: Spatial dependence of correlation function C^{SSS}_{ijklmn}. Comparison between measured correlation (top) and theoretical expression Eq. (D.3) (bottom). Bars are normalised by the first element. Error bars indicate one standard deviation.

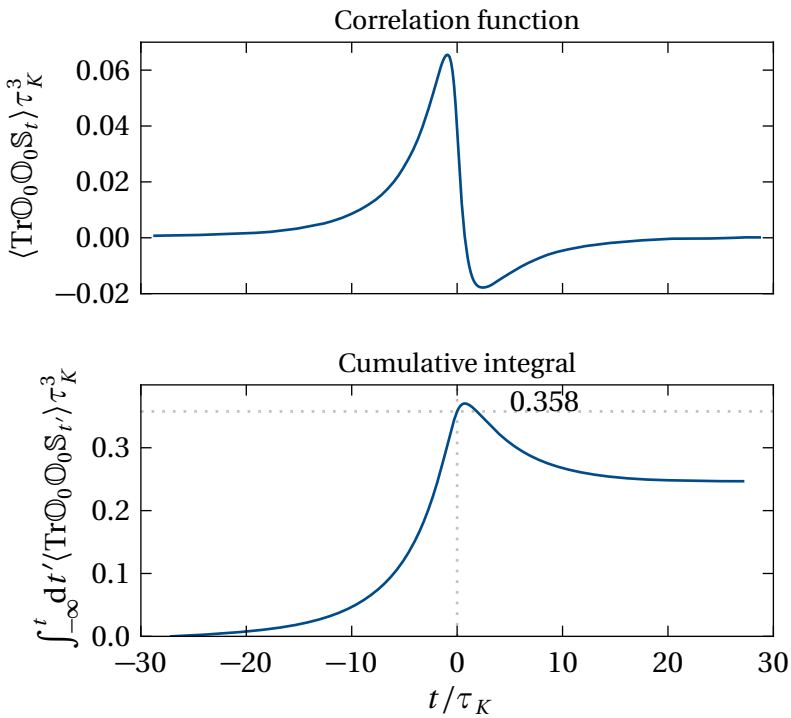

Figure 5.4: Top panel: Time dependence of correlation function $C^{OOS}_{ijklmn}(0,t)$. Bottom panel: Cumulative integral of correlation function. The integral in the expansion for rotation rates Eq. (5.7) correspond to the value at $t=0$, in this case 0.358.

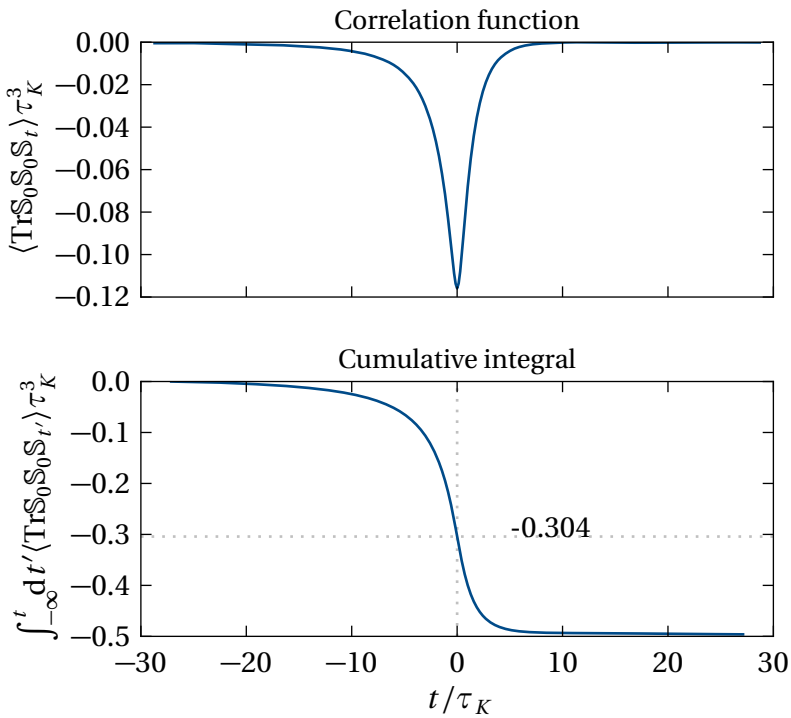

Figure 5.5: Top panel: Time dependence of correlation function $C^{SSS}_{ijklmn}(0,t)$. Bottom panel: Cumulative integral of correlation function. The integral in the expansion for rotation rates Eq. (5.7) correspond to the value at $t=0$, in this case −0.304.

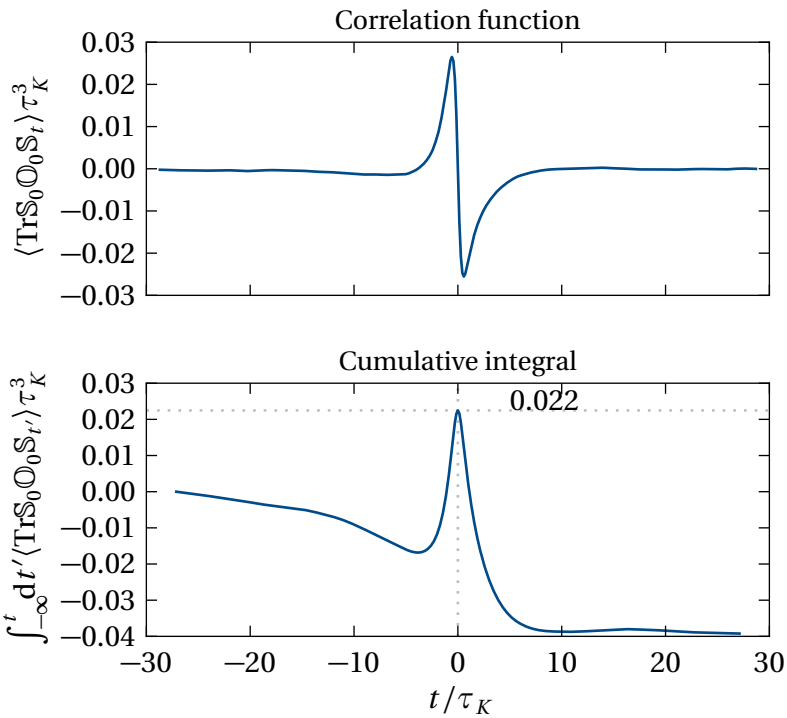

Figure 5.6: Top panel: Time dependence of correlation function $C^{SOS}_{ijklmn}(0,t)$. Bottom panel: Cumulative integral of correlation function. The integral in the expansion for rotation rates Eq. (5.7) correspond to the value at $t=0$, in this case 0.022.

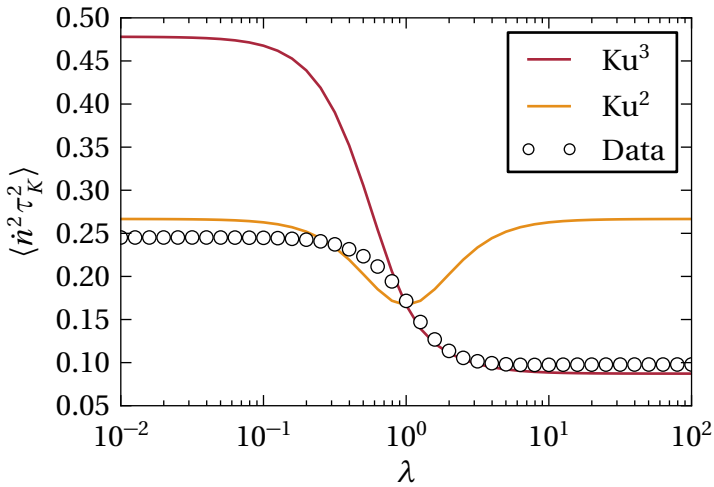

Figure 5.7: Average rotation rate of an axisymmetric particle as function of particle aspect ratio λ. Markers show numerical results from the JHU turbulence data set. Solid lines show the small-Ku expansions Eq. (5.4) (second order, orange line) and Eq. (5.7) (third order, red line), using the correlation functions shown in Figs. 5.4-5.6.

6 Outlook

Successful research needs good questions. And the more we know, the better questions we can ask. In this thesis, I have presented the main results of the past year's work. But perhaps the most important results are the new questions we are able to pose? I have already touched on the outlook for each project, but here I to conclude with a more complete summary.

I have described an experiment where we observe aperiodic tumbling of rod-like particles (see Section 3). We argue that the aperiodicity originates in the imperfect axisymmetry of the plastic particles used. The Jeffery theory predicts that if the observed particle is axisymmetric, we will observe periodic tumbling. We are currently pursuing refined experiments using very nearly axisymmetric particles. We expect that their results will conclusively show that we observe the quasi-periodic orbits of triaxial particles. However, there are several open theoretical questions concerning the dynamics of triaxial particles in simple shear flow. First, the orientational motion of triaxial ellipsoids are confined to tori, as described in Section 3. This fact tells us that there is a conserved quantity. But which quantity? In the case of axisymmetric particles, we know that the Jeffery orbit constant is preserved, but what is the correct set of variables in the triaxial case? We want to investigate whether there is a relation to the dynamical system known as "the standard map" [37].

Second, in Paper B (and Appendices B and C of this thesis) we explain how to compute orientational distributions on a sphere. The method described may be generalised to rotations of triaxial particles subject to Brownian noise [38, 39, 40]. We now know that even minor asymmetries of the particle shape may have a strong effect on the rotational dynamics. The question is whether a small amount of noise dominates this effect. Otherwise, it is important to consider the particle asymmetry when computing the orientational distribution.

Third, the results for weakly inertial particles described in Paper B may be extended to the case of triaxial particles. Numerical observations of inertial ellipsoids indicate the existence of a limit-

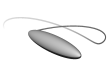

ing orbit, such that the minor particle axis aligns with the vorticity direction [41]. This periodic solution will correspond to a single point in the surface-of-section.

For axisymmetric particles in simple shear flow, the effect of fluid inertia ($\mathrm{Re_p} > 0$) stands out as an important topic. In Paper B we performed linear stability analysis of the log-rolling and tumbling modes, as function of particle shape. Our results are valid for small values of St, and $\mathrm{Re_p} = 0$. As mentioned in Section 4.2, calculations by Subramanian & Koch [29, 30] indicate that the result is qualitatively different when $\mathrm{Re_p} > 0$, and in particular when $\mathrm{Re_p} = \mathrm{St}$, corresponding to the case of neutrally buoyant particles. We will attempt to extend the stability analysis to finite particle Reynolds numbers by generalising the methods of [29, 30]. In particular, we believe that an adaptation of a "reciprocal theorem" [42] will enable us to perform the stability analysis without requiring the explicit solution of the Navier-Stokes equations.

In Paper C we ventured into the topic of non-spherical particles in random and turbulent flows. I will just mention two questions we are discussing at present. First, we believe that computing the relative angles of colliding non-spherical particles is important. The angle at which particles collide likely impacts the outcome of the collision. Second, sometimes the small Kubo-expansion described in Section 5 does not work. For example, when we compute the particle correlation function $\langle \boldsymbol{n}(0) \cdot \boldsymbol{n}(t) \rangle$, we find that the perturbation expansion contains secular terms: terms diverging as $t \to \infty$. Clearly, the correlation function cannot diverge in reality. The divergence is an artefact of the perturbation expansion. This raises the question of how to apply the methods of singular perturbation theory to the problem.

One of the delights, and at the same time torments, of theoretical work, is that it is rarely possible to foresee where your questions lead. We are confident that some of the above questions will bear fruit, but exactly which, and how, only time will tell.

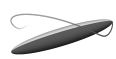

Bibliography

[1] DEVENISH, B. J, BARTELLO, P, BRENGUIER, J. L, COLLINS, L. R, GRABOWSKI, W. W, IJZERMANS, R. H. A, MALINOWSKI, S. P, REEKS, M. W, VASSILICOS, J. C, WANG, L. P & WARHAFT, Z 2012 Droplet growth in warm turbulent clouds. *Quarterly Journal of the Royal Meteorological Society* **138** (667), 1401–1429.

[2] WILKINSON, M, MEHLIG, B & USKI, V 2008 Stokes trapping and planet formation. *The Astrophysical Journal Supplement Series* **176** (2), 484–496.

[3] GUASTO, J. S, RUSCONI, R & STOCKER, R 2012 Fluid mechanics of planktonic microorganisms. *Annual Review of Fluid Mechanics* **44** (1), 373–400.

[4] BAYOD, E, WILLERS, E. P & TORNBERG, E 2008 Rheological and structural characterization of tomato paste and its influence on the quality of ketchup. *LWT - Food Science and Technology* **41** (7), 1289–1300.

[5] COUSSOT, P, NGUYEN, Q. D, HUYNH, H. T & BONN, D 2002 Avalanche behavior in yield stress fluids. *Physical Review Letters* **88** (17), 175501.

[6] MATHER, T, PYLE, D & OPPENHEIMER, C 2003 Tropospheric volcanic aerosol. In *Volcanism and the Earth's Atmosphere* (ed. A Robock & C Oppenheimer), p. 189–212. American Geophysical Union.

[7] GASTEIGER, J, GROSS, S, FREUDENTHALER, V & WIEGNER, M 2011 Volcanic ash from Iceland over Munich: mass concentration retrieved from ground-based remote sensing measurements. *Atmos. Chem. Phys.* **11** (5), 2209–2223.

[8] DUBOVIK, O, HOLBEN, B. N, LAPYONOK, T, SINYUK, A, MISHCHENKO, M. I, YANG, P & SLUTSKER, I 2002 Non-spherical aerosol retrieval method employing light scattering by spheroids. *Geophysical Research Letters* **29** (10), 54–1.

[9] MARCOS, SEYMOUR, J. R, LUHAR, M, DURHAM, W. M, MITCHELL, J. G, MACKE, A & STOCKER, R 2011 Microbial alignment in flow changes ocean light climate. *Proceedings of the National Academy of Sciences* PMID: 21368125.

[10] SABINE, E 1829 On the reduction to a vacuum of Captain Kater's convertible pendulum. *Philosophical Transactions of the Royal Society of London* **119**, 331–338.

[11] STOKES, G. G 1851 On the effect of the internal friction of fluids on the motion of pendulums. *Transactions of the Cambridge Philosophical Society* **IX**, 8, reprinted in Cambridge Library Collection: Mathematical and Physical Papers Vol. 3. ISBN 9780511702266.

[12] VEYSEY, J & GOLDENFELD, N 2007 Simple viscous flows: From boundary layers to the renormalization group. *Reviews of Modern Physics* **79** (3), 883–927.

[13] JEFFERY, G. B 1922 The motion of ellipsoidal particles immersed in a viscous fluid. *Proceedings of the Royal Society of London. Series A* **102** (715), 161–179.

[14] BRENNER, H 1974 Rheology of a dilute suspension of axisymmetric Brownian particles. *International Journal of Multiphase Flow* **1** (2), 195–341.

[15] KIM, S & KARRILA, S. J 1991 *Microhydrodynamics: principles and selected applications*. Boston: Butterworth-Heinemann.

[16] ZIMMERMANN, R, GASTEUIL, Y, BOURGOIN, M, VOLK, R, PUMIR, A, PINTON, J.-F & INTERNATIONAL COLLABORATION FOR TURBULENCE 2011 Tracking the dynamics of translation and absolute orientation of a sphere in a turbulent flow. *Review of Scientific Instruments* **82** (3), 033906.

[17] PARSA, S, CALZAVARINI, E, TOSCHI, F & VOTH, G. A 2012 Rotation rate of rods in turbulent fluid flow. *Physical Review Letters* **109** (13), 134501.

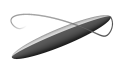

[18] KUNDU, P. K & COHEN, I. M 2004 *Fluid mechanics*, 3rd edn. Amsterdam; Boston: Elsevier Academic Press.

[19] HAPPEL, J. R & BRENNER, H 1965 *Low Reynolds Number Hydrodynamics: With Special Applications to Particulate Media*. Springer.

[20] EICHHORN, R 2010 Microfluidic sorting of stereoisomers. *Physical Review Letters* **105** (3), 034502.

[21] ARISTOV, M, EICHHORN, R & BECHINGER, C 2013 Separation of chiral colloidal particles in a helical flow field. *Soft Matter* **9** (8), 2525–2530.

[22] BRETHERTON, F. P 1962 The motion of rigid particles in a shear flow at low Reynolds number. *Journal of Fluid Mechanics* **14** (02), 284–304.

[23] KAMPEN, N. G. V 2007 *Stochastic processes in physics and chemistry*, 3rd edn. Amsterdam ; Boston: Elsevier.

[24] HINCH, E. J & LEAL, L. G 1972 The effect of Brownian motion on the rheological properties of a suspension of non-spherical particles. *Journal of Fluid Mechanics* **52** (04), 683–712.

[25] MISHRA, Y. N, EINARSSON, J, JOHN, O. A, ANDERSSON, P, MEHLIG, B & HANSTORP, D 2012 A microfluidic device for studies of the orientational dynamics of microrods. *Proc. SPIE* **8251**, 825109.

[26] HINCH, E. J & LEAL, L. G 1979 Rotation of small non-axisymmetric particles in a simple shear flow. *Journal of Fluid Mechanics* **92** (03), 591–607.

[27] YARIN, A. L, GOTTLIEB, O & ROISMAN, I. V 1997 Chaotic rotation of triaxial ellipsoids in simple shear flow. *Journal of Fluid Mechanics* **340**, 83–100.

[28] LUNDELL, F & CARLSSON, A 2010 Heavy ellipsoids in creeping shear flow: Transitions of the particle rotation rate and orbit shape. *Physical Review E* **81** (1), 016323.

[29] SUBRAMANIAN, G & KOCH, D. L 2006 Inertial effects on the orientation of nearly spherical particles in simple shear flow. *Journal of Fluid Mechanics* **557**, 257–296.

[30] SUBRAMANIAN, G & KOCH, D. L 2005 Inertial effects on fibre motion in simple shear flow. *Journal of Fluid Mechanics* **535**, 383–414.

[31] GUSTAVSSON, K & MEHLIG, B 2011 Distribution of relative velocities in turbulent aerosols. *Physical Review E* **84** (4), 045304.

[32] CHERTKOV, M, PUMIR, A & SHRAIMAN, B. I 1999 Lagrangian tetrad dynamics and the phenomenology of turbulence. *Physics of Fluids* **11** (8), 2394–2410.

[33] LÜTHI, B, HOLZNER, M & TSINOBER, A 2009 Expanding the Q–R space to three dimensions. *Journal of Fluid Mechanics* **641**, 497–507.

[34] SHIN, M & KOCH, D. L 2005 Rotational and translational dispersion of fibres in isotropic turbulent flows. *Journal of Fluid Mechanics* **540**, 143–173.

[35] LI, Y, PERLMAN, E, WAN, M, YANG, Y, MENEVEAU, C, BURNS, R, CHEN, S, SZALAY, A & EYINK, G 2008 A public turbulence database cluster and applications to study Lagrangian evolution of velocity increments in turbulence. *Journal of Turbulence* **9** (31).

[36] PUMIR, A & WILKINSON, M 2011 Orientation statistics of small particles in turbulence. *New Journal of Physics* **13** (9), 093030.

[37] OTT, E 2002 *Chaos in dynamical systems*, 2nd edn. Cambridge, U.K. ; New York: Cambridge University Press.

[38] FAVRO, L. D 1960 Theory of the rotational Brownian motion of a free rigid body. *Physical Review* **119** (1), 53–62.

[39] BRENNER, H & CONDIFF, D. W 1972 Transport mechanics in systems of orientable particles. III. Arbitrary particles. *Journal of Colloid and Interface Science* **41** (2), 228–274.

[40] HUBBARD, P. S 1972 Rotational Brownian motion. *Physical Review A* **6** (6), 2421–2433.

[41] LUNDELL, F 2011 The effect of particle inertia on triaxial ellipsoids in creeping shear: From drift toward chaos to a single periodic solution. *Physics of Fluids* **23** (1), 011704.

[42] LOVALENTI, P. M & BRADY, J. F 1993 The hydrodynamic force on a rigid particle undergoing arbitrary time-dependent motion at small Reynolds number. *Journal of Fluid Mechanics* **256**, 561–605.

[43] JACKSON, J. D 1999 *Classical electrodynamics*, 3rd edn. New York: Wiley.

[44] DOI, M & EDWARDS, S. F 1987 *The theory of polymer dynamics*. Oxford [Oxfordshire]; New York: Clarendon Press ; Oxford University Press.

[45] SCHERAGA, H. A 1955 Non-Newtonian viscosity of solutions of ellipsoidal particles. *The Journal of Chemical Physics* **23** (8), 1526–1532.

[46] PETERLIN, A 1938 Über die viskosität von verdünnten lösungen und suspensionen in abhängigkeit von der teilchenform. *Zeitschrift für Physik* **111** (3-4), 232–263.

[47] ARFKEN, G 1970 *Mathematical Methods for Physicists, Second Edition*. Academic Press.

[48] SAKURAI, J. J 1994 *Modern quantum mechanics*, rev. edn. Reading, Mass: Addison-Wesley Pub. Co.

[49] https://github.com/jeinarsson/fpe_sphere.

[50] ANDREWS, D. L & THIRUNAMACHANDRAN, T 1977 On three–dimensional rotational averages. *The Journal of Chemical Physics* **67** (11), 5026.

[51] EINARSSON, J, JOHANSSON, A, MAHATO, S. K, MISHRA, Y. N, ANGILELLA, J. R, HANSTORP, D & MEHLIG, B 2013 Periodic and

aperiodic tumbling of microrods advected in a microchannel flow. *Acta Mechanica* **224** (10), 2281–2289.

[52] EINARSSON, J, ANGILELLA, J. R & MEHLIG, B 2013 Orientational dynamics of weakly inertial axisymmetric particles in steady viscous flows. arXiv e-print 1307.2821.

[53] GUSTAVSSON, K, EINARSSON, J & MEHLIG, B 2013 Tumbling of small axisymmetric particles in random and turbulent flows. arXiv e-print 1305.1822.

PART III
APPENDICES

A Triaxial particle in a linear flow

In this Appendix I derive the torque-free equation of motion for an triaxial ellipsoidal particle in a general linear flow. It is the generalisation of the Jeffery equation to triaxial particles.

We represent the orientation of the particle with a rotation matrix $\mathbb{R}(t)$, which transforms the world-fixed cartesian coordinate frame $(\boldsymbol{e}_1, \boldsymbol{e}_2, \boldsymbol{e}_3)$ to the particle-fixed coordinate frame $(\boldsymbol{n}_1, \boldsymbol{n}_2, \boldsymbol{n}_3)$. The ellipsoid is defined by the lengths of its three half-axes, we denote them a_1, a_2 and a_3. Each a_i is the length along the corresponding particle axis $\boldsymbol{n}_i$.

The end result of this calculation is an equation of motion for $\boldsymbol{n}_1$ and $\boldsymbol{n}_2$. The two orthogonal vectors describe fully the orientation of the rigid body.

The kinematic equation of motion for a rotating vector is

$$\dot{\boldsymbol{n}}_i = \boldsymbol{\omega} \times \boldsymbol{n}_i, \tag{A.1}$$

where $\boldsymbol{\omega}$ is the angular velocity of the particle. Jeffery [13] computed the components of the angular velocity vector in the particle frame of reference. Updated to the present notation, his Eq. (37) reads

$$\begin{aligned}
(\boldsymbol{n}_1 \cdot \boldsymbol{\omega}) &= \boldsymbol{n}_1 \cdot \boldsymbol{\Omega} + \frac{a_2^2 - a_3^2}{a_2^2 + a_3^2} \left(\boldsymbol{n}_2^{\mathrm{T}} \mathbb{S} \boldsymbol{n}_3 \right), \\
(\boldsymbol{n}_2 \cdot \boldsymbol{\omega}) &= \boldsymbol{n}_2 \cdot \boldsymbol{\Omega} + \frac{a_3^2 - a_1^2}{a_3^2 + a_1^2} \left(\boldsymbol{n}_3^{\mathrm{T}} \mathbb{S} \boldsymbol{n}_1 \right), \\
(\boldsymbol{n}_3 \cdot \boldsymbol{\omega}) &= \boldsymbol{n}_3 \cdot \boldsymbol{\Omega} + \frac{a_1^2 - a_2^2}{a_1^2 + a_2^2} \left(\boldsymbol{n}_1^{\mathrm{T}} \mathbb{S} \boldsymbol{n}_2 \right).
\end{aligned}$$

Here $\boldsymbol{\Omega}$ is such that $\boldsymbol{\Omega}\times x = \mathbb{O}\boldsymbol{x}$, where $\mathbb{S}$ and $\mathbb{O}$ are the symmetric and antisymmetric parts of the flow gradient:

$$\mathbb{O} = \frac{1}{2}(\mathbb{A}-\mathbb{A}^{\mathrm{T}}), \quad \mathbb{S} = \frac{1}{2}(\mathbb{A}+\mathbb{A}^{\mathrm{T}}), \quad \mathbb{A} = \nabla\boldsymbol{u} = \mathbb{O}+\mathbb{S}.$$

We can put Jeffery's expression into a single vector expression

$$\boldsymbol{\omega} = \boldsymbol{\Omega} + \frac{a_2^2-a_3^2}{a_2^2+a_3^2}\left(\boldsymbol{n}_2^{\mathrm{T}}\mathbb{S}\boldsymbol{n}_3\right)\boldsymbol{n}_1 + \frac{a_3^2-a_1^2}{a_3^2+a_1^2}\left(\boldsymbol{n}_3^{\mathrm{T}}\mathbb{S}\boldsymbol{n}_1\right)\boldsymbol{n}_2 + \frac{a_1^2-a_2^2}{a_1^2+a_2^2}\left(\boldsymbol{n}_1^{\mathrm{T}}\mathbb{S}\boldsymbol{n}_2\right)\boldsymbol{n}_3.$$

In order to ease the notation we introduce the two aspect ratios $\lambda = a_3/a_1$ and $\kappa = a_2/a_3$:

$$\boldsymbol{\omega} = \boldsymbol{\Omega} + K\left(\boldsymbol{n}_2^{\mathrm{T}}\mathbb{S}\boldsymbol{n}_3\right)\boldsymbol{n}_1 - \Lambda\left(\boldsymbol{n}_3^{\mathrm{T}}\mathbb{S}\boldsymbol{n}_1\right)\boldsymbol{n}_2 + \frac{K-\Lambda}{K\Lambda-1}\left(\boldsymbol{n}_1^{\mathrm{T}}\mathbb{S}\boldsymbol{n}_2\right)\boldsymbol{n}_3,$$

where

$$K = \frac{\kappa^2-1}{\kappa^2+1}, \qquad \Lambda = \frac{\lambda^2-1}{\lambda^2+1}.$$

Now, take the equations of motion for $\boldsymbol{n}_1$ and $\boldsymbol{n}_2$,

$$\begin{aligned}
\dot{\boldsymbol{n}}_1 &= \boldsymbol{\omega}\times\boldsymbol{n}_1 \\
&= \boldsymbol{\Omega}\times\boldsymbol{n}_1 + \Lambda\left(\boldsymbol{n}_3^{\mathrm{T}}\mathbb{S}\boldsymbol{n}_1\right)\boldsymbol{n}_3 + \frac{K-\Lambda}{K\Lambda-1}\left(\boldsymbol{n}_1^{\mathrm{T}}\mathbb{S}\boldsymbol{n}_2\right)\boldsymbol{n}_2, \\
\dot{\boldsymbol{n}}_2 &= \boldsymbol{\omega}\times\boldsymbol{n}_2 \\
&= \boldsymbol{\Omega}\times\boldsymbol{n}_2 + K\left(\boldsymbol{n}_2^{\mathrm{T}}\mathbb{S}\boldsymbol{n}_3\right)\boldsymbol{n}_3 - \frac{K-\Lambda}{K\Lambda-1}\left(\boldsymbol{n}_1^{\mathrm{T}}\mathbb{S}\boldsymbol{n}_2\right)\boldsymbol{n}_1.
\end{aligned}$$

The final step is to eliminate $\boldsymbol{n}_3$ from the equations. This elimination is accomplished by noting that

$$\mathbb{S}\boldsymbol{x} = (\boldsymbol{n}_1^{\mathrm{T}}\mathbb{S}\boldsymbol{x})\boldsymbol{n}_1 + (\boldsymbol{n}_2^{\mathrm{T}}\mathbb{S}\boldsymbol{x})\boldsymbol{n}_2 + (\boldsymbol{n}_3^{\mathrm{T}}\mathbb{S}\boldsymbol{x})\boldsymbol{n}_3,$$

implying

$$(\boldsymbol{n}_3^{\mathrm{T}}\mathbb{S}\boldsymbol{x})\boldsymbol{n}_3 = \mathbb{S}\boldsymbol{x} - (\boldsymbol{n}_1^{\mathrm{T}}\mathbb{S}\boldsymbol{x})\boldsymbol{n}_1 - (\boldsymbol{n}_2^{\mathrm{T}}\mathbb{S}\boldsymbol{x})\boldsymbol{n}_2.$$

Take the equation for $\dot{\boldsymbol{n}}_1$,

$$\begin{aligned}
\dot{\boldsymbol{n}}_1 &= \boldsymbol{\Omega}\times\boldsymbol{n}_1 + \Lambda\big(\boldsymbol{n}_3^{\mathrm{T}}\mathbb{S}\boldsymbol{n}_1\big)\boldsymbol{n}_3 + \frac{K-\Lambda}{K\Lambda-1}\big(\boldsymbol{n}_1^{\mathrm{T}}\mathbb{S}\boldsymbol{n}_2\big)\boldsymbol{n}_2 \\
&= \boldsymbol{\Omega}\times\boldsymbol{n}_1 + \Lambda\big(\mathbb{S}\boldsymbol{n}_1 - (\boldsymbol{n}_1^{\mathrm{T}}\mathbb{S}\boldsymbol{n}_1)\boldsymbol{n}_1 - (\boldsymbol{n}_2^{\mathrm{T}}\mathbb{S}\boldsymbol{n}_1)\boldsymbol{n}_2\big) + \frac{K-\Lambda}{K\Lambda-1}\big(\boldsymbol{n}_1^{\mathrm{T}}\mathbb{S}\boldsymbol{n}_2\big)\boldsymbol{n}_2 \\
&= \boldsymbol{\Omega}\times\boldsymbol{n}_1 + \Lambda\big(\mathbb{S}\boldsymbol{n}_1 - (\boldsymbol{n}_1^{\mathrm{T}}\mathbb{S}\boldsymbol{n}_1)\boldsymbol{n}_1\big) + \frac{K-\Lambda-\Lambda(K\Lambda-1)}{K\Lambda-1}\big(\boldsymbol{n}_1^{\mathrm{T}}\mathbb{S}\boldsymbol{n}_2\big)\boldsymbol{n}_2 \\
&= \boldsymbol{\Omega}\times\boldsymbol{n}_1 + \Lambda\big(\mathbb{S}\boldsymbol{n}_1 - (\boldsymbol{n}_1^{\mathrm{T}}\mathbb{S}\boldsymbol{n}_1)\boldsymbol{n}_1\big) + \frac{K(1-\Lambda^2)}{K\Lambda-1}\big(\boldsymbol{n}_1^{\mathrm{T}}\mathbb{S}\boldsymbol{n}_2\big)\boldsymbol{n}_2.
\end{aligned}$$

In the same fashion, we find for $\dot{\boldsymbol{n}}_2$,

$$\begin{aligned}
\dot{\boldsymbol{n}}_2 &= \boldsymbol{\Omega}\times\boldsymbol{n}_2 + K\big(\boldsymbol{n}_2^{\mathrm{T}}\mathbb{S}\boldsymbol{n}_3\big)\boldsymbol{n}_3 - \frac{K-\Lambda}{K\Lambda-1}\big(\boldsymbol{n}_1^{\mathrm{T}}\mathbb{S}\boldsymbol{n}_2\big)\boldsymbol{n}_1 \\
&= \boldsymbol{\Omega}\times\boldsymbol{n}_2 + K\big(\mathbb{S}\boldsymbol{n}_2 - (\boldsymbol{n}_1^{\mathrm{T}}\mathbb{S}\boldsymbol{n}_2)\boldsymbol{n}_1 - (\boldsymbol{n}_2^{\mathrm{T}}\mathbb{S}\boldsymbol{n}_2)\boldsymbol{n}_2\big) - \frac{K-\Lambda}{K\Lambda-1}\big(\boldsymbol{n}_1^{\mathrm{T}}\mathbb{S}\boldsymbol{n}_2\big)\boldsymbol{n}_1 \\
&= \boldsymbol{\Omega}\times\boldsymbol{n}_2 + K\big(\mathbb{S}\boldsymbol{n}_2 - (\boldsymbol{n}_2^{\mathrm{T}}\mathbb{S}\boldsymbol{n}_2)\boldsymbol{n}_2\big) - \frac{K-\Lambda+K(K\Lambda-1)}{K\Lambda-1}\big(\boldsymbol{n}_1^{\mathrm{T}}\mathbb{S}\boldsymbol{n}_2\big)\boldsymbol{n}_1 \\
&= \boldsymbol{\Omega}\times\boldsymbol{n}_2 + K\big(\mathbb{S}\boldsymbol{n}_2 - (\boldsymbol{n}_2^{\mathrm{T}}\mathbb{S}\boldsymbol{n}_2)\boldsymbol{n}_2\big) + \frac{\Lambda(1-K^2)}{K\Lambda-1}\big(\boldsymbol{n}_1^{\mathrm{T}}\mathbb{S}\boldsymbol{n}_2\big)\boldsymbol{n}_1.
\end{aligned}$$

In most places in this thesis, I write the cross product with $\boldsymbol{\Omega}$ as the matrix product with $\mathbb{O}$ instead. We also rename $\boldsymbol{n} = \boldsymbol{n}_1$ and $\boldsymbol{p} = \boldsymbol{n}_2$:

$$\begin{aligned}
\dot{\boldsymbol{n}} &= \mathbb{O}\boldsymbol{n} + \Lambda\big(\mathbb{S}\boldsymbol{n} - (\boldsymbol{n}^{\mathrm{T}}\mathbb{S}\boldsymbol{n})\boldsymbol{n}\big) + \frac{K(1-\Lambda^2)}{K\Lambda-1}\big(\boldsymbol{n}^{\mathrm{T}}\mathbb{S}\boldsymbol{p}\big)\boldsymbol{p}, \\
\dot{\boldsymbol{p}} &= \mathbb{O}\boldsymbol{p} + K\big(\mathbb{S}\boldsymbol{p} - (\boldsymbol{p}^{\mathrm{T}}\mathbb{S}\boldsymbol{p})\boldsymbol{p}\big) + \frac{\Lambda(1-K^2)}{K\Lambda-1}\big(\boldsymbol{n}^{\mathrm{T}}\mathbb{S}\boldsymbol{p}\big)\boldsymbol{n}
\end{aligned}$$

In terms of the aspect ratios λ and κ the equations read

$$\begin{aligned}
\dot{\boldsymbol{n}} &= \mathbb{O}\boldsymbol{n} + \frac{\lambda^2-1}{\lambda^2+1}\big(\mathbb{S}\boldsymbol{n} - \boldsymbol{n}^{\mathrm{T}}\mathbb{S}\boldsymbol{n})\boldsymbol{n}\big) + \frac{2\lambda^2(1-\kappa^2)}{(\lambda^2+\kappa^2)(\lambda^2+1)}(\boldsymbol{n}^{\mathrm{T}}\mathbb{S}\boldsymbol{p})\boldsymbol{p}, \\
\dot{\boldsymbol{p}} &= \mathbb{O}\boldsymbol{p} + \frac{\kappa^2-1}{\kappa^2+1}\big(\mathbb{S}\boldsymbol{p} - \boldsymbol{p}^{\mathrm{T}}\mathbb{S}\boldsymbol{p})\boldsymbol{p}\big) + \frac{2\kappa^2(1-\lambda^2)}{(\kappa^2+\lambda^2)(\kappa^2+1)}(\boldsymbol{n}^{\mathrm{T}}\mathbb{S}\boldsymbol{p})\boldsymbol{n}.
\end{aligned}$$

This equation is identical to Eq. (3.1). It is further discussed in Section 3.2.

B Fokker-Planck equation on the sphere

The Fokker-Planck equation takes the familiar form in cartesian coordinates:

$$\partial_t P = -\nabla \cdot [\boldsymbol{v} P] + \mathscr{D} \nabla^2 P. \tag{B.1}$$

This equation is usually called the diffusion equation, because for a particle advected by the *drift* $\boldsymbol{v}$ and randomly kicked around with the *diffusion constant* $\mathscr{D}$, Eq. (B.1) governs the evolution of the probability $P(\boldsymbol{x}, t)$ of finding the particle at $\boldsymbol{x}$ at time t. As it is written, Eq. (B.1) is valid for isotropic and homogenous diffusion. In other words, the random kicks do not depend on the position of the particle, and they are equally probable in all directions.

When the particle does not move in cartesian space, but confined to the unit sphere there are two plausible ways of defining a Fokker-Planck equation. The first, and perhaps most straightforward, is to find out how to represent the operator ∇ on the surface of the sphere, and use Eq. (B.1) directly. The second way is to derive the Fokker-Planck equation from the microscopic equations of motion, as described for instance in the book by van Kampen [23]. This approach has certain advantages. First, it allows for the case that the random kicks have non-standard statistics. For instance, the random kicks may be stronger in one direction than another. The random kicks may also depend on the current state of the system $\boldsymbol{x}$. Deriving the Fokker-Planck equation will automatically give the correct amendments to Eq. (B.1). Second, the calculation gives an explicit expression for the diffusion constant $\mathscr{D}$. In the case of thermal diffusion, there exists a fluctuation-dissipation theorem that relates $\mathscr{D}$ to the temperature and fluid drag. But what if the source of noise is different? For example, if the random kicks originate in random fluctuations of the flow gradients, what is $\mathscr{D}$?

In the case of isotropic and homogenous noise, the two approaches must clearly be equivalent. In this appendix I will derive the Fokker-Planck equation for a unit vector $\boldsymbol{n}$ subject to random rotations $\boldsymbol{\omega}$, expressed in cartesian coordinates. I will show that the equation so obtained is equivalent to the angular portion of

the Laplacian in spherical coordinates.

In the following ∇ represents the usual gradient in cartesian space, and $\partial_{\boldsymbol{n}}$ denotes the surface gradient confined to the sphere. Then in the end, $\partial_{\boldsymbol{n}}$ and $\partial^2_{\boldsymbol{n}}$ will be replace ∇ and ∇^2 in Eq. (B.1) to give the correct Fokker-Planck equation on the unit sphere.

B.1 The standard way

The surface gradient on a sphere is defined as the projection of ∇ onto the surface $|\boldsymbol{n}| = 1$:

$$\partial_{\boldsymbol{n}} = (\mathbb{I} - \boldsymbol{n}\boldsymbol{n}^{\mathrm{T}})\nabla. \tag{B.2}$$

The interpretation is straightforward. Take the gradient ∇f, which is a vector, and subtract the component in the outwards direction from the sphere, $-\boldsymbol{n}(\boldsymbol{n}\cdot\nabla f)$. The result is the portion of the gradient vector tangent to the sphere at $\boldsymbol{n}$.

In the following derivations I will often use index notation with implicit summation over repeated indices, in which Eq. (B.2) reads

$$(\partial_{\boldsymbol{n}})_i = (\delta_{ij} - n_i n_j)\partial_j.$$

Here $\partial_j \equiv \partial/\partial n_j$, and δ_{ij} is the Kronecker symbol. We proceed and also compute $\partial^2_{\boldsymbol{n}}$ on component form:

$$\begin{aligned}
\partial^2_{\boldsymbol{n}} &= (\partial_{\boldsymbol{n}})_i(\partial_{\boldsymbol{n}})_i \\
&= (\delta_{ij} - n_i n_j)\partial_j(\delta_{ik} - n_i n_k)\partial_k \\
&= \underbrace{\delta_{ij}\partial_j\delta_{ik}\partial_k}_{\partial_i\partial_i} - \underbrace{\delta_{ij}\partial_j n_i n_k\partial_k}_{A} - \underbrace{n_i n_j\partial_j\delta_{ik}\partial_k}_{-n_i n_j\partial_i\partial_j} + \underbrace{n_i n_j\partial_j n_i n_k\partial_k}_{B}
\end{aligned} \tag{B.3}$$

In order to compute A and B we evaluate product derivatives according to

$$\partial_i f g = \partial_i[f]g + f\,\partial_i[g] + f g\,\partial_i,$$

where the last term is kept because we are manipulating an operator. Further, we use that

$$\begin{aligned}\partial_i n_j &= \delta_{ij},\\ n_i n_i &= 1,\\ \delta_{ii} &= 3,\end{aligned}$$

where the number 3 is the number of spatial dimensions. Continuing,

$$\begin{aligned}A &= -\delta_{ij}\partial_j n_i n_k \partial_k\\ &= -\partial_i n_i n_k \partial_k\\ &= -(\delta_{ii} n_k \partial_k + n_i \delta_{ik}\partial_k + n_i n_k \partial_i \partial_k)\\ &= -(3 n_k \partial_k + n_i \partial_i + n_i n_k \partial_i \partial_k)\\ B &= n_i n_j \partial_j n_i n_k \partial_k\\ &= n_i n_j \delta_{ij} n_k \partial_k + n_i n_j n_i \delta_{jk}\partial_k + n_i n_j n_i n_k \partial_j \partial_k\\ &= n_k \partial_k + n_k \partial_k + n_j n_k \partial_j \partial_k\\ &= 2 n_k \partial_k + n_j n_k \partial_j \partial_k\end{aligned}$$

Upon inserting A and B into Eq. (B.3) we obtain

$$\partial_{\boldsymbol{n}}^2 = \partial_i \partial_i - n_i n_j \partial_i \partial_j - 2 n_i \partial_i. \tag{B.4}$$

This is the result to which we will compare the result of our subsequent derivations.

B.1.1 Relation to Laplace operator in spherical coordinates

I now show that $\partial_{\boldsymbol{n}}^2$ corresponds to the angular part of the Laplace operator, as written in spherical coordinates (r, θ, φ):

$$\nabla^2 = \frac{1}{r^2}\partial_r r^2 \partial_r + \frac{1}{r^2 \sin\theta}\partial_\theta \sin\theta \partial_\theta + \frac{1}{r^2 \sin^2\theta}\partial_\varphi^2.$$

Expand derivatives in r and put $r = 1$ to obtain

$$\nabla^2 = \partial_r^2 + 2\partial_r + \frac{1}{\sin\theta}\partial_\theta \sin\theta \partial_\theta + \frac{1}{\sin^2\theta}\partial_\varphi^2.$$

Now we use this relation to express $\partial_{\boldsymbol{n}}^2$ in spherical coordinates:

$$\begin{aligned}\partial_{\boldsymbol{n}}^2 &= \nabla^2 - n_i n_j \partial_i \partial_j - 2 n_i \partial_i \\ &= \nabla^2 - \big((\boldsymbol{n}\cdot\nabla)^2 - \boldsymbol{n}\cdot\nabla\big) - 2\boldsymbol{n}\cdot\nabla \\ &= \nabla^2 - (\boldsymbol{n}\cdot\nabla)^2 - \boldsymbol{n}\cdot\nabla\end{aligned}$$

We know that $\boldsymbol{n}\cdot\nabla = r\,\partial_r$ in spherical coordinates:

$$= \nabla^2 - (r\,\partial_r)^2 - r\,\partial_r$$

And like above, expand derivatives in r and put $r = 1$ to obtain

$$\begin{aligned}&= \nabla^2 - \partial_r^2 - 2\partial_r \\ &= \frac{1}{\sin\theta}\partial_\theta \sin\theta\,\partial_\theta + \frac{1}{\sin^2\theta}\partial_\varphi^2. \qquad \blacksquare\end{aligned}$$

B.1.2 Relation to angular momentum operators

Another common way of writing down differential operators on the surface of a sphere is to use the orbital angular momentum operator $\hat{\boldsymbol{L}}$ [43]:

$$\hat{\boldsymbol{L}} = -i\,\boldsymbol{n}\times\nabla,$$

from which it follows

$$-i\,\boldsymbol{n}\times\hat{\boldsymbol{L}} = (\mathbb{I} - \boldsymbol{n}\boldsymbol{n}^{\mathrm{T}})\nabla = \partial_{\boldsymbol{n}}, \tag{B.5}$$

$$-\hat{\boldsymbol{L}}^2 = (\mathbb{I} - \boldsymbol{n}\boldsymbol{n}^{\mathrm{T}})\nabla\cdot(\mathbb{I} - \boldsymbol{n}\boldsymbol{n}^{\mathrm{T}})\nabla = \partial_{\boldsymbol{n}}^2. \tag{B.6}$$

There are several variants in literature, for example Doi & Edwards [44] defines the rotation operator $\mathscr{R} = i\,\hat{\boldsymbol{L}}$. Although the prefactors change, the idea is always the same. The relations Eq. (B.5) and Eq. (B.6) are straightforward to prove by calculation.

Proof of Eq. (B.5)

$$\begin{aligned}-i(\boldsymbol{n}\times\hat{\boldsymbol{L}})_i &= i^2 \varepsilon_{ijk} n_j \varepsilon_{kpq} n_p \partial_q \\ &= -(\delta_{ip}\delta_{jq} - \delta_{iq}\delta_{jp}) n_j n_p \partial_q \\ &= -(n_q n_i \partial_q - n_p n_p \partial_i) \\ &= (\delta_{iq} - n_i n_q)\partial_q \qquad \blacksquare\end{aligned}$$

Proof of Eq. (B.6)

$$\begin{aligned}
-\hat{L}_i\hat{L}_i &= \varepsilon_{ijk}n_j\partial_k\varepsilon_{ipq}n_p\partial_q \\
&= (\delta_{jp}\delta_{kq}-\delta_{jq}\delta_{kp})n_j\partial_k n_p\partial_q \\
&= n_j\partial_k n_j\partial_k - n_j\partial_k n_k\partial_j \\
&= \partial_k\partial_k + n_j\partial_j - n_j n_k\partial_j\partial_k - 3n_j\partial_j \\
&= \partial_k\partial_k - n_i n_j\partial_i\partial_j - 2n_i\partial_i
\end{aligned}$$ ■

B.2 Derivation from equations of motion

We now turn to the derivation of the Fokker-Planck equation from the equation of motion of a single particle. The general procedure is described in detail in the book by van Kampen [23], here I simply state the recipe: for a dynamical system of several variables we compute the drift for each variable n_i over a short time interval δt as

$$a_i^{(1)} = \lim_{\delta t\to 0}\frac{\langle\delta n_i\rangle}{\delta t}, \tag{B.7}$$

and the diffusion covariance matrix between all combinations of variables:

$$a_{ij}^{(2)} = \lim_{\delta t\to 0}\frac{\langle(\delta n_i)(\delta n_j)\rangle}{\delta t}. \tag{B.8}$$

The resulting Fokker-Planck equation for $P(\boldsymbol{n},t)$ is

$$\frac{\partial P}{\partial t} = -\frac{\partial}{\partial n_i}\left[a_i^{(1)}P\right] + \frac{1}{2}\frac{\partial^2}{\partial n_i\partial n_j}\left[a_{ij}^{(2)}P\right].$$

B.2.1 Formulas for the displacements $\delta\boldsymbol{n}$

We start with the equation of motion for the vector $\boldsymbol{n}(t)$. Its time evolution is governed by

$$\dot{\boldsymbol{n}} = \boldsymbol{f}(\boldsymbol{n}(t),t).$$

In general, the displacement $\delta \boldsymbol{n}$ after a small time δt is

$$\begin{aligned}\delta \boldsymbol{n} &= \boldsymbol{n}(\delta t) - \boldsymbol{n}_0 \\ &= \int_0^{\delta t} \mathrm{d}t_1 \boldsymbol{f}(\boldsymbol{n}(t_1), t_1) \\ &= \int_0^{\delta t} \mathrm{d}t_1 \boldsymbol{f}\left(\boldsymbol{n}_0 + \int_0^{t_1} \mathrm{d}t_2 \boldsymbol{f}(\boldsymbol{n}(t_2), t_2), t_1\right) \\ &= \int_0^{\delta t} \mathrm{d}t_1 \boldsymbol{f}(\boldsymbol{n}_0, t_1) + \int_0^{\delta t} \mathrm{d}t_1 \mathbb{F}(\boldsymbol{n}_0, t_1) \int_0^{t_1} \mathrm{d}t_2 \boldsymbol{f}(\boldsymbol{n}_0, t_2) + \ldots \end{aligned} \tag{B.9}$$

where $\mathbb{F}$ denotes the matrix of derivates

$$\mathbb{F}(\boldsymbol{n}, t) = \frac{\mathrm{d}\boldsymbol{f}}{\mathrm{d}\boldsymbol{n}}.$$

The function $\boldsymbol{f}(\boldsymbol{n}, t)$ may in general include both deterministic terms and terms including Gaussian white noise. The deterministic part of $\boldsymbol{f}$ results in the *drift* $\boldsymbol{v}$ in Eq. (B.1). In the following we will assume that $\boldsymbol{f}$ contains no deterministic terms in order to focus on the diffusion operator.

B.2.2 Random angular velocities

For a particle orientation $\boldsymbol{n}$ driven by only random angular velocities

$$\boldsymbol{f}(\boldsymbol{n}, t) = \boldsymbol{\omega}(t) \times \boldsymbol{n}, \qquad \begin{aligned} \langle \omega_i(t) \rangle &= 0, \\ \langle \omega_i(0) \omega_j(t) \rangle &= 2\mathscr{D} \delta_{ij} \delta(t), \end{aligned} \tag{B.10}$$

where I anticipate the diffusion constant $\mathscr{D}$. For mathematical convenience, rewrite the cross product in terms of an antisymmetric matrix $\mathbb{O}$, such that $\mathbb{O}\boldsymbol{n} = \boldsymbol{\omega} \times \boldsymbol{n}$, meaning

$$\begin{aligned} \boldsymbol{f}(\boldsymbol{n}, t) &= \mathbb{O}(t)\boldsymbol{n}, \\ \mathbb{F} &= \mathbb{O}, \end{aligned}$$

where $\mathbb{O}$ is defined by

$$O_{ij} = -\varepsilon_{ijp} \omega_p,$$

and has statistics

$$\begin{aligned}\left\langle O_{ij}(t)\right\rangle &= 0,\\ \left\langle O_{ij}(0)O_{kl}(t)\right\rangle &= \left\langle \varepsilon_{ijp}\omega_p(0)\varepsilon_{klq}\omega_q(t)\right\rangle\\ &= \varepsilon_{ijp}\varepsilon_{klq}\left\langle \omega_p(0)\omega_q(t)\right\rangle\\ &= 2\mathscr{D}\varepsilon_{ijp}\varepsilon_{klq}\delta_{pq}\delta(t)\\ &= 2\mathscr{D}(\delta_{ik}\delta_{jl}-\delta_{il}\delta_{jk})\delta(t).\end{aligned}$$

By insertion of $\boldsymbol{f}$ and $\mathbb{F}$ into Eq. (B.9) we may now compute the average displacement. In order to ease the notation I call the initial condition $\boldsymbol{n}_0$ simply $\boldsymbol{n}$.

$$\begin{aligned}\langle\delta\boldsymbol{n}\rangle &= \int_0^{\delta t}\mathrm{d}t_1\left\langle\mathbb{O}(t_1)\right\rangle\boldsymbol{n}+\int_0^{\delta t}\mathrm{d}t_1\int_0^{t_1}\mathrm{d}t_2\left\langle\mathbb{O}(t_1)\mathbb{O}(t_2)\right\rangle\boldsymbol{n}+\mathscr{O}(\delta t^2)\\ &= \mathscr{D}\int_0^{\delta t}\mathrm{d}t_1(\mathbb{I}-3\mathbb{I})\boldsymbol{n}+\mathscr{O}(\delta t^2)\\ &= -2\mathscr{D}\delta t\,\boldsymbol{n}+\mathscr{O}(\delta t^2).\end{aligned}$$

Similarly we obtain the second moments of the displacements $\delta\boldsymbol{n}$ up to $\mathscr{O}(\delta t)$:

$$\begin{aligned}\langle\delta\boldsymbol{n}\delta\boldsymbol{n}^{\mathrm{T}}\rangle &= \int_0^{\delta t}\mathrm{d}t_1\int_0^{\delta t}\mathrm{d}t_2\left\langle\boldsymbol{f}(\boldsymbol{n},t_1)\boldsymbol{f}^{\mathrm{T}}(\boldsymbol{n},t_2)\right\rangle+\mathscr{O}(\delta t^2)\\ &= \int_0^{\delta t}\mathrm{d}t_1\int_0^{\delta t}\mathrm{d}t_2\left\langle\mathbb{O}(t_1)\boldsymbol{n}\boldsymbol{n}^{\mathrm{T}}\mathbb{O}(t_2)^{\mathrm{T}}\right\rangle+\mathscr{O}(\delta t^2).\end{aligned}$$

Insert the statistics for $\mathbb{O}$ to obtain

$$\begin{aligned}&= 2\mathscr{D}\int_0^{\delta t}\mathrm{d}t_1\int_0^{\delta t}\mathrm{d}t_2\delta(t_1-t_2)(\mathbb{I}|\boldsymbol{n}|^2-\boldsymbol{n}\boldsymbol{n}^{\mathrm{T}})+\mathscr{O}(\delta t^2)\\ &= 2\mathscr{D}\delta t(\mathbb{I}|\boldsymbol{n}|^2-\boldsymbol{n}\boldsymbol{n}^{\mathrm{T}})+\mathscr{O}(\delta t^2).\end{aligned}\tag{B.11}$$

At this point we must refrain from using the fact that, eventually, $|\boldsymbol{n}|=1$. The equation of motion (B.10) only implies that $|\boldsymbol{n}|$ is conserved, not at which value. As a direct consequence the mean

square displacements (B.11) ensure that the random jumps also conserve $|\boldsymbol{n}|$. If we were to change this fact by letting $|\boldsymbol{n}| = 1$, while clearly the term $-\boldsymbol{n}\boldsymbol{n}^{\mathrm{T}}$ is proportional to $|\boldsymbol{n}|^2$, the random jumps will no longer conserve $|\boldsymbol{n}|$. The resulting Fokker-Planck equation would contain terms describing this erronous flux normal to the unit sphere[1]. Now, however, we conclude the derivation of the correct Fokker-Planck equation.

By the definitions in Eqns. (B.7) and (B.8), the coefficients $a^{(1)}$ and $a^{(2)}$ are

$$\begin{aligned} a_i^{(1)} &= \lim_{\delta t \to 0} \left\langle \frac{\delta n_i}{\delta t} \right\rangle = -2\mathscr{D} n_i, \\ a_{ij}^{(2)} &= \lim_{\delta t \to 0} \left\langle \frac{\delta n_i \delta n_j}{\delta t} \right\rangle = 2\mathscr{D}(\delta_{ij} n_k n_k - n_i n_j). \end{aligned} \tag{B.12}$$

The Fokker-Planck equation for the orientational distribution is then

$$\begin{aligned} \frac{\partial P}{\partial t} &= -\partial_i \left[a_i^{(1)} P \right] + \frac{1}{2} \partial_i \partial_j \left[a_{ij}^{(2)} P \right] \\ &= 2\mathscr{D} \partial_i [n_i P] + \mathscr{D} \partial_i \partial_j \left[(\delta_{ij} n_k n_k - n_i n_j) P \right]. \end{aligned} \tag{B.13}$$

This equation should correspond to the diffusion equation Eq. (B.1), with the drift $\boldsymbol{v} = 0$ and the spherical surface Laplacian Eq. (B.4) substituted for ∇^2. In order to make the comparison to $\partial_{\boldsymbol{n}}^2$ in Eq. (B.4), we remove $\mathscr{D}$ and expand the product derivatives of the operator in the right hand side of Eq. (B.13).

$$\begin{aligned} & 2\partial_i n_i + \partial_i \partial_j \left(\delta_{ij} n_k n_k - n_i n_j \right) \\ &= 2\delta_{ii} + 2n_i \partial_i + \partial_i [2\delta_{ik} n_k + n_k n_k \partial_i] \\ &\quad - \partial_i \left[\delta_{ij} n_j + n_i \delta_{jj} + n_i n_j \partial_j \right] \\ &= 6 + 2n_i \partial_i + 2\delta_{kk} + 2n_i \partial_i + 2\delta_{ik} n_k \partial_i + n_k n_k \partial_i \partial_i \\ &\quad - \delta_{jj} - n_j \partial_j - 3\delta_{ii} - 3n_i \partial_i \\ &\quad - \delta_{ii} n_j \partial_j - n_i \delta_{ij} \partial_j - n_i n_j \partial_i \partial_j \end{aligned}$$

[1] In fact, using $|\boldsymbol{n}| = 1$ at this point leads to the Fokker-Planck equation $\partial_t P = \nabla \cdot (\mathbb{I} - \boldsymbol{n}\boldsymbol{n}^{\mathrm{T}}) \nabla P$.

Here we may use $|\boldsymbol{n}|=1$, when it occurs outside derivatives:

$$\begin{aligned}
&= 6 + 2n_i\partial_i + 6 + 2n_i\partial_i + 2n_i\partial_i + \partial_i\partial_i \\
&\quad -3 - n_j\partial_j - 9 - 3n_i\partial_i \\
&\quad -3n_j\partial_j - n_i\partial_i - n_i n_j \partial_i\partial_j \\
&= \partial_i\partial_i - n_i n_j\partial_i\partial_j - 2n_i\partial_i = \partial^2_{\boldsymbol{n}}.
\end{aligned}$$

This concludes the derivation of the Fokker-Planck equation for a vector $\boldsymbol{n}$ undergoing random rotations.

B.2.3 Remark on drift terms

In the above we neglected the deterministic terms of $\boldsymbol{f}(\boldsymbol{n},t)$, in order to derive the correct diffusion operator. If we allow for a deterministic term in Eq. (B.10), the equation of motion becomes

$$\boldsymbol{f}(\boldsymbol{n},t) = \boldsymbol{\Omega}\times\boldsymbol{n} + \boldsymbol{\omega}(t)\times\boldsymbol{n}, \qquad \begin{aligned} \langle\omega_i(t)\rangle &= 0, \\ \langle\omega_i(0)\omega_j(t)\rangle &= 2\mathscr{D}\delta_{ij}\delta(t). \end{aligned} \tag{B.14}$$

The deterministic term transfers directly to the average displacement

$$\langle\delta\boldsymbol{n}\rangle = (\boldsymbol{\Omega}\times\boldsymbol{n} - 2\mathscr{D}\boldsymbol{n})\delta t + \mathscr{O}(\delta t^2).$$

The corresponding Fokker-Planck equation thus has a drift term

$$\partial_t P = -\nabla\cdot(\boldsymbol{\Omega}\times\boldsymbol{n}P) + \partial^2_{\boldsymbol{n}}P. \tag{B.15}$$

Now, this may seem to contradict what I stated above: the Fokker-Planck equation on the sphere is Eq. (B.1) with $\partial_{\boldsymbol{n}}$ substituted for ∇. But the contradiction is only apparent. We may replace ∇ with $\partial_{\boldsymbol{n}}$ in Eq. (B.15) without any change, because

$$\begin{aligned}
(\nabla - \partial_{\boldsymbol{n}})\cdot[\boldsymbol{\Omega}\times\boldsymbol{n}P] &= n_i n_j \partial_j \varepsilon_{ikl}\Omega_k n_l P \\
&= n_i n_j \varepsilon_{ikl}[\partial_j\Omega_k]n_l P + n_i n_j \varepsilon_{ikl}\Omega_k \delta_{jl} P \\
&\quad + n_i n_j \varepsilon_{ikl}\Omega_k n_l \partial_j P \\
&= 0.
\end{aligned}$$

Therefore Eq. (B.15) may be written as

$$\partial_t P = -\partial_{\boldsymbol{n}} \cdot (\boldsymbol{\Omega} \times \boldsymbol{n} P) + \partial_{\boldsymbol{n}}^2 P, \tag{B.16}$$

or, by relations Eq. (B.5) and Eq. (B.6)

$$= i\boldsymbol{n} \times \hat{\boldsymbol{L}}(\boldsymbol{\Omega} \times \boldsymbol{n} P) - \hat{\boldsymbol{L}}^2 P. \tag{B.17}$$

B.3 Orientational diffusion in a random flow

In the introduction of this appendix I argued that the explicit derivation of the Fokker-Planck equation gives an expression for $\mathscr{D}$. I will briefly illustrate this by computing the diffusion constant for an axisymmetric particle in a random flow. The calculation proceeds exactly as shown in detail above, but here we will use the Jeffery equation for $\boldsymbol{f}(\boldsymbol{n}, t)$:

$$\begin{aligned}
\boldsymbol{f}(\boldsymbol{n}, t) &= \mathbb{O}\boldsymbol{n} + \Lambda\left(\mathbb{S}\boldsymbol{n} - \boldsymbol{n}\boldsymbol{n}^{\mathrm{T}}\mathbb{S}\boldsymbol{n}\right), \\
\mathbb{F}(\boldsymbol{n}, t) &= \frac{\mathrm{d}\boldsymbol{f}}{\mathrm{d}\boldsymbol{n}} \\
&= \mathbb{O} + \Lambda(\mathbb{S} - \mathbb{I}\boldsymbol{n}^{\mathrm{T}}\mathbb{S}\boldsymbol{n} - 2\boldsymbol{n}\boldsymbol{n}^{\mathrm{T}}\mathbb{S}) \\
&= \mathbb{O} + \Lambda((\mathbb{I} - 2\boldsymbol{n}\boldsymbol{n}^{\mathrm{T}})\mathbb{S} - \mathbb{I}\boldsymbol{n}^{\mathrm{T}}\mathbb{S}\boldsymbol{n})
\end{aligned} \tag{B.18}$$

Here $\mathbb{A} = \mathbb{O} + \mathbb{S}$ is the matrix of flow gradients. The relevant gradient statistics of an homogenous, isotropic, and incompressible flow are

$$\begin{aligned}
\left\langle \mathbb{O}_{ij}(0)\mathbb{O}_{kl}(t) \right\rangle &= -\frac{\mathrm{Tr}\langle \mathbb{A}^{\mathrm{T}}\mathbb{A} \rangle}{12}\left(\delta_{ik}\delta_{jl} - \delta_{il}\delta_{jk}\right)\delta(t) \\
\left\langle \mathbb{S}_{ij}(0)\mathbb{S}_{kl}(t) \right\rangle &= \frac{\mathrm{Tr}\langle \mathbb{A}^{\mathrm{T}}\mathbb{A} \rangle}{60}\left(-2\delta_{ij}\delta_{kl} + 3\delta_{ik}\delta_{jl} + 3\delta_{il}\delta_{jk}\right)\delta(t) \\
\left\langle \mathbb{S}_{ij}(0)\mathbb{O}_{kl}(t) \right\rangle &= 0 \\
\left\langle \mathbb{S}_{ij}(t) \right\rangle &= 0 \\
\left\langle \mathbb{O}_{ij}(t) \right\rangle &= 0
\end{aligned} \tag{B.19}$$

Inserting Eq. (B.18) in Eq. (B.9), and taking averages leads to the Fokker-Planck equation coefficients

$$\boldsymbol{a}^{(1)} = \frac{1}{2}\left\langle \mathbb{O}\mathbb{O}\boldsymbol{n} + \Lambda^2\left(\mathbb{S}\mathbb{S}\boldsymbol{n} - 2\boldsymbol{n}\boldsymbol{n}^{\mathrm{T}}\mathbb{S}\mathbb{S}\boldsymbol{n} - 2(\boldsymbol{n}^{\mathrm{T}}\mathbb{S}\boldsymbol{n})\mathbb{S}\boldsymbol{n} + 3(\boldsymbol{n}^{\mathrm{T}}\mathbb{S}\boldsymbol{n})^2\boldsymbol{n}\right)\right\rangle$$
$$\mathbb{A}^{(2)} = \left\langle -\mathbb{O}\boldsymbol{n}\boldsymbol{n}^{\mathrm{T}}\mathbb{O} + \Lambda^2\left(\mathbb{S}\boldsymbol{n}\boldsymbol{n}^{\mathrm{T}}\mathbb{S} - (\boldsymbol{n}^{\mathrm{T}}\mathbb{S}\boldsymbol{n})(\mathbb{S}\boldsymbol{n}\boldsymbol{n}^{\mathrm{T}} + \boldsymbol{n}\boldsymbol{n}^{\mathrm{T}}\mathbb{S} - \boldsymbol{n}\boldsymbol{n}^{\mathrm{T}}(\boldsymbol{n}^{\mathrm{T}}\mathbb{S}\boldsymbol{n}))\right)\right\rangle$$

And finally, inserting the statistics for a homogenous, isotropic and incompressible flow Eq. (B.19) contracts the Fokker-Planck coefficients to

$$\boldsymbol{a}^{(1)} = -\frac{\mathrm{Tr}\langle\mathbb{A}^{\mathrm{T}}\mathbb{A}\rangle}{60}\left(5+3\Lambda^2\right)\boldsymbol{n}$$
$$\mathbb{A}^{(2)} = \frac{\mathrm{Tr}\langle\mathbb{A}^{\mathrm{T}}\mathbb{A}\rangle}{60}\left(5+3\Lambda^2\right)\left(\mathbb{I}|\boldsymbol{n}|^2 - \boldsymbol{n}\boldsymbol{n}^{\mathrm{T}}\right).$$

By comparison with Eq. (B.12) we conclude that the diffusion constant for a non-spherical particle in a random flow is

$$\mathscr{D} = \frac{\mathrm{Tr}\langle\mathbb{A}^{\mathrm{T}}\mathbb{A}\rangle}{120}\left(5+3\Lambda^2\right).$$

C Numerical orientational distributions

In this Appendix I explain how to compute numerical approximations of the solutions to the Fokker-Planck equation on the sphere. The method works for arbitrary polynomial drift and diffusion terms, however it was developed specifically for the drift term described in Paper B. The content of this Appendix is similar to the Appendix of Paper B.

The method of spectral decomposition is not new. As early as 1955, Scheraga [45] computed the orientational distribution of an axisymmatric particle in a simple shear flow up to $\mathrm{Pe} = 60$ with this method. The matrix elements needed for that calculation were computed in 1938 by Peterlin [46]. Here I explain the method and give a procedure to compute the matrix elements of any polynomial operator on the sphere. In particular we employ this method on the Fokker-Planck equation in Paper B.

C.1 Spectral decomposition of equation

We start from the Fokker-Planck equation governing the evolution of the probability density $P(\boldsymbol{n}, t)$ of finding a particle with orientation vector $\boldsymbol{n}$ at time t:

$$\partial_t P(\boldsymbol{n}, t) = -\partial_{\boldsymbol{n}} [\dot{\boldsymbol{n}} P] + \mathrm{Pe}^{-1} \partial_{\boldsymbol{n}}^2 P \equiv \hat{J} P \tag{C.1}$$

with the normalisation condition

$$\int_{S_2} P(\boldsymbol{n}, t) \mathrm{d}\boldsymbol{n} = 1. \tag{C.2}$$

The differential operator $\partial_{\boldsymbol{n}}$ is the gradient on the sphere, defined by taking the usual gradient ∇ in R^3 projected onto the unit sphere, $\partial_{\boldsymbol{n}} \equiv (\mathbb{I} - \boldsymbol{n}\boldsymbol{n}^{\mathrm{T}})\nabla$. We approximate the solution of Eq. (C.1) by an expansion in spherical harmonics [45], the eigenfunctions of the quantum mechanical angular momentum operators, which form a complete basis on S_2. We use bra-ket notation,

$$P(\boldsymbol{n}, t) = \langle \boldsymbol{n} | P(t) \rangle = \sum_{l=0}^{\infty} \sum_{m=-l}^{l} c_l^m(t) \langle \boldsymbol{n} | l, m \rangle \tag{C.3}$$

where

$$\langle \boldsymbol{n}|l,m\rangle = Y_l^m(\boldsymbol{n}) = (-1)^m \sqrt{\frac{2l+1}{4\pi}\frac{(l-m)!}{(l+m)!}} P_l^m(\cos\theta) e^{im\varphi}. \quad \text{(C.4)}$$

We use the standard spherical harmonics defined in for example Arfken (p. 571) [47]. The functions P_l^m are the associated Legendre polynomials. We call the time-dependent coefficients for each basis function $c_l^m(t)$, and the fact that P is real-valued puts a constraint on the coefficients that

$$c_l^{-m} = (-1)^m \overline{c_l^m}, \quad \text{(C.5)}$$

where the bar denotes complex conjugation. Then Eq. (C.1) for the time evolution of the state ket $|P(t)\rangle$ reads

$$\partial_t |P(t)\rangle = \hat{J}|P(t)\rangle$$

Inserting the expansion yields

$$\sum_{l=0}^{\infty}\sum_{m=-l}^{l} \partial_t c_l^m(t)|l,m\rangle = \sum_{l=0}^{\infty}\sum_{m=-l}^{l} c_l^m(t)\hat{J}|l,m\rangle. \quad \text{(C.6)}$$

Multiplying with the bra $\langle p,q|$, and using the orthogonality of the spherical harmonics we arrive at a system of coupled ordinary differential equations for the coefficients $c_l^m(t)$

$$\dot{c}_p^q(t) = \sum_{l=0}^{\infty}\sum_{m=-l}^{l} c_l^m(t)\langle p,q|\hat{J}|l,m\rangle, \quad \text{(C.7)}$$

$$c_0^0 = \frac{1}{\sqrt{4\pi}}. \quad \text{(C.8)}$$

C.2 Computation of matrix elements

In order to solve Eq. (C.7) it remains to compute the matrix elements of the operator $\hat{J}$. This is achieved by expressing $\hat{J}$ as a combination of the angular momentum operators. How the angular momentum operators act on the spherical harmonics is well known, see for example Arfken [47].

The angular momentum operator $\hat{\boldsymbol{L}}$ is given by

$$\hat{\boldsymbol{L}} = -i\hat{\boldsymbol{n}} \times \nabla.$$

In terms of $\hat{\boldsymbol{L}}$ we have

$$\partial_{\boldsymbol{n}}^2 = (\mathbb{I} - \hat{\boldsymbol{n}}\hat{\boldsymbol{n}}^{\mathrm{T}})\nabla \cdot (\mathbb{I} - \hat{\boldsymbol{n}}\hat{\boldsymbol{n}}^{\mathrm{T}})\nabla = -\hat{\boldsymbol{L}}^2,$$

and

$$\partial_{\boldsymbol{n}} = (\mathbb{I} - \hat{\boldsymbol{n}}\hat{\boldsymbol{n}}^{\mathrm{T}})\nabla = -i\hat{\boldsymbol{n}} \times \hat{\boldsymbol{L}}.$$

The states $|l,m\rangle$ are the eigenfunctions of $\hat{\boldsymbol{L}}^2$ and $\hat{L}_3$ with eigenvalues $l(l+1)$ and m. Now, to evaluate the drift term $\partial_{\boldsymbol{n}}\dot{\boldsymbol{n}}$ we need to know how $\hat{L}_1$, $\hat{L}_2$, and $\hat{\boldsymbol{n}}$ act on $|l,m\rangle$. The first two are known through the use of ladder operators, defined by

$$\hat{L}_\pm = \hat{L}_1 \pm i\hat{L}_2 \implies \hat{L}_1 = \frac{1}{2}(\hat{L}_+ + \hat{L}_-), \quad \hat{L}_2 = -\frac{i}{2}(\hat{L}_+ - \hat{L}_-)$$

and their effect is

$$\hat{L}_\pm |l,m\rangle = \sqrt{(l \mp m)(1 + l \pm m)}\,|l, m \pm 1\rangle.$$

Next, the drift term we consider is a polynomial in $\hat{n}_1, \hat{n}_2$ and $\hat{n}_3$ (the components of $\hat{\boldsymbol{n}}$), we therefore need to evaluate the action of a monomial $\hat{n}_1^\alpha \hat{n}_2^\beta \hat{n}_3^\gamma$ on $|l,m\rangle$. Any such monomial of order $k = \alpha + \beta + \gamma$ may be written as a linear combination of spherical tensor operators of up to order k:

$$\hat{n}_1^\alpha \hat{n}_2^\beta \hat{n}_3^\gamma = \sum_{l=0}^{k} \sum_{m=-l}^{l} a_l^m(\alpha,\beta,\gamma)\hat{Y}_l^m.$$

The action of $\hat{Y}_p^q$ is computed with the Clebsch-Gordan coefficients (see for example Sakurai p.216 [48])

$$\hat{Y}_p^q |l,m\rangle = \sum_{\Delta l=-p}^{p} K(p,q,l,m,l+\Delta l, m+q)|l+\Delta l, m+q\rangle,$$

where

$$K(l_1,m_1,l_2,m_2,l,m)=\sqrt{\frac{(2l_1+1)(2l_2+1)}{4\pi(2l+1)}}\times\langle l_1 l_2;00|l_1 l_2;l0\rangle\langle l_1 l_2;m_1 m_2|l_1 l_2;l\,m\rangle$$

The Clebsch-Gordan coefficients are in the notation of Sakurai denoted $\langle l_1 l_2;m_1 m_2|l_1 l_2;l\,m\rangle$, and they are available in Mathematica by the function `ClebschGordan[l1,m1,l2,m2,l,m]`. Finally, we order the operators, so that as many terms as possible cancel before we actually begin evaluating the operators. In particular we want to reorder $\hat{n}_i$ against $\hat{L}_i$, and we make use of the commutator

$$[\hat{n}_p,\hat{L}_q]=i\varepsilon_{pqj}\hat{n}_j,$$

where ε_{ijk} is the Levi-Civita tensor.

Let us consider an example. In the special case of $\hat{J}_0=\mathrm{Pe}^{-1}\partial^2_{\boldsymbol{n}}$ (that is, $\dot{\boldsymbol{n}}=0$) we immediately see that $\hat{J}_0=-\mathrm{Pe}^{-1}\hat{\boldsymbol{L}}^2$. It follows:

$$\hat{J}_0|l,m\rangle=-\mathrm{Pe}^{-1}\hat{\boldsymbol{L}}^2|l,m\rangle=-l(l+1)\mathrm{Pe}^{-1}|l,m\rangle.$$

Knowing how $\hat{J}$ acts on $|l,m\rangle$ fully specifies Eq. (C.7) which becomes

$$\dot{c}^q_p(t)=-p(p+1)\mathrm{Pe}^{-1}c^q_p(t).$$

This means that the diffusion operator exponentially suppresses all modes with $p>0$, and the lowest mode $p=0$ is determined by the normalisation condition Eq. (C.8). This is the solution of the diffusion equation on the sphere, with the uniform distribution as steady state.

Now take the for the drift term the standard Jeffery equation $\dot{\boldsymbol{n}}=\mathbb{O}\boldsymbol{n}+\Lambda(\mathbb{S}\boldsymbol{n}-\boldsymbol{n}\boldsymbol{n}^{\mathrm{T}}\mathbb{S}\boldsymbol{n})$, and call this operator $\hat{J}_1=-\partial_{\boldsymbol{n}}\dot{\boldsymbol{n}}+\mathrm{Pe}^{-1}\partial^2_{\boldsymbol{n}}$. We find

$$\begin{aligned}\hat{J}_1=&\,i\sqrt{\frac{\pi}{30}}\Lambda\hat{L}_-\hat{Y}_2^{-1}+i\sqrt{\frac{\pi}{30}}\hat{L}_-\hat{Y}_2^{1}-i\sqrt{\frac{\pi}{30}}\Lambda\hat{L}_+\hat{Y}_2^{1}\\&-i\sqrt{\frac{\pi}{30}}\hat{L}_+\hat{Y}_2^{-1}-i\sqrt{\frac{2\pi}{15}}\Lambda\hat{L}_3\hat{Y}_2^{-2}-i\sqrt{\frac{2\pi}{15}}\Lambda\hat{L}_3\hat{Y}_2^{2}\\&+\frac{2}{3}i\sqrt{\pi}\hat{L}_3\hat{Y}_0^{0}-\frac{2}{3}i\sqrt{\frac{\pi}{5}}\hat{L}_3\hat{Y}_2^{0}-\mathrm{Pe}^{-1}\hat{\boldsymbol{L}}^2.\end{aligned}$$

The fact that the operator $\hat{J}$ is real implies that the matrix elements must have the symmetry

$$\langle p,q|\hat{J}|l,m\rangle = (-1)^q \overline{\langle p,-q|\hat{J}|l,m\rangle}.$$

We can understand the reason for this because the system of differential equations in Eq. (C.7) needs to preserve the condition that P is real, as stated in Eq. (C.5). It implies we have only to compute half of the matrix elements.

Upon including the correction due to weak particle inertia (see Eq.(8) in Paper B), the expression for the operator $\hat{J}$ becomes too lengthy to include here. However, we have implemented the identities and rules described in this appendix in a publicly available Mathematica notebook [49]. Given an operator $\hat{J}$ expressed in terms of $\hat{\boldsymbol{n}}$ and $\hat{\boldsymbol{L}}$, it converts the expression into sums of angular momentum operators as exemplified above. We also provide an additional Mathematica notebook that, given the matrix elements, assembles a sparse matrix $\mathbb{J}$, up to a desired order $l_{\max}$. This matrix can then be used to solve the truncated version of Eq. (C.7) numerically:

$$\dot{\boldsymbol{c}} = \mathbb{J}\boldsymbol{c},$$

where $\boldsymbol{c}$ is a vector containing all the c_l^m. Or alternatively, the matrix can be solved for the stationary values of $\boldsymbol{c}$. All results shown in this paper were computed using $l_{\max} = 400$, which leads to very good convergence in all cases shown. Only when solutions approach delta peaks, as for example the limiting stable orbits in the large PeSt case, the expansion procedure does not converge. All orders $l \to \infty$ are required to represent such peaked functions.

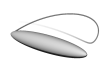

D Lagrangian statistics in isotropic & incompressible flow

In this appendix I derive the general form of the Lagrangian statistics of velocity gradients in an isotropic and incompressible flow. Let me introduce some notation for Lagrangian correlation functions. We denote the matrix of flow gradients by

$$\mathbb{A}(\boldsymbol{r}(t),t)=\nabla\boldsymbol{u}(\boldsymbol{r}(t),t),$$

or in component notation

$$A_{ij}(\boldsymbol{r}(t),t)=\frac{\partial}{\partial r_j}u_i(\boldsymbol{r}(t),t).$$

The correlation functions between matrix elements are denoted

$$C^{AA}_{ijkl}(t_1)\equiv\left\langle A_{ij}(\boldsymbol{r}(0),0)A_{kl}(\boldsymbol{r}(t_1),t_1)\right\rangle,$$
$$C^{AAA}_{ijklmn}(t_1,t_2)\equiv\left\langle A_{ij}(\boldsymbol{r}(0),0)A_{kl}(\boldsymbol{r}(t_1),t_1)A_{mn}(\boldsymbol{r}(t_2),t_2)\right\rangle,$$

and so on. Later we will instead use the shorthand $\mathbb{A}_t\equiv\mathbb{A}(\boldsymbol{r}(t),t)$ for gradients evaluated along particle trajectories.

D.1 Two-point correlation functions

Since we are considering isotropic flows, the correlation function must also be isotropic. The most general isotropic tensor of rank four is

$$C^{AA}_{ijkl}(t)=\alpha_1(t)\delta_{ij}\delta_{kl}+\alpha_2(t)\delta_{ik}\delta_{jl}+\alpha_3(t)\delta_{il}\delta_{kj},$$

where $\alpha_k(t)$ are arbitrary functions of time. The incompressibility condition, $\partial_i u_i=0$, translates into:

$$C^{AA}_{iikk}=d^2\alpha_1(t)+d(\alpha_2(t)+\alpha_3(t))=0,$$

where d is the number of spatial dimensions. We may choose $\alpha_1=-(\alpha_2+\alpha_3)/d$:

$$C^{AA}_{ijkl}(t)=-\frac{1}{d}(\alpha_2(t)+\alpha_3(t))\delta_{ij}\delta_{kl}+\alpha_2(t)\delta_{ik}\delta_{jl}+\alpha_3(t)\delta_{il}\delta_{kj},$$

We are out of symmetries to apply, and two arbitrary functions of t remain in the correlation function. The non-trivial mix of time and space dependence is not convenient to deal with in calculations. But it turns out we can separate the two arbitrary functions by separating $\mathbb{A}$ in its symmetric and antisymmetric parts:

$$\mathbb{O} = \frac{1}{2}(\mathbb{A} - \mathbb{A}^{\mathrm{T}}), \quad \mathbb{S} = \frac{1}{2}(\mathbb{A} + \mathbb{A}^{\mathrm{T}}), \quad \mathbb{A} = \mathbb{O} + \mathbb{S}.$$

It follows that

$$\begin{aligned}
C^{OO}_{ijkl}(t) &= \frac{1}{4}\Big(C^{AA}_{ijkl}(t) - C^{AA}_{ijlk}(t) - C^{AA}_{jikl}(t) + C^{AA}_{jilk}(t)\Big) \\
&= \frac{\alpha_3(t) - \alpha_2(t)}{2}(\delta_{il}\delta_{jk} - \delta_{ik}\delta_{jl}), \\
C^{SS}_{ijkl}(t) &= \frac{1}{4}\Big(C^{AA}_{ijkl}(t) + C^{AA}_{ijlk}(t) + C^{AA}_{jikl}(t) + C^{AA}_{jilk}(t)\Big) \\
&= \frac{\alpha_2(t) + \alpha_3(t)}{2d}(d\delta_{il}\delta_{jk} + d\delta_{ik}\delta_{jl} - 2\delta_{ij}\delta_{kl}), \\
C^{SO}_{ijkl}(t) &= \frac{1}{4}\Big(C^{AA}_{ijkl}(t) - C^{AA}_{ijlk}(t) + C^{AA}_{jikl}(t) - C^{AA}_{jilk}(t)\Big) = 0.
\end{aligned}$$

We relate the time correlation functions $\alpha_k(t)$ to the respective matrices by computing

$$\begin{aligned}
\big\langle \mathrm{Tr}\mathbb{O}_0\mathbb{O}_t \big\rangle &= C^{OO}_{ijji}(t) = \frac{\alpha_3(t) - \alpha_2(t)}{2} d(d-1), \\
\big\langle \mathrm{Tr}\mathbb{S}_0\mathbb{S}_t \big\rangle &= C^{SS}_{ijji}(t) = \frac{\alpha_2(t) + \alpha_3(t)}{2}(d^2 + d - 2).
\end{aligned} \tag{D.1}$$

For an isotropic, incompressible flow the two-point gradient statistics are on the form

$$\begin{aligned}
C^{OO}_{ijkl}(t) &= \frac{\big\langle \mathrm{Tr}\mathbb{O}_0\mathbb{O}_t \big\rangle}{d(d-1)}(\delta_{il}\delta_{jk} - \delta_{ik}\delta_{jl}), \\
C^{SS}_{ijkl}(t) &= \frac{\big\langle \mathrm{Tr}\mathbb{S}_0\mathbb{S}_t \big\rangle}{d(d-1)(d+2)}(d\delta_{il}\delta_{jk} + d\delta_{ik}\delta_{jl} - 2\delta_{ij}\delta_{kl}), \\
C^{SO}_{ijkl}(t) &= 0.
\end{aligned} \tag{D.2}$$

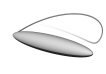

On this form the time- and space dependence of the correlation functions factorise, which enables us to find a simple expression like Eq. (4) in Paper C. The time correlation functions $\left\langle \mathrm{Tr}\mathbb{O}_0\mathbb{O}_t \right\rangle$ and $\left\langle \mathrm{Tr}\mathbb{S}_0\mathbb{S}_t \right\rangle$ are specific to the flow, and must be measured or computed from a flow model.

D.2 Three-point correlation functions

The same type of factorisation can be found for the three-point correlations, for example $C^{SSS}_{ijklmn}(t)$. The procedure is the same, but the algebra expands a fair bit. The general isotropic tensor of rank six has 15 free parameters [50]:

$$\begin{aligned} C^{AAA}_{ijklmn}(t_1,t_2) = {} & \beta_1\delta_{ij}\delta_{kl}\delta_{mn} + \beta_2\delta_{ij}\delta_{km}\delta_{ln} + \beta_3\delta_{ij}\delta_{kn}\delta_{lm} \\ & + \beta_4\delta_{ik}\delta_{jl}\delta_{mn} + \beta_5\delta_{ik}\delta_{jm}\delta_{ln} + \beta_6\delta_{ik}\delta_{jn}\delta_{lm} \\ & + \beta_7\delta_{il}\delta_{jk}\delta_{mn} + \beta_8\delta_{il}\delta_{jm}\delta_{kn} + \beta_9\delta_{il}\delta_{jn}\delta_{km} \\ & + \beta_{10}\delta_{im}\delta_{jk}\delta_{ln} + \beta_{11}\delta_{im}\delta_{jl}\delta_{kn} + \beta_{12}\delta_{im}\delta_{jn}\delta_{kl} \\ & + \beta_{13}\delta_{in}\delta_{jk}\delta_{lm} + \beta_{14}\delta_{in}\delta_{jl}\delta_{km} + \beta_{15}\delta_{in}\delta_{jm}\delta_{kl}. \end{aligned}$$

The $\beta_k = \beta_k(t_1,t_2)$ are also here arbitrary functions of time, but the explicit time dependence is left out for brevity. The incompressibility condition $A_{ii} = 0$ gives the equations

$$C^{AAA}_{iiklmn} = C^{AAA}_{ijkkmn} = C^{AAA}_{ijklmm} = 0,$$

which when solved reduce the number of free parameters to eight:

$$\begin{aligned}
\beta_3 &= -\frac{1}{2}\beta_1 d - \beta_2,\\
\beta_7 &= -\frac{1}{2}\beta_1 d - \beta_4,\\
\beta_{11} &= \beta_2 d - \beta_4 d - \beta_6 + \beta_9 + \beta_{10},\\
\beta_{12} &= -\frac{2\beta_9}{d} - \frac{2\beta_{10}}{d} - \beta_2 + \beta_4,\\
\beta_{13} &= \frac{1}{2}\beta_1 d^2 + \beta_4 d - \beta_8 - \beta_9 - \beta_{10},\\
\beta_{14} &= \beta_2(-d) - \beta_5 - \beta_9 - \beta_{10},\\
\beta_{15} &= -\frac{1}{2}\beta_1 d + \frac{2\beta_9}{d} + \frac{2\beta_{10}}{d} + \beta_2 - \beta_4.
\end{aligned}$$

Again, it turns out that the splitting of $\mathbb{A}$ into $\mathbb{O}$ and $\mathbb{S}$ separates the eight parameters, one for each of the eight combinations of $\mathbb{O}$ and $\mathbb{S}$. Take for example $\mathbb{SSS}$,

$$\begin{aligned}
C^{SSS}_{ijklmn}(t_1,t_2) &= \frac{1}{8}\Big(C^{AAA}_{ijklmn}(t_1,t_2) + C^{AAA}_{ijklnm}(t_1,t_2) + C^{AAA}_{ijlkmn}(t_1,t_2)\\
&\quad + C^{AAA}_{ijlknm}(t_1,t_2) + C^{AAA}_{jiklmn}(t_1,t_2) + C^{AAA}_{jiklnm}(t_1,t_2)\\
&\quad + C^{AAA}_{jilkmn}(t_1,t_2) + C^{AAA}_{jilknm}(t_1,t_2)\Big)\\
&= \frac{\beta_1}{16}\big(d^2\delta_{in}\delta_{jl}\delta_{km} + d^2\delta_{il}\delta_{jn}\delta_{km} + d^2\delta_{im}\delta_{jl}\delta_{kn}\\
&\quad + d^2\delta_{il}\delta_{jm}\delta_{kn} + d^2\delta_{in}\delta_{jk}\delta_{lm} + d^2\delta_{ik}\delta_{jn}\delta_{lm}\\
&\quad + d^2\delta_{im}\delta_{jk}\delta_{ln} + d^2\delta_{ik}\delta_{jm}\delta_{ln} - 4d\delta_{in}\delta_{jm}\delta_{kl}\\
&\quad - 4d\delta_{im}\delta_{jn}\delta_{kl} - 4d\delta_{ij}\delta_{kn}\delta_{lm} - 4d\delta_{ij}\delta_{km}\delta_{ln}\\
&\quad - 4d\delta_{il}\delta_{jk}\delta_{mn} - 4d\delta_{ik}\delta_{jl}\delta_{mn} + 16\delta_{ij}\delta_{kl}\delta_{mn}\big)
\end{aligned}$$

We relate β_1 to the trace of $\mathbb{SSS}$ by

$$C^{SSS}_{ijjkki}(t_1,t_2) = \left\langle \mathrm{Tr}\mathbb{S}_0\mathbb{S}_{t_1}\mathbb{S}_{t_2}\right\rangle = \frac{\beta_1}{16}d\left(d^4 + 3d^3 - 8d^2 - 12d + 16\right)$$

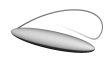

The same procedure is repeated for all eight combinations of $\mathbb{S}$ and $\mathbb{O}$. The result is

$$\begin{aligned}
C^{SSS}_{ijklmn}(t_1,t_2) = \frac{\left\langle \mathrm{Tr}\mathbb{S}_0\mathbb{S}_{t_1}\mathbb{S}_{t_2}\right\rangle}{d\left(d^4+3d^3-8d^2-12d+16\right)}\big(&d^2\delta_{in}\delta_{jl}\delta_{km}\\
&+d^2\delta_{il}\delta_{jn}\delta_{km}+d^2\delta_{im}\delta_{jl}\delta_{kn}+d^2\delta_{il}\delta_{jm}\delta_{kn}\\
&+d^2\delta_{in}\delta_{jk}\delta_{lm}+d^2\delta\delta_{jn}\delta_{lm}+d^2\delta_{im}\delta_{jk}\delta_{ln}\\
&+d^2\delta\delta_{jm}\delta_{ln}-4d\delta_{in}\delta_{jm}\delta_{kl}-4d\delta_{im}\delta_{jn}\delta_{kl}\\
&-4d\delta_{ij}\delta_{kn}\delta_{lm}-4d\delta_{ij}\delta_{km}\delta_{ln}-4d\delta_{il}\delta_{jk}\delta_{mn}\\
&-4d\delta_{ik}\delta_{jl}\delta_{mn}+16\delta_{ij}\delta_{kl}\delta_{mn}\big), \qquad \text{(D.3)}\\
C^{SSO}_{ijklmn}(t_1,t_2) = \frac{\left\langle \mathrm{Tr}\mathbb{S}_0\mathbb{S}_{t_1}\mathbb{O}_{t_2}\right\rangle}{(d-1)d(d+2)}\big(&\delta_{in}\delta_{jl}\delta_{km}+\delta_{il}\delta_{jn}\delta_{km}\\
&-\delta_{im}\delta_{jl}\delta_{kn}-\delta_{il}\delta_{jm}\delta_{kn}+\delta_{in}\delta_{jk}\delta_{lm}\\
&+\delta_{ik}\delta_{jn}\delta_{lm}-\delta_{im}\delta_{jk}\delta_{ln}-\delta_{ik}\delta_{jm}\delta_{ln}\big), \qquad \text{(D.4)}\\
C^{SOS}_{ijklmn}(t_1,t_2) = -\frac{\left\langle \mathrm{Tr}\mathbb{S}_0\mathbb{O}_{t_1}\mathbb{S}_{t_2}\right\rangle}{(d-1)d(d+2)}\big(&\delta_{in}\delta_{jl}\delta_{km}+\delta_{il}\delta_{jn}\delta_{km}\\
&+\delta_{im}\delta_{jl}\delta_{kn}+\delta_{il}\delta_{jm}\delta_{kn}-\delta_{in}\delta_{jk}\delta_{lm}\\
&-\delta_{ik}\delta_{jn}\delta_{lm}-\delta_{im}\delta_{jk}\delta_{ln}-\delta_{ik}\delta_{jm}\delta_{ln}\big), \qquad \text{(D.5)}\\
C^{SOO}_{ijklmn}(t_1,t_2) = -\frac{\left\langle \mathrm{Tr}\mathbb{S}_0\mathbb{O}_{t_1}\mathbb{O}_{t_2}\right\rangle}{(d-2)(d-1)d(d+2)}\big(&d\delta_{in}\delta_{jl}\delta_{km}+d\delta_{il}\delta_{jn}\delta_{km}\\
&-d\delta_{im}\delta_{jl}\delta_{kn}-d\delta_{il}\delta_{jm}\delta_{kn}-d\delta_{in}\delta_{jk}\delta_{lm}\\
&-d\delta_{ik}\delta_{jn}\delta_{lm}+d\delta_{im}\delta_{jk}\delta_{ln}+d\delta_{ik}\delta_{jm}\delta_{ln}\\
&-4\delta_{ij}\delta_{km}\delta_{ln}+4\delta_{ij}\delta_{kn}\delta_{lm}\big), \qquad \text{(D.6)}\\
C^{OSS}_{ijklmn}(t_1,t_2) = \frac{\left\langle \mathrm{Tr}\mathbb{O}_0\mathbb{S}_{t_1}\mathbb{S}_{t_2}\right\rangle}{(d-1)d(d+2)}\big(&\delta_{in}\delta_{jl}\delta_{km}-\delta_{il}\delta_{jn}\delta_{km}\\
&+\delta_{im}\delta_{jl}\delta_{kn}-\delta_{il}\delta_{jm}\delta_{kn}+\delta_{in}\delta_{jk}\delta_{lm}\\
&-\delta_{ik}\delta_{jn}\delta_{lm}+\delta_{im}\delta_{jk}\delta_{ln}-\delta_{ik}\delta_{jm}\delta_{ln}\big), \qquad \text{(D.7)}
\end{aligned}$$

$$C^{OSO}_{ijklmn}(t_1,t_2)=\frac{\left\langle \mathrm{Tr}\mathbb{O}_0\mathbb{S}_{t_1}\mathbb{O}_{t_2}\right\rangle}{(d-2)(d-1)d(d+2)}\big(d\delta_{in}\delta_{jl}\delta_{km}-d\delta_{il}\delta_{jn}\delta_{km}$$
$$-d\delta_{im}\delta_{jl}\delta_{kn}+d\delta_{il}\delta_{jm}\delta_{kn}+d\delta_{in}\delta_{jk}\delta_{lm}$$
$$-d\delta_{ik}\delta_{jn}\delta_{lm}-d\delta_{im}\delta_{jk}\delta_{ln}+d\delta_{ik}\delta_{jm}\delta_{ln}$$
$$-4\delta_{in}\delta_{jm}\delta_{kl}+4\delta_{im}\delta_{jn}\delta_{kl}\big), \tag{D.8}$$

$$C^{OOS}_{ijklmn}(t_1,t_2)=-\frac{\left\langle \mathrm{Tr}\mathbb{O}_0\mathbb{O}_{t_1}\mathbb{S}_{t_2}\right\rangle}{(d-2)(d-1)d(d+2)}\big(d\delta_{in}\delta_{jl}\delta_{km}-d\delta_{il}\delta_{jn}\delta_{km}$$
$$+d\delta_{im}\delta_{jl}\delta_{kn}-d\delta_{il}\delta_{jm}\delta_{kn}-d\delta_{in}\delta_{jk}\delta_{lm}$$
$$+d\delta_{ik}\delta_{jn}\delta_{lm}-d\delta_{im}\delta_{jk}\delta_{ln}+d\delta_{ik}\delta_{jm}\delta_{ln}$$
$$+4\delta_{il}\delta_{jk}\delta_{mn}-4\delta_{ik}\delta_{jl}\delta_{mn}\big), \tag{D.9}$$

$$C^{OOO}_{ijklmn}(t_1,t_2)=-\frac{\left\langle \mathrm{Tr}\mathbb{O}_0\mathbb{O}_{t_1}\mathbb{O}_{t_2}\right\rangle}{(d-2)(d-1)d}\big(\delta_{in}\delta_{jl}\delta_{km}-\delta_{il}\delta_{jn}\delta_{km}$$
$$-\delta_{im}\delta_{jl}\delta_{kn}+\delta_{il}\delta_{jm}\delta_{kn}-\delta_{in}\delta_{jk}\delta_{lm}$$
$$+\delta_{ik}\delta_{jn}\delta_{lm}+\delta_{im}\delta_{jk}\delta_{ln}-\delta_{ik}\delta_{jm}\delta_{ln}\big). \tag{D.10}$$

D.3 Homogeneity

When the correlation is evaluated at the particle, that is $t = 0$, we may also exploit the homogeneity of the flow. In a homogenous and incompressible flow $\langle \mathrm{Tr}\mathbb{A}^2 \rangle = \langle \mathrm{Tr}\mathbb{A}^3 \rangle = 0$, which implies

$$\begin{aligned} 0 = C^{AA}_{ijji}(t) &= (d-1)(\alpha_2(0) + (1+d)\alpha_3(0)), \\ \Rightarrow \alpha_2(0) &= -\alpha_3(0)(1+d). \end{aligned}$$

and

$$\begin{aligned} \beta_1 &= \frac{12\beta_9}{d(d+1)} \\ \beta_2 &= -\frac{4\beta_9}{d} \\ \beta_4 &= -\frac{4\beta_9}{d} \\ \beta_5 &= \beta_9 \\ \beta_6 &= \beta_9 \\ \beta_8 &= -\frac{3\beta_9}{d+1} \\ \beta_{10} &= \beta_9 \end{aligned}$$

By insertion into Eq. (D.1), and the equivalent for the three-matrix traces we find that

$$\begin{aligned} \frac{1}{2}\langle \mathrm{Tr}\mathbb{A}_0^{\mathrm{T}}\mathbb{A}_0 \rangle &= \langle \mathrm{Tr}\mathbb{S}_0\mathbb{S}_0 \rangle \\ &= -\langle \mathrm{Tr}\mathbb{O}_0\mathbb{O}_0 \rangle \end{aligned}$$

and

$$\begin{aligned} \frac{1}{4}\langle \mathrm{Tr}\mathbb{A}_0^{\mathrm{T}}\mathbb{A}_0\mathbb{A}_0 \rangle &= \frac{1}{3}\langle \mathrm{Tr}\mathbb{S}_0\mathbb{S}_0\mathbb{S}_0 \rangle \\ &= -\langle \mathrm{Tr}\mathbb{S}_0\mathbb{O}_0\mathbb{O}_0 \rangle \\ &= -\langle \mathrm{Tr}\mathbb{O}_0\mathbb{S}_0\mathbb{O}_0 \rangle \\ &= -\langle \mathrm{Tr}\mathbb{O}_0\mathbb{O}_0\mathbb{S}_0 \rangle. \end{aligned}$$

The last three lines are identically equal because the trace of a matrix product is invariant under cyclic permutations.

Part IV
Research papers

Paper A

Periodic and aperiodic tumbling of microrods advected in a microchannel flow

arXiv e-print available at http://arxiv.org/abs/1211.5672

Paper B

Orientational dynamics of weakly inertial axisymmetric particles in steady viscous flows

arXiv e-print available at http://arxiv.org/abs/1307.2821

Paper C

Tumbling of small axisymmetric particles in random and turbulent flows

arXiv e-print available at http://arxiv.org/abs/1305.1822